DISRUPTION OF THE K-Cl COTRANSPORTER-3 LEADS TO SEVERE PERIPHERAL NEUROPATHY

By

Nellie Eunjoo Byun

Dissertation

Submitted to the Faculty of the

Graduate School of Vanderbilt University

in partial fulfillment of the requirements

for the degree of

DOCTOR OF PHILOSOPHY

in

Neuroscience

December, 2007

Nashville, Tennessee

Approved by:

Professor Bruce D. Carter

Professor Eric Delpire

Professor Robert L. Macdonald

Professor W. Gray Jerome

Professor William M. Valentine

ACKNOWLEDGEMENTS

.

Many people were instrumental in kindling my curiosity in neuroscience into a passion for research as well as guiding me through graduate school. This dissertation would not have been possible without them. First, I need to thank my advisor Dr. Eric Delpire for allowing me to me take on my research project as well as for his enthusiasm, advice, and patient teaching. No matter how busy he was, his office door was always open. The support of Dr. Bruce Carter, my committee chair, not only in welcoming me into his lab to learn techniques, but as a student advocate was invaluable. My committee members, Drs. Bob Macdonald, Jay Jerome, and Bill Valentine have each guided me with their expertise, and their direction has been invaluable. I greatly appreciate the generosity of Drs. Amanda Peltier and Mike Macdonald who spent time to train me on equipment and share their resources. I admire the dedication of Drs. Elaine Sanders-Bush and Lou DeFelice to all students and science, and their advice continues to be indispensable. Drs. Ken Gagnon and Kerstin Piechotta should know that I value their mentorship, friendship, and all their help. Finally, I wouldn't be here today without Dr. Ann McPartland.

My parents have been supportive in all my endeavors, and I thank them for all the years of encouragement and providing me with so many opportunities. My little sister is always there to talk to no matter how mundane the topic, and I wish her success as a budding neurologist. My grandmothers in Korea traveled to Buddhist temples to wish me luck, and really my great luck is all the love and support from my family and friends.

TABLE OF CONTENTS

Page

LIST OF FIGURES

LIST OF TABLES

LIST OF ABBREVIATIONS

AATYK	apoptosis-associated tyrosine kinase
ACCPN	peripheral neuropathy associated with agenesis of the corpus callosum
CAP	compound action potential
CIP	CCC interacting protein
CCC	cation chloride cotransporter
CLC	chloride channel
CMAP	compound muscle action potential
CMTD	Charcot-Marie-Tooth disease
CMTX	Charcot-Marie-Tooth X-linked
CNPase	2',3'-cyclic nucleotide 3'-phosphodiesterase
CNS	central nervous system
Co-IP	co-immunoprecipitation
CSF	cerebrospinal fluid
Cx	connexin
DIDS	4,4'-diisothiocyanostilbene disulphonic acid
DIOA	dihydro-1-oxo-1H-inden-5-yl-oxy acetic acid
DRG	dorsal root ganglion
dSMAV	distal spinal muscular atrophy V
DSS	Dejerine-Sottas syndrome
ECM	extracellular matrix
ECS	extracellular space

EM	electron microscopy
EMG	electromyography
ER	endoplasmic reticulum
ES	embryonic stem
GAN	giant axonal neuropathy
GARS	glycyl transfer RNA synthetase
GCK	germinal center kinase
GDAP1	ganglioside-induced differentiation-associated protein-1
HMSN	hereditary motor and sensory neuropathy
HNPP	hereditary neuropathy with liability to pressure palsies
KCC	K-Cl cotransporter
KIF1B	kinesin family member 1B
Kv	voltage gated potassium channel
MAG	myelin associated glycoprotein
MFN2	mitofusin 2
MTMR2	myotubularin-related protein-2
Nav	voltage-gated sodium channel
NKCC	Na-K-2Cl cotransporter
NCC	Na-Cl cotransporter
NCV	nerve conduction velocity
NEM	N-ethylmaleimide
NMJ	neuromuscular junction
Nrg	neuregulin

NTR	neurotrophin receptor
OSR1	oxidative stress-response protein 1
PBS	phosphate-buffered saline
P0	myelin protein zero
Prx	periaxin
PHAII	Pseudohypoaldosteronism type II
PMP22	peripheral myelin protein 22
PNS	peripheral nervous system
PP1	protein phosphatase 1
PPI	prepulse inhibition
RBC	red blood cell
RT	room temperature
RVI	regulatory volume increase
RVD	regulatory volume decrease
SLC	solute carrier
SLI	Schmidt-Lanterman incisure
SLSJ	Saguenay-Lac-St.-Jean
SOX10	sex determining region Y box 10
SPAK	Ste20-related proline alanine rich kinase
SSEP	somatosensory evoked potential
TALH	thick ascending loop of Henle
TBST	tris-buffered saline with Tween 20
TM	transmembrane

Wld^S	Wallerian degeneration slowed
WNK	with-no-K (lysine)

CHAPTER I

CATION CHLORIDE COTRANSPORTERS

Introduction

All cells, whether a single unit organism or part of a multicellular conglomerate, need to stabilize their intracellular ion and fluid compositions in the face of changing and oftentimes harsh external environments with differential molecular compositions and osmolarities. Cells must adjust and adapt to these ionic and osmotic stresses by changing their internal ionic milieu and volumes, an ability that is critical for normal cellular metabolism, integration with other cells, and survival. The necessity for ion and volume control led to the evolution of proteins, including cation chloride cotransporters (CCCs), which regulate the movement of salts. In response to osmotic stress, cells maintain osmotic and volume homeostasis through controlled ion and obligate fluid movement through the processes of regulatory volume increase (RVI) and decrease (RVD). Fluid secretion and absorption, the main function of epithelial tissues—including salivary, lung, kidney, pancreas, and choroid plexus—is also directly linked to ion flux. Neuronal communication via propagating action potentials depends on intracellular ion concentrations that determine the resting membrane potential and thus the signaling outcome. CCCs directly mediate these processes and have also been implicated in other fundamental cellular activities such as ion buffering and pH regulation as well as proliferation, motility, and apoptosis, which are related to cell volume changes. After the recent discovery of key signaling molecules that interact with CCCs, great headway is

being made in determining the molecular regulation of each cotransporter in different cell types, bringing us closer to the ever elusive osmosensors. Due to their clinical significance, studying the physiology of these cotransporters is also crucial. Recent studies have linked CCCs to a wide range of human diseases including cancer, epilepsy, schizophrenia, and bipolar disorder, and investigators have made both expected and surprising discoveries of mutations in cotransporter genes that cause renal and nervous system syndromes. Mouse models have helped to uncover the physiological, cellular, and molecular functions of each CCC as well as mechanisms of disease pathogenesis.

Membrane transport is crucial in all cells for the homeostasis of inorganic ions, amino acids, neurotransmitters, sugars, and other molecules. CCCs belong to one group of transporters in the solute carrier (SLC) gene class (*SLC1-46*) that encodes for 298 human transporter genes, which include uniporters, cotransporters, and exchangers (Hediger et al., 2004). The CCC superfamily encoded by the *SLC12* genes is comprised of proteins that mediate the coupled, electroneutral transport of inorganic cations with chloride across plasma membranes (Haas, 1994; Hebert et al., 2004). In vertebrates, the Na-dependent subfamily includes one Na-Cl cotransporter (NCC) and two Na-K-Cl cotransporters (NKCCs), while the four K-Cl cotransporters (KCCs), CCC9, and CCC interacting protein (CIP) belong to the Na-independent line (Table 1-1). A homology tree schematically delineates these two distinct branches and the relationships between the proteins (Figure 1-1). Several cotransporters with homology to the KCCs exist in invertebrates, including the Drosophila KCC *kazachoc* (Colmenero-Flores et al., 2007; Hekmat-Scafe et al., 2006) and even plants express a *bona fide* NKCC (Colmenero-Flores et al., 2007).

Table 1-1. The seven vertebrate cation chloride cotransporters

Cotransporter Name	Human Gene	Human Chromosome	Tissue Distribution	Human Disease	Knockout Phenotype
NCC, TSC	Slc12a3	16q13	Kidney	Gitelman syndrome	Kidney
NKCC1, BSC2	Slc12a2,	5q23.2	Ubiquitous: Epithelial cells (basolateral). Nonepithelial: Brain Spinal cord Sciatic nerve	Not known (possibly deafness, epilepsy, renal)	Inner ear/ vestibular *shaker/waltzer*; Sensory (nociception); Intestinal; Salivary; Male sterility
NKCC2, BSC1	Slc12a1	15q15-q21.1	Kidney apical thick ascending limb	Bartter syndrome	Kidney
KCC1	Slc12a4	16q22.1	Ubiquitous: Brain Colon Heart Kidney Liver Lung Spleen, Stomach Pancreas Muscle RBCs, etc.	Not known (possibly hemoglobin-apthies)	No phenotype
KCC2	Slc12a5	20q13	Brain Spinal cord (Neurons only)	Not known (possibly epilepsy)	Embryonic lethal; Seizures in hypomorph
KCC3	Slc12a6	15q13-14	Widespread: Brain Spinal cord DRG Kidney Lung Heart Pancreas RBC	ACCPN (Andermann syndrome)	Locomotor; Sensory (nociception); PPI disruption; Hypertension
KCC4	Slc12a7	5p15.3	Kidney Heart Brain	Not known (possibly renal)	Sensorineural deafness; Renal acidosis
CCC9	SLC12a8	3q21	Widespread	Not known	Not reported
CIP	SLC12A9	7q22	Widespread	Not known	Not reported

Abbreviations: RBCs=red blood cells; ACCPN=peripheral neuropathy associated with agenesis of the corpus callosum; PPI=prepulse inhibition.

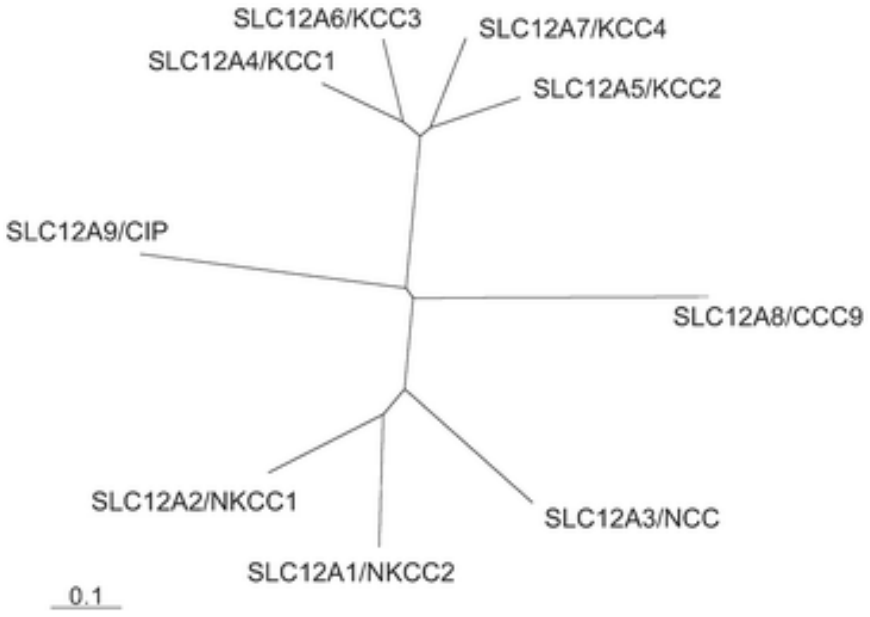

Figure 1-1. Homology tree of the vertebrate cation chloride cotransporters

Hebert et al. calculated this homology tree of CCCs using human sequences in the Clustal program at www.ebi.ac.uk/clustalw. The homology tree, which is labeled with both the gene and protein acronyms, delineates the distinct branches of Na-dependent (NCC, NKCC1-2) and Na-independent cotransporters (KCC1-4) and their relationships with CCC9 and CIP. The scale bar corresponds to a distance of 10 substitutions per 100. Figure from (Hebert et al., 2004)

Although the functions of CCC9 and CIP are not known, the other seven vertebrate cotransporters (NCC, NKCC1-2, and KCC1-4) are well characterized. They all share a basic 12 transmembrane structural motif as well as all of the functional criteria of CCCs: electroneutral ion transport driven by their concentration gradients, dependence on the presence of all transported ions, and sensitivity to loop diuretics and cell volume changes (Delpire & Mount, 2002). Despite these similarities, their differential expression patterns, activation/deactivation pathways, cellular localizations, ion sensitivities, and phosphorylation and protein binding sites confer their unique physiological functions and distinct pathologies from dysfunction.

General Protein Structure

Kyte-Doolittle hydropathy analyses predict each CCC as a 12 transmembrane (TM) domain protein with a large extracellular loop and intracellular amino- and carboxy-termini based on their putative alpha-helices and two flanking hydrophilic regions (Figure 1-2). Their homology is strongest within the central 12 hydrophobic domains, specifically TM3-TM12, which is homologous to the amino acid permease pfam00324. TM2 determines the CCCs differential ion binding affinities (Isenring et al., 1998). The placement of the large N-glycosylated extracellular loop differs between KCCs and N(K)CCs; it lies between TM5 and TM6 in KCCs and CIP, but for NCC/NKCCs it is situated between TM7 and TM8. The cytoplasmic domains contain phosphorylation and protein binding sites, which have been determined in part by mutagenesis and yeast 2-hybrid mapping experiments. The most variability between CCCs lies in their amino-termini, suggesting that this region is responsible for differential

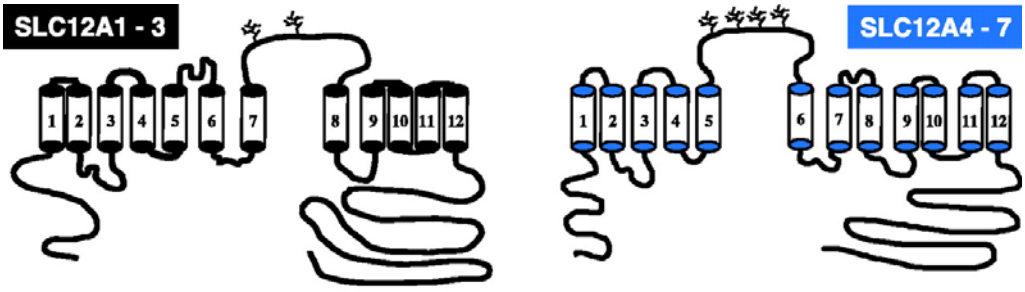

Figure 1-2. Basic structures of the vertebrate cation chloride cotransporters

CCCs are comprised of 12 transmembrane domains, a large extracellular loop, and intracellular amino and carboxyl tails as predicted by Kyte-Doolittle hydropathy analyses. The major difference between the Na-dependent cotransporters SLC12A1-3 (NCC, NKCC2, NKCC1) and Na-independent cotransporters SLC12A4-7 (KCC1-4) are the positions of the glycosylated extracellular loops. Figure from (Gamba, 2005).

regulatory mechanisms.

Each cotransporter most likely functions as a homodimer. Supporting evidence for homooligomeric quaternary structure include: crosslinking experiments that double the size of detected bands corresponding to NKCC1 (Moore-Hoon & Turner, 2000); yeast 2-hybrid analyses and GST-pull downs demonstrating two self-interacting domains in the carboxy-termini of NKCC1 and NKCC2 (Brunet et al., 2005; Simard et al., 2004); and the co-immunoprecipitation (co-IP) of 2 NKCC2s and 2 NCCs when heterologously expressed in *Xenopus* oocytes (de Jong et al., 2003; Starremans et al., 2003). More recently, Simard et al. demonstrated homodimeric structure of KCCs through yeast 2-hybrid mapping and confirmatory co-IP assays (Simard et al., 2007). Furthermore, KCCs could form heterooligomeric structures in the *Xenopus* oocyte system. Whether or not heterodimers are physiologically relevant structures is not known. The authors state that the overlap in the phenotypes of deafness and neuronal excitability in several different cotransporter knockouts support physiological heterooligomerization (Simard et al., 2007). This proposal, however, is not well grounded since the most striking phenotypes of each KCC knockout are extremely unique and the extent of the common defects in question—deafness of KCC4$^{-/-}$ and KCC3$^{-/-}$ mice and neuronal excitability in KCC2$^{-/-}$ and KCC3$^{-/-}$ animals—are not at comparable levels. For example, despite some colocalization of KCC3 and KCC4 proteins in the inner ear, KCC3 is present alone on Type I and III fibrocytes. Also, a completely different degeneration pattern ensues in the inner ear of KCC3$^{-/-}$ mice than in KCC4$^{-/-}$ mice (Boettger et al., 2002; Boettger et al., 2003). This example indirectly supports that KCCs (at least KCC3 and KCC4) do not

heterooligomerize. Otherwise, a similar histopathology and pathogenesis of deafness would be expected in both knockouts.

Simard et al. have, however, opened the possibility that in some cell types heterooligomerization may occur (Simard et al., 2007). This hypothesis should be further tested using intact, natural, nonheterologous systems, such as co-IP experiments from brain tissue or cultured neurons, or a heterologous system utilizing a much more powerful detection method, such as fluorescence resonance energy transfer of fluorescent-tagged (e.g., GFP, YFP, CFP) CCCs. This technique has successfully demonstrated interactions between many membrane proteins, not just their oligomerization states, but also the location, timing, and ligand effects on the process, such as the homodimerization of epidermal growth factor receptors (Liu et al., 2007); homodimerization of the serotonin receptor 5-HT2C in the endoplasmic reticulum (Herrick-Davis et al., 2006); timing of assembly of the cytokine receptor gp 130 (Tenhumberg et al., 2006); and ligand-induced structural changes in the dimeric metabotropic glutamate receptor 1 alpha (Tateyama et al., 2004). Functionality of cotransporter heterodimers could be assayed in *Xenopus* oocytes using concatenated homo- and hetero-dimers for ^{86}Rb flux assays, or in other systems such as ghost red blood cells or resealed vesicles.

Electroneutral ion transport

Cation chloride cotransport is an electrically silent, passive process dependent on the existing ion gradients (Geck et al., 1980; Jennings & Adame, 2001). CCCs require the presence of all transported ions on the same side of the plasma membrane; for example, absence of any of the three transported ions shuts down NKCC1 (Russell, 2000). In most

situations, NKCCs carry ions at a 1Na:1K:2Cl ratio and KCCs at 1K:1Cl. This stoichiometry leads to electroneutral transport since there is no net charge crossing the plasma membrane. Because CCCs are secondary transporters that do not utilize ATP, the direction of ion movement depends on the established gradients created by primary transporters, mainly the Na-K ATPase (Dunham et al., 1980; Geck et al., 1980; Lauf & Theg, 1980). Since Na-K pump activity is constant, it is the cation gradient(s) that drives chloride movement through the cotransporters. Thus, under physiological conditions, the high extracellular Na^+ concentration drives Cl^- inward through N(K)CCs resulting in Cl^- accumulation, while the high intracellular K^+ levels drives Cl^- out of the cell, along with K^+, through KCCs. Since the Na-K ATPase returns Na^+ and K^+ concentrations to physiological levels, cotransport activity is able to net changes in intracellular Cl^- levels, which is a major cellular function of many CCCs. Theoretically, however, NKCCs and KCCs can move ions in either direction and are able to switch when thermodynamics allow for it.

Regulation

Like many other proteins, CCCs are regulated by phosphorylation and dephosphorylation. The fact that NKCCs and KCCs hold an inverse, reciprocal activation-deactivation relationship where phosphorylation activates NKCCs and dephosphorylation activates KCCs (Gagnon et al., 2006; Jennings & Schulz, 1991; Lauf et al., 1992; Mercado et al., 2000; Reisert et al., 2005; Starke & Jennings, 1993) indicates a coordinated balance between cation-chloride influx/efflux and suggests coexpression of NKCCs and KCCs. Although the role of protein phosphatase 1 (PP1) was recognized

from ion flux experiments using PP1 inhibitors (Jennings & Schulz, 1991; Kaji & Tsukitani, 1991; Krarup & Dunham, 1996; Krarup et al., 1998) and mutagenesis of the putative PP1 consensus binding motif (Darman et al., 2001), the phosphorylating agents remained a mystery until Piechotta et al. identified two related kinases, Ste20-related proline alanine rich kinase (SPAK) and oxidative stress-response protein 1 (OSR1), in yeast 2-hybrid screens that demonstrated their interactions with the amino-termini of KCC3, NKCC1, and NKCC2 (Piechotta et al., 2002). Gagnon et al. showed that SPAK activated NKCC1 via phosphorylation, revealing its functional significance (Gagnon et al., 2006).

SPAK (pas domain-containing serine-threonine kinase, or PASK, in rat), a protein expressed by neurons and epithelial cells, was originally cloned from rat brain (Ushiro et al., 1998), but its substrate was not known until Piechotta et al. determined that KCC3, NKCC1, and NKCC2 were putative binding partners (Piechotta et al., 2002). It is not surprising that cell types with an abundance of CCCs also express SPAK at high levels. SPAK was detected along the plasma membrane of epithelial tissues following the pattern of NKCC1; for example, both were detected on salivary gland tissue basolaterally (Piechotta et al., 2002). Since SPAK is not a membrane protein, its localization is most likely due to interaction with the cotransporter. This is supported by immunostaining results of NKCC1$^{-/-}$ choroid plexus epithelial cells in which SPAK appears completely cytosolic, most likely from the loss of its scaffolding protein (Piechotta et al., 2002). SPAK is a member of the germinal center kinase (GCK)-VI subfamily, which includes other Ste20 serine/threonine kinases such as *Drosophila* Fray (Leiserson et al., 2000) and *C. elegans* Gck-3 (Denton et al., 2005). Ste20 kinases respond to osmotic/volume stress

even in yeast, demonstrating their evolutionarily conserved roles in ion/fluid homeostasis (Strange et al., 2006). Interestingly, the regulatory domain of SPAK contains putative sequences for caspase-3 cleavage and nuclear targeting, suggesting that SPAK can mediate signaling between the cytoplasm and nucleus (Johnston et al., 2000). In fractionation and immunostaining studies, however, SPAK is both cytosolic and associated with the plasma membrane (Piechotta et al., 2002; Tsutsumi et al., 2002), the latter mediated through interaction with integral membrane proteins such as CCCs (Piechotta et al., 2003). It is not known whether CCCs can change the localization of the kinase, but interestingly, exposure to cellular stresses such as hypertonicity, oxidative stress (hydrogen peroxide), and heat shock led to the translocation of SPAK from cytoplasm to cytoskeleton (Tsutsumi et al., 2002). Although it is tempting to speculate that responses to different cellular stresses converge on SPAK to activate NKCCs and inactivate KCCs, it is likely that this is only the case for osmotic stress; other stress conditions may induce SPAK to interact with other proteins. This hypothesis should be tested by evaluating phosphorylation states and protein/mRNA levels of other proteins that interact with SPAK after exposing cells to different types of stresses. In fact, a yeast 2-hybrid screen with SPAK as bait yielded gelsolin, an actin-binding protein that has been shown to respond to oxidative stress and heat shock protein 105 as putative interacting proteins (Piechotta et al., 2003). Other potential SPAK-binding partners fished from the screen, such as apoptosis-associated tyrosine kinase (AATYK) and With-no-K (lysine) (WNK) kinase-4 (Piechotta et al., 2003), were later shown to regulate CCC activity (Gagnon et al., 2006; Garzon-Muvdi et al., 2007).

It is now clear that protein phosphatases, Ste20 kinases, and WNKs are part of the signaling complex that regulates CCCs (Figure 1-3), but the biochemical pathway has not been completely mapped. Of the four vertebrate WNKs (WNK1-4), WNK4 interacts directly with SPAK, activating it via phosphorylation (Vitari et al., 2005), presumably allowing phospho-SPAK to phosphorylate and activate NKCC1. Indeed, the processes of NKCC1 activation and KCC2 inhibition both required the coexpression of WNK4 and SPAK in *Xenopus* oocytes (Gagnon et al., 2006). It appears that WNK4 can also regulate surface expression of at least one CCC as WNK4 decreased NCC surface expression in a *Xenopus* oocyte model (Wilson et al., 2003). Related to this, it is now known that the kidney disorder Gitelman syndrome is caused by mutations in WNK4 that increase NCC activity, which could be through increased expression. On the other hand, mutations in NCC that decrease cotransporter activity cause the kidney disorder pseudohypoaldosteronism type II (PHAII), and thiazides, which inhibit NCCs, are used to treat the disease (Mayan et al., 2002). Knockin mice with a mutated *Wnk4* gene (D561A/+) phenotypically presented with PHAII and their kidney tissues had increased levels of both phosphorylated NCC and SPAK/OSR1 compared to wild-type, which support the postulated WNK4—SPAK/OSR1—cotransporter pathway and also demonstrate that increased NCC activity cause PHAII (Yang et al., 2007a). Whether WNK4 affects the surface expression of other cotransporters has not been reported. Also complicating this pathway are the effects of the other WNKs on CCCs, suggesting multiple levels of regulation.

WNK3 can inhibit KCC3 flux in hypotonic (activating) environments, and inversely, stimulates Na-dependent cotransporters in deactivating conditions (Kahle, et al.

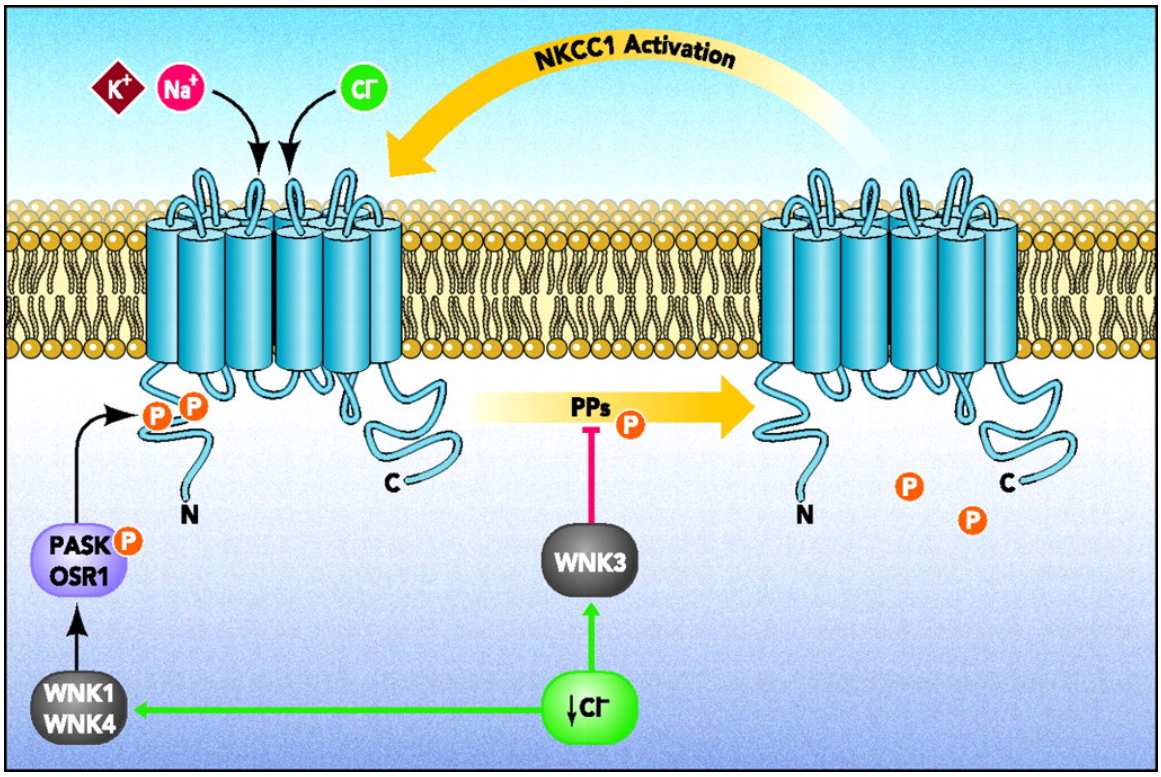

Figure 1-3. Regulation of cation chloride cotransporters

NKCCs are activated by phosphorylation while KCCs are inhibited by phosphorylation. PASK is the rat homolog of mouse SPAK. In this example, after phosphorylation by WNK, PASK/OSR1 adds phosphate groups to key cotransporter residues, which activates NKCCs (and would inhibit KCCs). WNK3 also promotes the activation of NKCCs by inhibting protein phophatases (PPs), specifically PP1. Stress signals from changes in intracellular ion concentration, cell volume, and/or extracellular tonicity are transduced by the stress-sensing molecule(s)—either WNKs or upstream proteins—can switch the downstream kinases from an inactive to an active state. Since chloride-sensitive WNKs are activated by hypertonicity and/or low intracellular chloride, these proteins may be the sensors and the transducers. The upstream playesrs are not known, but clearly, WNKs, PASK/SPAK/OSR1, and PP1 coordinate the activity CCCs. Figure from (Kahle et al., 2006).

2005). WNK3, however, does not directly interact with cotransporters, but rather inhibits protein phosphatases via phosphorylation, which in turn increases NKCC activity and reduces KCC activity (de Los Heros et al., 2006; Rinehart et al., 2005). This again demonstrates the reciprocal regulation of NKCCs and KCCs, which balances the net transport of ions through entry and efflux pathways. Since the kidney regulates ion reabsorption for secretion, it is a popular model for studying WNKs and cotransporters. More recently, however, the role of WNKs on cotransport activity has been studied in neuronal models due to the importance of intracellular chloride regulation that directly affects GABAergic/glycinergic signaling pathways. Quite interestingly, WNK3 colocalizes with KCC2 in hippocampal, cerebellar, and cortical neurons that receive GABAergic input and its developmental postnatal upregulation pattern mirrors that of KCC2 (Holden et al., 2004; Kahle et al., 2005). If WNK3 truly regulates KCC2 by reducing its activity, then overexpression or overactivity of WNK3 could lead to a similar CNS phenotype as KCC2-hypomorphs (i.e., hyperexcitability, seizures). Although it is clear that WNK3 directly affects phosphatases, its ability to interact with and/or phosphorylate SPAK cannot be ruled out since its sequence contains a SPAK binding motif. Whether SPAK is a scaffold for WNK3 or is phosphorylated by WNK3 remains to be determined.

Although the discovery of SPAK-cotransporter interaction in our laboratory (Piechotta et al., 2003; Piechotta et al., 2002) has led to a greater understanding of CCC regulation, more work needs to be done to unravel the ambiguities (e.g., regulation of activity versus expression levels), tease out the different pathways for each CCC in different cell types, and uncover the actual osmosensors, which WNKs themselves may

prove to be. Interestingly, inactivating mutations in the *Drosophila* homolog of SPAK, Fray, led to bulging of abdominal nerves from fluid accumulation. This swelling phenotype was due to a glial defect, which could be rescued by rat PASK (Leiserson et al., 2000), showing the importance of SPAK and its homologs as signaling molecules in the volume- and osmo-control pathway. The fluid defect is compatible with the kinase's ability to regulate membrane proteins that adjust volume through ion movement. It is not known whether Fray participates in ion/volume regulation in adult cells since embryonic lethality in *Drosophila* precluded such investigations. Just as RNAi knockdown of gck-3 expression in *C. elegans* led to constitutive activation of the chloride channel CLH-3b in nematode oocytes (Denton et al., 2005), the targeted deletion of the SPAK gene in mice could increase activation of KCC3 while deactivating NKCC1. However, one downside in studying rodent SPAK knockout or knockdown models is that partial compensation by the other mammalian Ste-kinase OSR-1 may ameliorate the defects and would likely result in milder phenotypes than that of NKCC1-null mice. A transgenic mouse line that overexpresses KCC3 has not yet been reported.

Phosphorylation/dephosphorylation is the endpoint control step of CCCs already at the plasma membrane, and possibly for trafficking from the ER. However, each CCC must be differentially regulated for their precise tissue distributions, cellular expressions, and functions. Since the promoter of the NCC gene *SLC12a3* contains the consensus sequence for the hepatocyte fork head homolog-3 transcription factor, it likely controls the kidney-specific expression of NCC (MacKenzie et al., 2001). NCC transcription is also under the regulation of hormones and Na/Cl load itself as mineralocorticoids and low salt diets can both decrease NCC mRNA levels in the distal convoluted tubule of the

kidney (Kim et al., 2006; Masilamani et al., 2002). The renal specificity of NKCC2 is also regulated at the gene transcription level as demonstrated by nuclear run-off and luciferase assays of promoter deletion mutants in kidney and fibroblasts cells, and the existence of a promoter binding site for the hepatocyte nuclear factor-1 transcription factor (Igarashi et al., 1996). NKCC2 protein expression is also hormonally controlled, i.e., vasopressin-mediated increase (Ecelbarger et al., 2001). NKCC2 on the apical side of thick ascending loop of Henle (TALH) cells remain active from constant hormone stimulation through Gs-coupled receptors for vasopressin, parathyroid hormone, and the beta-adrenergic receptor agonist isoproterenol (Ecelbarger et al., 2001; Flemmer et al., 2002; Gimenez & Forbush, 2003; Knepper et al., 1999; Mount, 2006). The neuronal-restricted expression of KCC2 is also transcriptionally regulated, and is mediated by the neuron-restrictive silencer factor (Karadsheh & Delpire, 2001), also known as RE1-binding silencer protein, which is only expressed by non-neuronal cells and neuronal precursors (Kraner et al., 1992). By binding to the 21-bp neuronal-restrictive silencing element, or repressor element-1, of the *SLC12a5* gene, it suppresses transcription (Karadsheh & Delpire, 2001) by covalent modification of chromatin through a deacetylase complex (Ballas et al., 2001; Ballas et al., 2005; Roopra et al., 2000). Thus, KCC2 expression can be said to be controlled by epigenetic factors. Extensive promoter bashing has not been carried out for KCC3 gene regulatory sequences, but it may be worthwhile to do so as Meyer et al. have demonstrated linkage between two mutations in the *SLC12a6* promoter and a subset of bipolar disorder (Meyer et al., 2005).

In summary, it appears that CCCs need to be activated by hormones or cell stressors (i.e., volume and ion disturbances), except for the constitutively active KCC2.

Even the "housekeeping" property of NKCC2 in the kidney is driven by constant hormonal input.

Splice forms

Multiple open reading frames/initiation start sites and alternative splicing are two mechanisms that increase protein diversity and function, including for CCCs. Interestingly, there are at least six alternatively spliced forms of NKCC2, three of which are expressed in different regions of the TALH (Payne & Forbush, 1994). NKCC2a, NKCC2b, and NKCC2f differ in TM2, which, as mentioned earlier, determines ion binding affinities (Isenring et al., 1998), and indeed, their chloride affinities differ (Km is 22-45 mM, 9-12 mM, and 110 mM for NKCC2a, NKCC2b, and NKCC2f, respectively) (Gagnon et al., 2003; Gimenez et al., 2002; Plata et al., 2002). The brain splice variant of NKCC1, or NKCC1b, lacks a short segment of the carboxy-terminus containing a PKA consensus sequence (Randall et al., 1997), suggesting differential regulation. There are at least six open reading frames for human KCC1 as well as several splice variants, but the physiological significance of each one is not known (Crable et al., 2005). Transcriptional initiation at two different coding exons (1a and 1b) generates the two major KCC3 isoforms, KCC3a and KCC3b, resulting in two distinct amino-terminal domains with 1,150 and 1,099 residues, respectively. Although KCC3b is considered the kidney isoform, brain and other tissues express both KCC3a and KCC3b. Surprisingly, alternative splicing produces even more forms of KCC3, specifically KCC3a-x2M and KCC3b-x2M (Mercado et al., 2005). The physiological significance of the various KCC3 isoforms is not known, but multiple isoforms suggest different biological roles. Do the

various isoforms account for the different roles it may perform, e.g., chloride accumulation versus volume regulation? Aside from volume regulation in proximal tubules and hippocampal neurons (Boettger et al., 2003), not enough is known about the contribution of KCC3 for ion release in other tissues or cells since other cotransporters and ion channels have much more dominant roles. Unlike for NKCC2, however, none of the KCC3 isoforms vary in activation set point as measured by cotransport activity in different osmolarities (Mercado et al., 2005). NKCC2 is an import pathway, with isoform expression organized along the extracellular ion concentration gradient in the kidney, which varies tremendously. However, the intracellular concentrations of cells do not vary as much as extracellular levels, so wide ranges of activation set points make less sense for an export pathway. But since the KCC3 isoforms all differ in length at their amino-terminals that contain phosphorylation sites (Mercado et al., 2005), the shorter versions are likely differentially regulated compared to the full-length cotransporter, which could affect trafficking, surface expression, and/or degradation, as well as differential activation by various types and/or levels of stressors. With specific antibodies to each isoform, it would be interesting to assess differential upregulation of KCC3a, KCC3a-x2M, and KCC3b in the brain and other tissues under varying levels of oxidative stress (e.g., ischemia) and hypotonic osmotic stress. Clearly, much more work needs to be done to assess the levels of each isoform in various tissues by RT-PCR, for example, and eventually determine the roles of the KCC3 isoforms in native cell types instead of heterologous systems (e.g., *Xenopus* oocytes), which may not contain the necessary cellular machinery, such as signaling molecules, to differentially regulate each isoform.

Pharmacology

CCCs are also categorized by their sensitivity to thiazide and loop diuretics that act as inhibitors: (1) thiazide-sensitive NCC; (2) bumetanide-sensitive NKCCs; and (3) furosemide-sensitive KCCs (Delpire & Mount, 2002). "Loop" diuretics are so named because they reduce the amount of water in the body by acting at the loops of Henle in the kidneys, increasing urine flow. They also mechanically decrease blood pressure by vasodilation. Renal CCCs are targets of therapeutic drugs, including Bumex (bumetanide) for the treatment of congestive heart failure and Lasix (furosemide) for high blood pressure. These drugs are not used for the CNS, although they may be applicable if neonatal seizures, which do not respond to anti-convulsants used to treat adults (Ronen et al., 1999), are indeed proven to be caused by NKCC1 overactivity in neurons as suggested by studies by Dzhala et al. (Dzhala et al., 2005) or by the inhibition of interneurons or reduced extracellular K^+ clearance by astrocytic NKCC1 as proposed by Zhu et al. (personal communication).

Despite their categorical names, the loop diuretics bumetanide and furosemide are not specific to either NKCCs or KCCs as 1mM of furosemide can block both types of cotransporters (Lytle & McManus, 2002). In flux experiments, however, furosemide is often utilized to inhibit KCCs since the specificity issue can be overcome by omitting sodium from the bath solution to prevent NKCC activity. Bumetanide, on the other hand, is a much more potent inhibitor of NKCCs, so low concentrations (2-10 μM) are often used to inhibit NKCCs without blocking KCCs (Ki~0.1 μM for NKCCs versus Ki~25–50 μM for KCCs) (Payne et al., 2003). Furosemide and bumetanide can even inhibit the potent stimulating effect of N-ethylmaleimide (NEM) on KCCs. NEM's targets and

mechanism of action are not known; however, it reacts with sulfhydryl groups through alkylation, preventing cystine cross-linking. Besides NEM, staurosporine and the reduction of intracellular Mg^{2+} activate KCCs. Staurosporine, a broad-spectrum protein kinase inhibitor, most likely interferes with the ability of SPAK/OSR1 to shut down KCCs. Likewise, reduction of Mg^{2+} affects the ability of the kinases to phosphorylate its substrates. Other pharmacologic inhibitors commonly used to characterize wild-type and mutant KCCs in cells include 4,4'-diisothiocyanostilbene disulphonic acid (DIDS) and dihydro-1-oxo-1H-inden-5-yl-oxy acetic acid (DIOA). One useful advantage of DIDS and DIOA is that they do not affect Na-dependent cotransporters (Delpire & Lauf, 1992; Vitoux et al., 1989). All of the above molecules are the limited pharmacological tools available to study cation chloride cotransport, and since there are no specific inhibitors for each individual CCCs, genetic ablation and modifications in mouse and cell models continue to be crucial tools for studying them.

Overview of the major functions of CCCs

CCCs directly control three types of major cellular functions: (1) volume regulation; (2) ion and fluid secretion/absorption; and (3) intracellular Cl^- concentration maintenance. The processes of regulatory increase (RVI) and decrease (RVD), activated by extracellular changes in osmolarity, lead to the rapid movement of ions and water across the plasma membrane for cell swelling or shrinkage. The secretion and reabsorption of ions, and thus fluid, by a variety of epithelial tissues requires CCC activity. In neurons, the intracellular chloride concentration is crucial since GABA-A and glycine receptors are chloride channels; the expression levels and activity of NKCC1 and

KCC2 determine the direction of chloride movement through these neurotransmitter receptors, and thus contribute to modulating the excitability of the nervous system. Outside of their classical roles, other cellular processes such as proliferation, motility, and apoptosis have been linked to CCC activity. The physiological functions of individual CCCs have also been identified through genetic ablation of cotransporter genes in mice (Table 1-1) and studies of corresponding human disorders.

RVI and RVD

Cell volume regulation is one major, well-studied function of CCCs that requires the coordination of KCCs, NKCCs, and volume-sensitive ion channels. Cells utilize CCCs as one mechanism for intracellular osmolarity adjustment when challenged by external changes in osmolarity. When the extracellular osmolarity increases, water molecules move out of the cell to the space where it is less concentrated, which leads to cell shrinkage. To recover volume, shrunken cells activate channels and cotransporters to regain ions, which favor inward water movement. This RVI process is partially mediated by NKCC1. On the other hand, when the extracellular osmolarity decreases, becoming hypotonic relative to the inside of the cell, water influx swells the cell. This swelling activates the RVD response through which the cell attempts to return its volume to normal by triggering ion channels and cotransporters to release ions. CCC activity is affected by cellular responses to stress stimuli, including osmotic stress (Tsutsumi et al., 2002) and as described earlier, are substrates of stress-activated kinases SPAK and OSR-1.

Various osmolyte transport proteins in vertebrate cells respond to acute changes in cell volume. The RVI participants are NKCCs, Na^+/H^+ exchangers, and in some cells, shrink-activated Na^+ channels (Alexander & Grinstein, 2006). Upon cell swelling, the main RVD effectors are KCCs, K^+ and Cl^- channels, and the K^+/H^+ exchanger coupled to the Cl^-/HCO_3^+ exchanger (Wehner et al., 2003). A genome-wide scan of mouse proteins containing the SPAK/OSR1 binding motif revealed potential interactors, including several ion channels (1 K^+ and 3 Na^+ channels), and a slightly less stringent screen also turned up the CLC-2 chloride channel (Delpire & Gagnon, 2007). Of course, the results of this *in silico* screen does not prove that the positive hits are regulated by SPAK, but they do warrant further investigation since Gck-3, the *C. elegans* SPAK homolog, can phosphorylate and modulate a chloride channel (Denton et al., 2005).

Epithelial transport

Epithelial ion transport by NCCs and NKCCs has been especially well studied in the kidney. Coordinated control of ion transport across basolateral and apical membranes is absolutely necessary to prevent huge ion and volume changes during reabsorption and secretion. The only CCC not involved epithelial transport is KCC2 due to its specific neuronal expression. The role of the other KCCs in epithelial transport is not as clear as for NCC and NKCCs. However, since KCC1, KCC3, and KCC4 are all expressed in several types of epithelial tissue (Mount et al., 1999), it is likely that they also mediate transepithelial ion movement. For example, KCC4 cycles K^+ in the inner ear (Boettger et al., 2002).

Intracellular chloride

As described earlier, CCCs are secondary transporters; the high extracellular Na^+ concentration drives Cl^- inward via Na-dependent cotransport while high intracellular K^+ levels drive Cl^- through KCCs, which allows cotransport activity to accumulate or lose Cl^-, respectively. Thus, the final intracellular Cl^- concentration gradient is dependent on the predominant cotransporter. In adult animals, low intracellular Cl^- concentration maintenance is a central function of KCC2 in CNS neurons (Hubner et al., 2001; Payne et al., 1996; Rivera et al., 1999; Woo et al., 2002) and NKCC1 in peripheral neurons (Alvarez-Leefmans et al., 1988; Sung et al., 2000). The precise regulation of intracellular Cl^- concentration is crucial in neurons since the chloride gradient determines the directionality and magnitude of GABAergic and glycinergic responses since $GABA_A$- and glycine-receptors are chloride channels. GABAergic and glycinergic inhibitory inputs are indispensable for balancing excitatory (i.e., glutamatergic) signals to prevent hyperexcitability that could lead to epileptic seizures and neuronal death.

Na-coupled Cotransport

NCC

NCC, also called thiazide sensitive cotransporter, was the first CCC to be molecularly characterized, cloned by Gamba et al. from flounder urinary bladder, which is functionally the fish kidney (Gamba et al., 1993), and later in rat renal cortex (Gamba et al., 1994). NCC is mainly a kidney protein localized to epithelial cells of the distal convoluted tubule (Bachmann et al., 1995; Obermuller et al., 1995) where it mediates apical Na and Cl reabsorption, filtering ~5% of the Na/Cl load (de Jong et al., 2003;

Delpire & Mount, 2002), which is considerable since the distal tubule reabsorbs 10% of the total Na/Cl load (Ellison et al., 1987). Before the advent of molecular biology techniques for cloning and antibody production, NCC localization to the DCT had already been established by labeling with a tritiated thiazide-based tracer [^{3}H] metolazone (Beaumont et al., 1988). Although NCC has always been considered to be kidney-specific, it is also expressed and functional in bone (Nicolet-Barousse et al., 2005).

Gitelman syndrome, a kidney disorder caused by mutations in the NCC gene, is, not surprisingly, characterized by abnormal salt levels: low serum calcium, magnesium, and potassium, and alkalosis (Nicolet-Barousse et al., 2005; Simon et al., 1996). Magnesium and calcium are affected because their absorption in the thick ascending loop of Henle (TALH) is dependent on Na^+ and Cl^- concentrations. Interestingly, an earlier hint of NCC involvement in this disorder was the lack of diuretic response to thiazides (Tsukamoto, 1995). NCC knockout mice exhibit similar symptoms of excessive urinary Ca^{2+} and Mg^{2+}, along with increased levels of renin (angiotensinogenase) and morphological changes in the distal convoluting tubule (Schultheis et al., 1998). These knockout mice have been advantageous for studying morphological changes related to NCC inactivation in the kidney (Schultheis et al., 1998), and in a more recent study, morphometric analysis of bone (Nicolet-Barousse et al., 2005).

NKCC2

The other renal-specific cotransporter, NKCC2, was first cloned from the outer medulla of the rat kidney (Gamba et al., 1994) and rabbit renal cDNA libraries (Payne & Forbush, 1994). It resides in the apical membranes of the cortical and medullary TALH

where it reabsorbs ions and concentrates urine (Gamba et al., 1994; Igarashi et al., 1995; Kaplan et al., 1996; Yang et al., 1996). TALH cells reabsorb chloride ions through NKCC2, which remains phosphorylated from constant hormonal activation. The chloride ions taken up by NKCC2 are then transported out of the cells into the renal interstitial space on the basolateral side by CLC-K/barttin chloride channels (Jentsch et al., 2005).

The correlation between the cotransporter and the salt-wasting disease Bartter syndrome was made after the cloning of NKCC2. Bartter syndrome is a heterogeneous systemic disorder of electrolyte wasting featuring low blood pressure from renal loss of NaCl (Karolyi et al., 1998). The physiological significance of the TALH is highlighted by the fact that mutations in the potassium channel Kir1.1a (ROMK) and the chloride channel CLC-NKB, which, along with NKCC2, are all expressed at the basolateral membrane of the TALH, cause Bartter syndrome (Karolyi et al., 1998; Landau, 2006). Renal tubular acidosis, however, is specific to NKCC2 mutations, and stems from the disruption of ammonium absorption from the tubular lumen (Good, 1994).

As a model of one form of Bartter syndrome, Takahashi et al. developed a NKCC2 knockout mouse (Takahashi et al., 2000). NKCC2-null pups showed signs of extracellular volume depletion at P1 as determined by hematocrit measurements (i.e., red blood cell volume), and by P7 were smaller than wild-type littermates and dehydrated with renal insufficiency (high plasma potassium and renin, metabolic acidosis). Only indomethacin, a nonselective cyclooxygenase inhibitor that increases K^+ and Na^+ plasma levels, likely by enhancing the effects of vasopressin, allowed NKCC2-null pups to survive beyond weaning (Takahashi et al., 2000). Recently, isoform-specific NKCC2a- and NKCC2b-knockouts were characterized and their kidney phenotypes provide

evidence that the two isoforms possess different Cl^- sensing abilities (Oppermann et al., 2006; Oppermann et al., 2007).

NKCC1

NKCC1, often referred to as the bumetanide sensitive cotransporter-2, was first cloned from shark rectal gland (Xu et al., 1994) and mouse IMCD3 kidney cells (Delpire et al., 1994). NKCC1 is expressed at the basolateral membranes for the promotion of salt and water release from various secretory epithelia, including lacrimal sweat, and salivary glands, and inner ear *stria vascularis* (Crouch et al., 1997; Evans et al., 2000; Hoffmann et al., 2006; Nejsum et al., 2005; Walcott et al., 2005) as well as in the kidney, muscle, and brain (Delpire & Mount, 2002). Tissue-specific splice variants, such as a shorter version in skeletal muscles exist (Payne et al., 1995), but the functional significance is not known. In the brain, epithelial secretory cells of the choroid plexus, neurons, and oligodendrocytes express NKCC1 (Plotkin et al., 1997).

In epithelial cells, NKCC1 maintains an uptake pathway for salt reabsorption (Hoffmann et al., 2006) while in neurons, it regulates intracellular chloride concentrations (Sung et al., 2000; Yamada et al., 2004). NKCC1 on the basolateral side of epithelia is a passage for collecting chloride ions that will be secreted at the apical side by other transport proteins, such as the well-known cystic fibrosis transmbrane regulator (Bachmann et al., 2003; Evans et al., 2000; Hoffmann et al., 2006). NKCC1's chloride accumulating ability is of particular importance in neurons as intracellular chloride concentration is intimately tied to GABAergic/glycinergic signaling. Peripheral neurons maintain high intracellular chloride concentrations through NKCC1-mediated

accumulation of chloride ions far above its electrochemical equilibrium potential (Alvarez-Leefmans et al., 1988; Sung et al., 2000), which results in GABA depolarizing responses at terminals that contributes to presynaptic inhibition, a likely mechanism for filtration of sensory noise (Laird et al., 2004; Sung et al., 2000; Willis, 1999). In the young brain—embryonic to early postnatal—high levels of NKCC1 also keep intraneuronal chloride concentrations at elevated levels, which leads to depolarizing GABAergic and glycinergic responses (Ben-Ari et al., 1989; Dzhala et al., 2005; Yamada et al., 2004). Thus in sensory neurons and immature CNS neurons, NKCC1 provides one major mechanism for controlling neuronal excitability. With age, NKCC1 levels diminish while the expression of the chloride-extruding KCC2 concomitantly increases and becomes the predominant neuronal cotransporter, positioning the chloride electrochemical gradient at the level for inhibitory GABAergic/glycinergic responses.

Most of the functional roles of NKCC1 have been determined by characterizing NKCC1 knockout mice (Delpire et al., 1999; Evans et al., 2000; Flagella et al., 1999; Grubb et al., 2000; Laird et al., 2004; Meyer et al., 2002; Pace et al., 2000; Sung et al., 2000). The most dramatic phenotype of NKCC1-null mice was their *shaker/waltzer* head-bobbing and circling behavior. Inner-ear dysfunction from the collapse of the endolymphatic cavity and Reissner's membrane, indicative of impaired secretion in the cochlea, led to imbalance and deafness (Delpire et al., 1999). Poor rotorod performance was attributed to spasticity (Delpire et al., 1999), but possibly could also stem from imbalance and limb weakness. Indeed, $NKCC1^{-/-}$ mice exhibited limb weakness ~P10, but subsequent *shaker/waltzer* movements made locomotor tests unfeasible. The knockouts' sensory phenotype—decreased perception to noxious stimuli—is likely linked

to diminished sensory input from the collapse of the chloride gradient in DRG neurons, which may lead to decreased depolarizing responses to sensory input (Laird et al., 2004; Sung et al., 2000). Other abnormalities include changes in intestinal ion transport and morphology, reduced saliva secretion, male sterility from deficient spermatocyte production, intestinal obstructions, and hypotension (Evans et al., 2000; Flagella et al., 1999; Grubb et al., 2000; Meyer et al., 2002; Pace et al., 2000; Wall et al., 2006; Wouters et al., 2006). Defects in such numerous tissues highlight its broad expression. No human disorder has been linked to mutations in the NKCC1 gene, but it is possible that there is a genetic link to infantile epilepsy, sensory deficits, deafness, and/or male sterility waiting to be uncovered in the future.

Na-independent cotransport

KCC1

Due to its wide expression (brain, colon, heart, kidney, liver, lung, spleen, stomach, pancreas, and muscle) and activation by hypotonic challenge, KCC1 is considered a housekeeping protein for cell volume regulation (Gillen et al., 1996; Mercado et al., 2000; Rust et al., 2007; Su et al., 1999). Unexpectedly, inactivation of the KCC1 gene in mice was not lethal; in fact, they did not display any obvious phenotype (Rust et al., 2007). Although previous KCC physiology studies in red blood cells (RBCs) attributed most activity to KCC1 (with some KCC3 and KCC4 involvement) and linked it to the dehydration of sickled erythrocytes and human sickle cell disease (Crable et al., 2005; Lauf et al., 1992), there were, surprisingly, no changes in RBC volume regulation in KCC1-null mice (Rust et al., 2007). Human and murine RBCs, however, may possess

different regulatory mechanisms, so KCC1 may still be relevant to human hemoglobinopathies. The normal life span of KCC1-null mice seems to demonstrate that KCC1 is not necessary for survival despite its ubiquitous expression, although upon immense challenge deficits may arise. Another explanation for their unexpected survival is that other KCCs may be compensating for the lack of KCC1. Theoretically, this is possible since KCC3 and KCC4 also exhibit similar widespread, overlapping expression patterns. And, for example, only RBCs from mice lacking both KCC1 and KCC3 showed significantly increased mean corpuscular volume and impaired volume regulation, while the RBCs of the single knockouts were unaffected. This hypothesis of cotransporter compensation could be tested by assessing KCC3 and KCC4 upregulation in different tissues from KCC1-null mice compared to wild-type by Western blotting or quantitative RT-PCR.

KCC2

The KCC2 gene was found in an EST database search and later cloned from a mouse cDNA library (Payne et al., 1996). Its ion cotransport capacity and loop diuretic sensitivity was demonstrated through flux experiments with furosemide and bumetanide (Payne et al., 1996). One unique feature of KCC2 is its strict neuronal expression. *In situ* hybridization and immunohistochemistry results by numerous groups demonstrated KCC2's CNS-confined expression. It is important to note, however, that not all neurons express KCC2 (Kanaka et al., 2001; Williams et al., 1999). Another unique feature of KCC2 is its constitutive activity in isotonic conditions, which is conferred by 15 residues in a unique span of 73 amino acids in its carboxy tail that is not present in the other KCCs

(Mercado et al., 2006). This isotonic transport activity can be transferred to other KCCs; for example, a chimera experiment swapping the unique region of KCC2 into KCC4 conferred the isotonic property (Mercado et al., 2006). The exact mechanism behind how this string of residues leads to constitutive, isotonic activity is not known since it does not encode for any known motifs for signaling or protein-protein interactions, nor does it share homology with other proteins; also, mutations of putative phosphorylation sites within the region had no affect on constitutive, isotonic activity (Mercado et al., 2006). Whether the secondary structure is important for blocking phosphorylation that inactivates KCCs has yet to be tested.

The temporal increase of KCC2 from low expression at birth with a steady rise during early postnatal development (Dzhala et al., 2005; Lu et al., 1999; Rivera et al., 1999) correlates with the switch of GABAergic and glycinergic responses from excitatory to inhibitory (Delpire, 2000; Fiumelli et al., 2005; Ganguly et al., 2001; Stein et al., 2004). KCC2 knockout mice die at birth due to motor neuron defects that affect the respiratory system (Hubner et al., 2001). The hypomorph model, with ~5% KCC2 expression, survived for ~2 weeks, but these mice suffered from generalized seizures (Woo et al., 2002). Clearly, the loss of KCC2 leads to CNS hyperexcitability. KCC2 plays a key role in regulating excitation in the CNS by controlling neuronal chloride concentrations (Zhu et al., 2005), which is critical because, as mentioned earlier, the intracellular chloride concentration determines whether GABA and glycine are excitatory or inhibitory. KCC2 is also involved in pain transduction (Coull et al., 2003; Mantyh & Hunt, 2004; Morales-Aza et al., 2004; Nomura et al., 2006). For example, Coull et al. demonstrated that the mechanism of disinhibition (loss of inhibition) in spinal dorsal horn

neurons after peripheral nerve injury was through the reduction of KCC2 levels that disrupted anion homeostasis (Coull et al., 2003). This establishes that neurons of the spinal cord also need to regulate intracellular chloride for normal inhibitory function, similar to the brain. Hyperexcitability of spinal neurons appears to manifest as abnormally increased pain threshold. No human disorders have been linked to mutations in the KCC2 gene, but if discovered, they will likely be connected to epilepsy.

KCC4

KCC4 was first identified by Mount et al. through an EST database search (Mount et al., 1999). It is abundant in the kidney and heart, but at low levels in the CNS. In the brain, KCC4 is mostly localized to cranial nuclei and nerves, and the apical membrane of the choroid plexus. Its developmentally regulated expression begins with early abundance in the proliferative zone around embryonic day E14.5 and by P0 its expression tapers to the choroids plexus and ventricles (Li et al., 2002).

No human disorder has yet been associated with KCC4, but the targeted deletion of the KCC4 gene resulted in early-onset deafness and renal tubular acidosis. Hearing deteriorated early at P14, and after only one week, the mice became completely deaf (Boettger et al., 2002; Boettger et al., 2003). This phenotype is attributed to the disruption of K^+ cycling in the inner ear, which supports a model in which KCC4 regulates K^+ cycling by absorbing K^+ into supporting Deiters cells from the fluid surrounding the outer hair cells, which allows the ions to enter gap junctions (Boettger et al., 2002). This is one rare example where a KCC functions as an inward pathway. The renal tubular acidosis implicates KCC4 in Cl^- extrusion across the basolateral membrane of alpha-intercalated

cells in the kidney (Boettger et al., 2002). Although the sciatic nerve expresses KCC4 (Karadsheh et al., 2004), KCC4-null mice did not exhibit any neuromuscular phenotypes and performed as well as wild-type on the rotorod (Boettger et al., 2002). This suggests that other potassium and chloride pathway(s) may be compensating for the loss of KCC4.

KCC3

The focus of the remaining chapter will be on KCC3, the topic of this dissertation. Although expressed by many tissues outside of the nervous system—including kidney, heart, lung, pancreas, muscle—inactivating mutations of KCC3 in both mice and humans predominantly affect the central and peripheral nervous systems, leading to peripheral neuropathy and other syndromic features of the severe neurological disorder 'peripheral neuropathy associated with agenesis of the corpus callosum' (ACCPN). The disorder will be detailed in the next chapter while part of the characterization of the knockout mice, which is a section of this thesis, will be detailed in Chapter 3. Here I outline several key properties of KCC3.

KCC3 was discovered independently by three separate research groups. Hiki et al. were the first to publish the cloning and characterization of the then novel cotransporter. Upon finding that one band consistently upregulated by vascular endothelial growth factor was 77% homologous to KCC1, they cloned this putative KCC and completed flux studies, demonstrating that the protein could move K^+ and Cl^- in a Na^+-independent fashion. Based on sequence, structure, and function, they were able to prove that this new molecule was indeed a KCC, and named it KCC3 (Hiki et al., 1999). Two other groups published their findings in the same year: one group used an *in silico* method of human

EST cDNA sequence analysis to clone human KCC3 while the other employed a homology cloning strategy and screened a human placenta cDNA library by PCR to isolate KCC3 clones (Mount et al., 1999; Race et al., 1999). Functional tests in heterologous systems included dose response experiments to bumetanide, furosemide, and DIOA as well as the KCC stimulating agents NEM, staurosporine, and hypotonicity (Hiki et al., 1999; Mount et al., 1999; Race et al., 1999).

An extra ~60 amino acid stretch at the amino-terminal of KCC3 makes it the longest KCC. Kyte-Doolittle hydropathy analysis of the primary sequence of KCC3 resulted in a virtually identical pattern to KCC1 of 12 membrane-spanning regions with a large extracellular loop between TM5 and TM6 and cytoplasmic amino- and carboxy-termini. There are five N-glycosylation consensus sites in the large extracellular domain.

Much of the functional analysis of KCCs has been carried out in heterologous systems such as *Xenopus* oocytes or HEK cells by measuring uptake of $^{86}Rb^{+}$ in isotonic and hypotonic conditions. For activating conditions, cells are incubated in a hypotonic potassium- and chloride-free medium with ouabain (1 mM) to block the Na-K ATPase. This is followed by an uptake period in hypotonic sodium-free solution containing KCl and $^{86}Rb^{+}$ tracer (Rb^{+} is a congener of K^{+}). The absence of extracellular sodium prevents the exchange of $^{86}Rb^{+}$ and K^{+} by any endogenous NKCCs, and the hypotonicity prevents NKCC activation as well. The amount of tracer is determined by scintillation counting. Mercado et al. determined the ion transport kinetics of KCC3 in *Xenopus* oocytes by varying concentrations of K^{+} and Cl^{-} (Mercado et al., 2005)

Northern analysis showed a broad tissue distribution of human KCC3—kidney, brain, skeletal muscle, heart, placenta, lung, liver, and pancreas—with the most transcript

in heart, brain, and kidney. Based on its broad tissue distribution, KCC3 has been proposed to possess other functions besides volume regulation, such as salt/fluid transport in epithelial tissues, and in the heart, skeletal muscle, and brain, buffering of potassium and chloride in cells and in the interstitial space as its potential bidirectionality could allow it to serve in this capacity (Race et al., 1999). KCC3 has been implicated in cell proliferation in human cancer cells as well, and has been shown to be expressed by glioblastomas (Gagnon et al., 2007; Shen et al., 2000; Shen et al., 2001).

After the development of a polyclonal anti-KCC3 antibody, Western blot analysis was performed on rodent tissues. Mouse kidney and brain were both positive for KCC3, but the proteins were of different sizes. Northern blots confirmed the existence of two forms, KCC3a and KCC3b, where the larger KCC3a is the predominant brain isoform and KCC3b is more abundant in the kidney. Following the expression levels of KCC3 in rat brain at different ages by Western blot analysis, Pearson et al. showed that its expression increases postnatally during development (Pearson et al., 2001), much like KCC2. The highest levels of KCC3 expression were in spinal cord, while it was very low in the DRG, and could not be detected by immunoblot in adult peripheral nerves. In agreement, Boettger et al. also showed that adult sciatic nerves do not express KCC3 (Boettger et al., 2003).

Although immunostaining experiments with anti-KCC3 antibody developed by Pearson et al. yielded a strong signal in myelinated tracts of the spinal cord (Pearson et al., 2001), Boettger et al.'s antibody was only reactive in grey matter (Boettger et al., 2003). Positive immunohistochemical results of hippocampal neuron and cerebellar Purkinje KCC3 expression, however, were in agreement (Boettger et al., 2003; Pearson et

al., 2001). The anti-KCC3 antibody also strongly labeled the base of the choroid plexus epithelium (Pearson et al., 2001). Probes designed for RNA *in situ* hybridization of whole mice at P0 detected KCC3 mRNA in the brain, spinal cord, and DRG as well as other tissues such as nasal epithelium, trachea, esophagus, stomach, gut, lung, kidney, and heart and these results matched their LacZ staining experiments in KCC3-null embryos (E14) and pups (P0) (Boettger et al., 2003).

Hiki et al. used fluorescence *in situ* hybridization to localize the human KCC3 gene to chromosome 15q13 (Hiki et al., 1999). Mount et al. narrowed down the location to chromosome 15q14 between two markers that flanked regions linked to two subtypes of generalized epilepsy, schizophrenia, and ACCPN (Mount et al., 1999). KCC3 was not linked to rolandic epilepsy in the families screened (Steinlein et al., 2001). However, through single-strand conformation polymorphism analysis, Howard et al. showed that mutations in the cotransporter cause the severe neurological disorder ACCPN (Howard et al., 2002b).

KCC3 knockout mice were generated by our laboratory (described in Chapter 3) as well as by Boettger et al. (Boettger et al., 2003). Both sets of KCC3 knockout mice phenocopied the locomotor symptoms of ACCPN well and also displayed CNS abnormalities. Boettger et al.'s finding that volume regulation in renal tubules and hippocampal neurons was KCC3-dependent was not surprising as this is a classical function of KCCs. The slow recovery of volume to original size after hypotonic stress has revealed one important cellular function of this cotransporter (Boettger et al., 2003), but it may play other roles as well. Although KCC3 is expressed in the kidney, it is not known whether it participates in epithelial transport. Besides the clinical features and the gene

involved in ACCPN, very little is known about the pathogenesis of the disorder. Because the genetic cause of ACCPN was only recently uncovered (Howard et al., 2002b), autopsies of ACCPN patients have been rare and the patients who were examined were of varying ages and with few sural nerve biopsies, so neither the peripheral neuropathy or central features of ACCPN were analyzed over age (Dupre et al., 2003). Therefore, these KCC3 knockout mice, after characterization to validate that they are indeed a good model of ACCPN, are valuable for the continued study of KCC3 and to start investigating the pathogenesis of the disorder at the tissue and cellular levels.

There are many questions open for study regarding KCC3, including its regulation in different cell types; promoter characterization; significance of its multiple isoforms; and physiological roles in various tissues and cell types. Boettger et al. showed that KCC3 is clearly involved in RVD in kidney and hippocampal neurons (Boettger et al., 2003), and although this important role in cell volume regulation likely applies to other cell types, this hypothesis remains to be tested. Of particular importance is elucidating the function of KCC3 in the nervous system and uncovering the pathophysiology in the disease state of ACCPN. One perplexing question that has not been answered is how the loss of KCC3 function leads to peripheral neuropathy. Thus, after characterizing the KCC3 knockout mouse, the main focus of this thesis work was on the peripheral neuropathy component of the disorder using the KCC3 knockout as an animal model of the disorder. Especially considering the lack of patient data, the availability of KCC3 knockout mice to study the peripheral neuropathy of ACCPN is advantageous. Since this study requires an understanding of peripheral nerve development, maintenance, and related disorders, they will be discussed in the following chapter.

CHAPTER II

PERIPHERAL NERVES AND NEUROPATHIES

Introduction

The peripheral nervous system is made up of the somatic nervous system and the autonomic nervous system. The somatic nervous system consists of nerve fibers that relay motor information from the spinal cord to skeletal muscles and sensory signals from the periphery through the dorsal root ganglion (DRG) to the CNS. The sympathetic nervous system, parasympathetic nervous system, and enteric nervous system compose the autonomic nervous system, which controls visceral muscles and glands.

Intact peripheral nerves are critical for the transmission of signals needed for proper movement, balance, sensation, and reflexes as well as normal autonomic function. Although most neuronal signals are initiated by chemicals (i.e., neurotransmitters), the propagation of information is carried by electrical currents through depolarizations along axons via voltage-gated ion channels. Proper nervous system function requires the balance between different signaling modalities (e.g., excitatory and inhibitory) and the ability of the nerves to propagate current with minimal loss in amplitude while maintaining fast conduction.

The efferent axons sending signals from the spinal cord to peripheral muscles are motor fibers while the afferent axons that convey information to the DRG are sensory fibers. All motor axons and large sensory A-alpha and A-beta fibers that convey low threshold non-noxious sensory information (i.e., proprioception) are myelinated while

unmyelinated fibers, which are strictly sensory C-fibers, are grouped in structures called Remak bundles by non-myelinating Schwann cells. The cell bodies of the motor axons reside in the gray matter of spinal cord while the somata of sensory axons lie in the DRG, which, as bipolar (pseudounipolar) cells, project into the spinal cord. Peripheral nerves are covered externally covered by connective tissue called the epineurium. Under the epineurium lies another layer, the perineurium. Peripheral nerves are split into separate bundles called fascicles by the endoneurial sheath (Parmantier et al., 1999).

Axon growth

Neural function depends on the proper numbers, structural integrity, and connections of neurons and their axons. Neurotrophins are critical for the survival of neurons and the morphological development of axons, such as extension and branching (Lentz et al., 1999; Patel et al., 2000; Tucker et al., 2001; Wright et al., 1997). The seminal work in the field of peripheral nerve growth and targeting made by Dr. Rita Levi-Montalcini with her discovery and isolation of nerve growth factor (NGF) led to her discovery of its positive function on axon growth. Neurite growth cone extension toward a target, steered by local guidance cues, occurs during embryogenesis (Tessier-Lavigne & Goodman, 1996). Briefly, axon growth includes elongation toward its target, sprouting and pruning of branches, and formation and disconnection of synapses. Extension is headed by the growth cone at the tip of the neurite, which deduces signals from secreted or interaction-dependent cues, in the local environment. Chemo-repellents and chemo-attractants, including semaphorins, netrins, Eph/Ephrins, Robo/Slit (Chilton, 2006; Ma & Tessier-Lavigne, 2007) regulate growth cone extension and collapse through small

GTPase-mediated cytoskeletal changes via Rac and Rho/Cdc42 (Luo, 2000; Meyer & Feldman, 2002) as well as Ca^{2+} transients (Chilton, 2006; Gomez et al., 2001; Gomez & Spitzer, 1999). Dynamic changes of microtubules and actin filaments allow for growth cone motility; actin filaments underlie the structure of lamellipodia and filopodia at the edges of the growth cone while the central region contains a high density of microtubules (Kalil & Dent, 2005). When the axon reaches its target region, the elongation phase is replaced by a terminal branching, or arborization, phase (Ma & Tessier-Lavigne, 2007). Spinal motor and sensory axons that fail to reach their targets are pruned by a an axon retraction and/or degeneration mechanism accompanied by axosome shedding that is cleared by Schwann cells (Koirala & Ko, 2004). This clearance is likely mediated by the vertebrate homolog of *Drosophila* Draper (Hoopfer et al., 2006; MacDonald et al., 2006). Since projection pathways to targets are established before development ends, axons need to elongate to match the growth of the fiber tract (Pfister et al., 2004).

Myelin and Schwann cells

Myelin is a specialized vertebrate adaptation for increasing nerve conduction velocity. It is produced by glial cells—Schwann cells in the PNS and oligodendrocytes in the CNS—as spiraling multilamellar sheaths of specialized membrane that concentrically wrap axons at precise intervals (Arroyo & Scherer, 2000; Poliak & Peles, 2003; Scherer & Arroyo, 2002). The interruptions in myelin at either ends of the sheath are gaps of bare axon, called nodes of Ranvier, which segregate voltage-gated sodium (Nav) channels. The nodal Nav channel clusters allow depolarizing signals to propagate toward its

synaptic target in a saltatory fashion, “leaping” from node to node instead of spreading current passively (Hartline & Colman, 2007).

The evolution of myelin has allowed for increasing neural complexity, so it has become absolutely critical for vertebrate function. Due to its insulating properties and the formation of nodes where Nav channels are clustered, myelin dramatically conserves space and energy: for an unmyelinated fiber, the increase in axon caliber that would be necessary to deliver impulses as quickly as a myelinated one would require the axon diameter to be 40 times greater, since conduction velocities increase with increasing calibers, consuming 5000 times more energy to propagate an electrical signal at an equivalent speed (Garbay et al., 2000). For a naked axon, the depolarizing current is passively spread through the axon because ion channels are not grouped, but rather, are distributed along the length of the fiber. Myelin wrappings around the axon electrically insulate the axonal membrane. Myelin increases the resistance of the fiber, which along with the formation of nodes of Ranvier promotes the rapid, saltatory conduction of action potentials, allowing for depolarization at widely-spaced intervals and maximal conduction velocities of up to 100 m/s (Garbay et al., 2000; Suter & Scherer, 2003).

The function of myelin in the PNS and CNS are essentially identical, but although structurally similar, many of their properties differ. First, the cell types producing myelin are different: Schwann cells in the PNS and oligodendrocytes in the CNS. Each Schwann cell myelinates only one axon while one oligodendrocyte ensheathes several axons. There are many more dramatic differences, including lipid and protein compositions. This chapter will center on Schwann cells and peripheral axons to focus on the main dissertation topic of the peripheral neuropathy of ACCPN.

Schwann cells, like DRG neurons, begin as multipotent neural crest cells that arise from the neuroepithelium of the neural tube (Figure 2-1). The transcription factor sex determining region Y box 10 (SOX10) triggers glial specification (Jessen & Mirsky, 2002) as gliogenesis is halted in *Sox10*-null mice, which lack satellite Schwann cells and Schwann cell precursors in spite of normal neurogenesis (Britsch et al., 2001). The major signaling pathways controlling gliogenesis from migrating neural crest cells involve neuregulin 1 (Nrg1) and Notch (Jessen & Mirsky, 2005). In mouse, Schwann cell precursors populate the embryonic nerves at E12-13 (rat E14-15) (Jessen & Mirsky, 2005). Both highly mitotic and migratory, these precursor cells associate with the extending PNS axons, which they depend on for survival (Winseck et al., 2002). For example, Schwann cell precursors depend on axon-secreted Nrg1 for survival, which has been demonstrated by the severely diminished amount of precursor cells in mice lacking the type III isoform of Nrg1 (Wolpowitz et al., 2000). Both neural crest cells and Schwann cell precursors express the low-affinity neurotrophin receptor P75 (P75 NTR), which is also required for proper myelination (Cosgaya et al., 2002). Schwann cell precursors and immature Schwann cells can be differentiated from neural crest cells by the cell adhesion molecule L1, intermediate filament nestin, growth associated protein-43, desert hedgehog, myelin protein zero (P0), peripheral myelin protein 22 (PMP22), and ErbB3 (Jessen & Mirsky, 2005).

At E13-15 (rat E15-17), an age correlating with nerve vascularization and perineurium development, Schwann cell precursors differentiate into immature Schwann cells and remain at that stage until birth (Jessen & Mirsky, 2005). Immature Schwann cells are clearly different from their paracrine signal-dependent precursors as they rely on

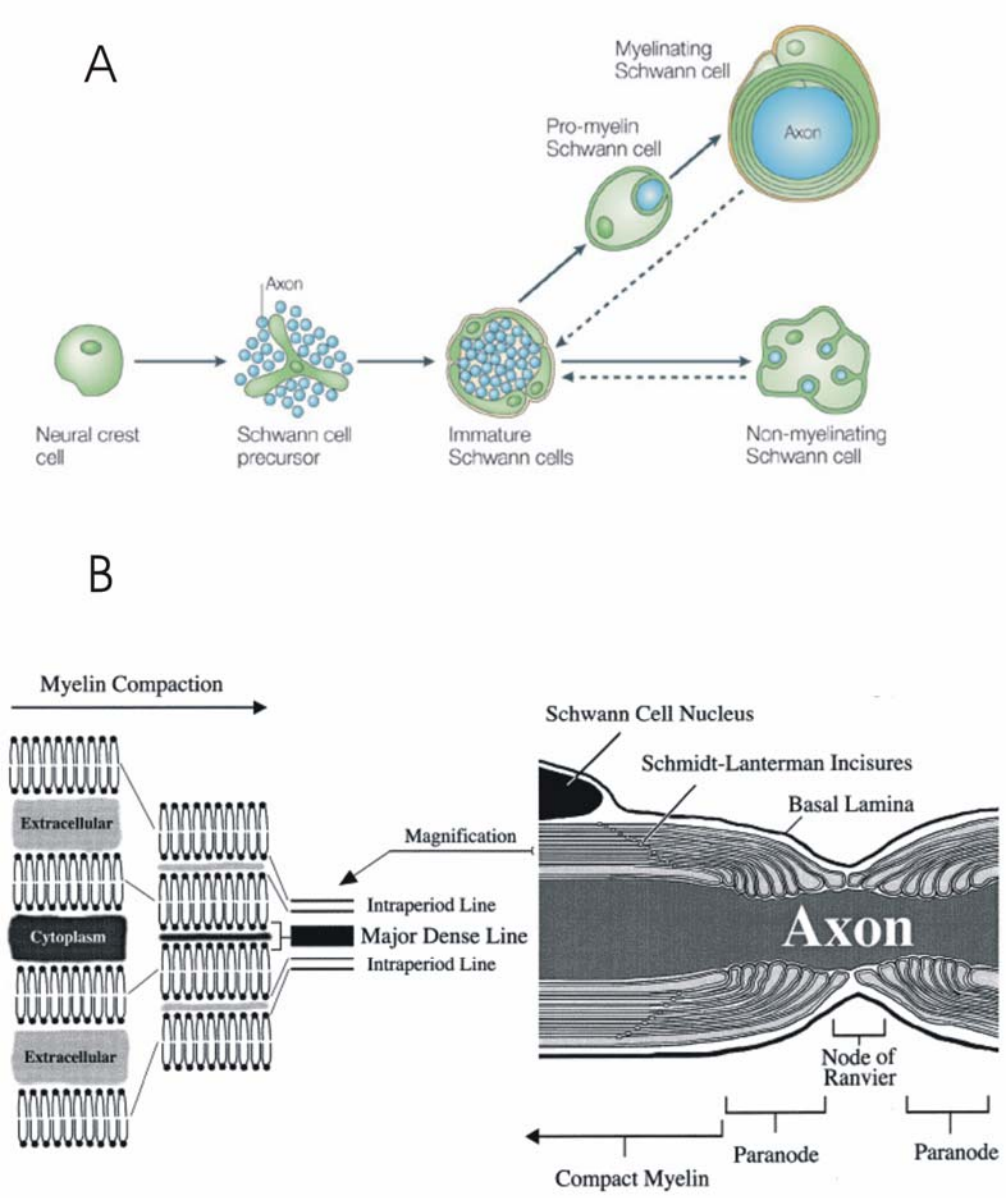

Fig. 2-1. Schwann development and myelin compaction

(A) Two types of Schwann cells develop from a common neural crest background. The transcription factors Oct-6, Krox20/Egr2, and Brn2 instruct an immature Schwan cell to a myelinating phenotype. Nonmyelinating Schwann cells group axons in Remak bundles. (B) The formation of compact myelin requires the extrusion of cytoplasm out of Schwann cell plasma membrane layers, which form the characteristic intraperiod and major dense lines that can be observed under electron microscopy. Nav chanels cluster at the node of Ranvier while paranodal loops anchored to the axon separate them from Kv channels at the juxtaparanode. Figure from (Garbay et al., 2000).

autocrine survival loops, utilizing insulin-like growth factor 2, neurotrophin 3, leukemia inhibitory factor, platelet-derived growth factor beta, and lysophosphatidic acid (Jessen & Mirsky, 2002; Jessen & Mirsky, 2005). Immature Schwann cells are characterized by their bipolar morphology and expression of cytoplasmic S100 calcium binding protein, glial fibrillary acidic protein, O4, and octamer binding transcription factor 6 (Oct-6) (Blanchard et al., 1996; Jessen & Mirsky, 2005). After E15 (rat E17), immature Schwann cells ensheath groups of axons. Myelination, however, requires the 1:1 segregation of the axon in a process called radial sorting by promyelinating Schwann cells (Jessen & Mirsky, 2005). Schwann cells that do not establish axon contacts undergo apoptosis. Activation of the nuclear factor kappa B pathway is essential for peripheral myelin formation as are other transcription factors, including Oct6, Krox20/EGR2, brain 2 class III POU domain protein, and protooncogene SKI (Atanasoski et al., 2004; Decker et al., 2006; Ghislain & Charnay, 2006; Nickols et al., 2003).

Mature Schwann cells either become myelinating or nonmyelinating depending on the size of the axon with which they associate. Schwann cells associating with larger diameter axons (>1 um) adopt a myelinating phenotype (Garbay et al., 2000). After axon segregation, Schwann cells form their initial wraps of membrane around the axon. The trailing edge, or inner lip, which is the Schwann cell membrane facing the axon, expresses adhesion molecules myelin associated glycoprotein (MAG), NCAM, and neurofascin to promote binding to the axolemma (Garbay et al., 2000; Martini et al., 1988; Martini & Schachner, 1986). Compact myelin is formed by extrusion of cytoplasm, which is paramount for establishing a non-conducting medium for insulation, and the fusion of plasma membrane layers, or lamellae, which is likely mediated by structural

proteins. Compaction of the membrane layers is facilitated by P0, an adhesion protein that forms tetramers in *cis*, which interact in *trans* to bring the opposing membranes together as structural components of compact myelin (D'Urso et al., 1990). In fact, the crystal structure of P0 supports this role (Shapiro et al., 1996). Some cytoplasm, however, does remain in non-compacted regions: Schmidt-Lanterman incisures (SLIs) and paranodes at the edges of each myelin segment (Garbay et al., 2000). SLIs, through gap junctions formed by connexin 32 (Cx32) proteins, connect the inner- and outer-most myelin layers by forming a radial diffusion pathway for the transport of ions, secondary messengers, and other small molecules, a much more efficient route than circular movement (Scherer et al., 1998). Nonmyelinating Schwann cells, on the other hand, encase a group of axons, surrounding them with their membrane extensions, and form structures called Remak bundles.

Myelinated nerve fiber domains

The morphologic and molecular domains of myelin and associated axons are defined by their location and protein constituents. The internode refers to the myelinated region. The length of the internode, and therefore nodal spacing, is proportional to the diameter of the underlying axon; nodal distance is ~100 times the diameter of the axon (Friede & Bischhausen, 1980; Friede et al., 1981). As described earlier, Nav channels cluster at the nodes of Ranvier. During myelin formation and development, however, neurofascin 155 and NCAM are first localized to the presumptive node (Davis et al., 1996). The cytoskeletal protein ankyrin G recruits and anchors sodium channels to the nodes, first binding to Nav 1.2, then later to Nav 1.6 in adult (Boiko et al., 2001). Adult

myelinated peripheral nerves are highly enriched with Nav channels (>11000 channels per μm^2) at the nodes compared to internodes (<25 channels per μm^2) or unymeylinated axons (~110 channels per μm^2) (Garbay et al., 2000; Shrager, 1989). Schwann cell microvilli, projections emanating from the outer edge of the Schwann cell, are directly coupled to the nodal axolemma (Ichimura & Ellisman, 1991). The late development of both myelin and nodes in the claw paw mouse (mutations in *Lgi4*) compared to wild-type, supports the hypothesis that nodal development is Schwann cell-dependent (Bermingham et al., 2006; Koszowski et al., 1998).

Myelinating Schwann cells synthesize adhesion molecules, integrins, and dystroglycan to form basal lamina (Court et al., 2006), which connect them to the extracellular matrix (ECM) (Previtali et al., 2001). Through Schwann cell-specific deletion, Feltri et al. demonstrated that Schwann cells lacking beta-1 integrin could not segregate axons, which left the nerve with a fetal-like morphology, highlighting the importance of basal lamina-Schwann cell interaction for proper myelination (Feltri et al., 2002). Since the Schwann cell is a polarized entity with one surface facing the ECM, referred to as abaxonal, and the other surface facing the axon, which is adaxonal, or apical, it has been likened to traditional epithelia (Salzer, 2003).

The paranode is a distinct region defined by its molecular constituents. Noncompact myelin at both edges of the myelin sheath form the paranodal loop structures (Salzer, 2003). Axon-glial contacts mediated by contactin with Schwann cell neurofascin 155 close off the myelin and form a physical barrier that limits the diffusion of ions and small molecules (Boyle et al., 2001). Caspr1/paranodin is also essential for the formation of the paranodal junction (Bhat, 2003; Bhat et al., 2001). The paranode

physically and electrically isolates the Nav channels at the node from the voltage-gated potassium channels Kv1.1 and Kv1.2 that cluster at the juxtaparanode, which is adjacent to the paranode (Arroyo & Scherer, 2000). Loss of adhesion at the paranode alters normal ion channel distribution; for example, contactin- and Caspr1-null mice with disrupted paranodal regions exhibited diffusion of the Nav clusters, which appeared as dispersed nodes of Ranvier in immunostaining experiments and abnormal diffusion of Kv1.1 and Kv1.2 into paranodes (Bhat et al., 2001; Boyle et al., 2001).

The proper development, function, maintenance, and post-injury regeneration of axons and Schwann cells require their reciprocal interaction from physical contacts as well as trophic support. Axons are the source of trophic support for Schwann cells (Jessen & Mirsky, 2005), beginning with axonal Nrg1, a survival signal for Schwann cell precursors and biochemical signal for myelin thickness through ErbB receptors (Michailov et al., 2004; Wolpowitz et al., 2000). The presence of axons is required for maintaining the myelinating phenotype of Schwann cells (Garbay et al., 2000). Likewise, Schwann cells provide trophic support for DRG neurons and peripheral nerve axons (Jessen & Mirsky, 2005).

Inherited Peripheral Neuropathies

Peripheral neuropathy is a term that broadly describes damage or injury to the peripheral nervous system, and can be either acquired or inherited. Acquired peripheral neuropathy can be caused by physical injury, tumors, toxins, diabetes, autoimmune responses, nutritional deficiencies, alcoholism, infections, and vascular and metabolic disorders. Genetic mutations can also lead to peripheral neuropathy. The following

presents a review of inherited peripheral neuropathies, focusing on Charcot-Marie-Tooth disease (CMTD), the most prevalent genetic peripheral nerve disorder. Background knowledge of other peripheral nerve diseases and their corresponding animal models aids in the evaluation and biological study of newly discovered neuropathies, not only for methodologies and insights into potential pathomechanisms, but also for connecting different proteins to molecular and cellular pathways. CMTD is categorized into demyelinating (CMT1) and axonal (CMT2) forms, which are helpful for comparing and contrasting newly discovered peripheral neuropathies.

Charcot-Marie-Tooth disease, named after the discoverers Drs. Charcot, Marie, and Tooth, all late 19th century neurologists, is an umbrella term for nonsyndromic inherited peripheral neuropathies. CMTD is also referred to as hereditary motor and sensory neuropathies (HMSNs). With the incidence of CMTD at 1/2500, it is the most common inherited neurological disease (Suter & Scherer, 2003). Following the advent of electrophysiological techniques, and later, the arrival of modern molecular biology, CMTD was found not to be one disorder, but encompassing many gene mutations. The various forms of CMTD have been well-studied by many research groups in patients and animal models, which in particular have been important in studying the pathophysiology peripheral disorders. Much of the information on Schwann cell and axonal proteins has been elucidated from animal models through genetic manipulation, behavioral analysis, biochemistry, electron microscopy, and other methods. Besides the gene involved in a particular peripheral neuropathy, key questions include whether the neuropathy is demyelinating, axonal, or mixed and if it is developmental or neurodegenerative. These

answers will eventually help in the development and utilization of the right therapeutic treatment for each form of peripheral neuropathy.

Electrophysiological evaluation can clinically differentiate two different types of neuropathy: in humans, forearm motor nerve conduction velocities (NCVs) less than 38 m/s is considered indicative of demyelination, as in CMT1, while normal NCVs with decreased amplitude is categorized as axonal neuropathy, as in CMT2 (Harding & Thomas, 1980; Suter & Scherer, 2003; Zuchner & Vance, 2006). Electrophysiological diagnosis, however, is not always clear-cut; gray areas include a mixture of both decreased NCV and amplitudes, myelin histopathology with decreased amplitudes, and/or axonal abnormalities with decreased nerve conduction speeds (Zuchner & Vance, 2006). This can indicate mixed axon and myelin pathology. The histopathology of nerve biopsies from classical CMT1 patients is predominantly segmental demyelination and remyelination with onion bulb structures; although axonal loss is also detected, it is considered to occur secondarily. CMT2, on the other hand, is associated with the loss of myelinated axons (Suter & Scherer, 2003). However, involvement of a single gene can lead to different phenotypes and severities, including intermediate forms. Therefore, a combination of genetic, behavior, histopathological, and electrodiagnostic analysis is important for pinpointing the underlying pathophysiology.

Demyelinating peripheral neuropathies

It seems intuitive that inactivation or disruption of key residues of myelin structural proteins would lead to demyelination of peripheral nerves from instability within the myelin sheath. Therefore, the fact that mutations in the gene encoding for the

myelin structural protein PMP22 lead to demyelination is not remarkable. In fact, PMP22 gene defects cause the most common form of CMTD. Mutations arise due to the structure of the gene: the two homologous DNA sequences flanking either side of *pmp22* promote unequal homologous recombination, leading to gene duplications and deletions. Gene duplication leads to CMTD with clinical onset during young adulthood with the lower limbs preferentially targeted, leading to weakness, sensory deficits, loss of reflexes, and ultimately atrophy, which are all, very interestingly, often preceded by decreased NCVs (~20 m/s) (Birouk et al., 1997; Thomas, 1999). Although this seems to indicate that demyelination, which decreases NCV, leads to the symptoms, this, surprisingly, is not the case. It is not myelin abnormalities, but rather, the reduction of motor amplitudes and axonal loss that correlate with patients' weakness and symptoms (Krajewski et al., 2000). So although demyelination reduces NCVs, the disorder seems to be aggravated by subsequent axonal problems. PMP22 deletions are the main cause of hereditary neuropathy with liability to pressure palsies (HNPP), which is clinically characterized by episodic neuropathies followed by a period of recovery (Chance et al., 1993). Unlike PMP22 duplications that lead to initial demyelination, abnormal histopathological features from PMP22 deletions also include tomacula (focal myelin thickening) along with segmental demyelination with remyelination, which are recapitulated in the genetically authentic $PMP22^{+/-}$ HNPP mouse model. Through the HNPP animal model, Adlkofer et al. showed that the main deficit leading to the symptoms was progressive demyelination (Adlkofer et al., 1997). Point mutations in *pmp22*, on the other hand, lead to even more severe phenotypes in human patients and mice than from excessive gene copies or loss (Trembler and Trembler-J heterozygotes), likely from dominant-negative

effects (Suter & Scherer, 2003). Clearly, normal PMP22 gene dosage as well as the correct sequence is crucial for proper myelination (Scherer & Chance, 1995).

Mutations in *mpz*, which encodes for another compact myelin structural protein, P0, causes CMT1B, Dejerine-Sottas syndrome (DSS), and congenital hypomyelination (Shy, 2006; Warner et al., 1996). The phenotypes, however, are extremely variable depending on the type of mutation, and can present as classical CMT1B, a severe CMTD, DSS, congenital hypomyelination, or even, unexpectedly, a CMT2-like neuropathy with pronounced axon loss (Suter & Scherer, 2003). The combination of uncompacted myelin and severe demyelination in nerves of $P0^{-/-}$ mice gave more evidence to the proposed role of P0 in both peripheral myelin compaction process and structural integrity, showing that P0 is necessary for the development of compact myelin as well as its maintenance (Giese et al., 1992; Martini et al., 1995). By ~2 weeks in age, the P0 knockout mice developed tremors, convulsions, locomotor deficits, and abnormal hind limb clasping when handled by the tail. Other Schwann cell proteins, PMP22, NCAM, and L1 were downregulated in mutant sciatic nerves. Similar to *pmp22*, gene dosage of *mpz* is crucial as reduction of P0 destabilizes myelin while overexpression leads to dysmyelination (Martini et al., 1995; Wrabetz et al., 2000). Overexpression of P0 in mice revealed that very high levels (20-30 fold) disabled Schwann cells to the point that they were unable to sort axons or produce myelin properly, which led to the neuropathy (Wrabetz et al., 2000).

Disruption of the connexin 32 (Cx32)-encoding gene *gjb1* leads to a primary demyelinating X-linked neuropathy (CMTX) in humans and mice (Anzini et al., 1997; Scherer et al., 1998) despite the existence of other connexins in the same regions of Schwann cell myelin (e.g., Cx29) (Altevogt et al., 2002). The different connexins cannot

functionally replace each other, which indicates that even those that colocalize to the same subregions do not interact, so they must be serving different purposes through variations in pore size and/or gating mechanisms. Six Cx32 subunits form a connexon, or hemichannel, which forms a gap junction with a connexon on the adjacent plasma membrane. Defects in this formation lead to a disease state that progresses to pronounced axonal loss, as demonstrated by nerve conduction and morphometric/ultrastructural analyses, despite the fact that Cx32 is not expressed on axons or neurons (Hahn et al., 2001; Hahn et al., 2000). This is similar to the cases of *pmp22* duplications and some forms of *mpz* mutations in which disruption of myelin proteins ultimately lead to axonal defects. Although axonal loss is considered secondary (Birouk et al., 1997; Thomas, 1999), it clearly aggravates symptoms and is a similar endpoint of many neuropathies that begin with myelin defects.

CMT4 also describes demyelinating peripheral neuropathies; however, unlike the subtypes of CMT1, they are inherited recessively. Ganglioside-induced differentiation-associated protein-1 (GDAP1) mutations cause CMT4A. Some mutations lead to a demyelinating neuropathy, other mutations cause a severe axonal neuropathy categorized as AR-CMT2, while another set of gene defects causes an intermediate form encompassing both pathological features. Mutations in the gene encoding myotubularin-related protein-2 (MTMR2), which belongs to a phosphatase family that dephosphorylates inositol phospholipids, cause CMT4B, an early-onset neuropathy. Despite the fact that MTMR2 is also highly expressed by neurons, histopathology of CMT4B peripheral nerves revealed that myelinating Schwann cells were mainly affected, resulting in abnormal myelin outfoldings and redundant myelin loops (Suter & Scherer,

2003). This was confirmed by Bolis et al. who demonstrated that inactivation of *Mtmr2* in Schwann cells, but not motor neurons, is sufficient and necessary to reproduce CMT4B peripheral neuropathy with myelin outfoldings (Bolis et al., 2005). CMT4D is caused by mutations in N-myc downstream-regulated gene-1 and also features hearing loss and dysmorphic features (Scherer, 2006). Patients with mutations in the periaxin (Prx) gene are diagnosed with CMT4F, which is characterized by delayed motor milestones, weakness, sensory and reflex loss, and sensory ataxia. Like most forms of CMTD, it is a peripheral neuropathy in which weakness is predominantly distal. Prx is exclusively expressed by Schwann cells. Curiously, during myelin development it shifts from the adaxonal membrane to the abaxonal membrane where it links the cytoskeleton of mature Schwann cells to the basal lamina. Thus, it is not surprising that fibers in $Prx^{-/-}$ mice initially formed myelin sheaths, but subsequently developed abnormal myelin outfoldings and demyelination at the stage when Prx is normally acting as a scaffolding protein (Gillespie et al., 2000).

Not surprisingly, mutations in transcription factors regulating myelin proteins also cause peripheral neuropathy, but with increased severity. Egr2/Krox20 knockout mice fail to generate myelin sheaths, and indeed, there are human patients with severe CMTD with mutations in Egr2/Krox20 (Berger et al., 2006; Warner et al., 1998). This phenotype is expected since Egr2/Krox20 directly targets the promoter of *mpz* and also works synergistically with Sox10 to regulate *mpz* and *gjb1* (Berger et al., 2006). Mutations in Sox10 lead to a syndromic disorder affecting both the PNS and CNS due its function in regulating neural crest stem cells (Britsch et al., 2001; Kim et al., 2003; Stolt et al., 2002). The discovery that mutations in transcription factors regulating myelin genes lead

to peripheral neuropathy connects the network of many genes and proteins involved in CMTD.

The earliest known alteration after demyelination is the reorganization of axonal membrane proteins, including nodal sodium channels (Dugandzija-Novakovic et al., 1995) and juxtaparanodal Kv1.1 and Kv1.2 channels, which disperse after demyelination and reorganize with remyelination (Rasband et al., 1998). Segmental demyelination itself leads to biophysical consequences on action potential conduction, and changes in Nav channel distribution can jeopardize it even further by diminishing the ability of the action potential to regenerate at nodes (Poliak & Peles, 2003). The *Shaker*-like Kv1.1 and Kv1.2 channels, on the other hand, limit the duration of action potentials, prevent aberrant firing after action potentials, and repolarize the membrane potential, thus controlling excitability. Although Kv1.1-null mice exhibited CNS hyperexcitabiility through spontaneous seizures, sciatic nerves electrophysiologically showed an increased refractory period (Smart et al., 1998). An increased refractory period was also demonstrated in contactin mutants with Kv1.1 and Kv1.2 mislocalization to paranodes (Boyle et al., 2001). This means that the initiation of a subsequent action potential is inhibited, which can profoundly affect nerve function if enough fibers are affected.

Axonal peripheral neuropathies

Mutations in proteins expressed by neurons/axons also lead to peripheral neuropathies, which are classified as CMT2. The common pathological hallmarks of CMT2-affected peripheral nerves are axon degeneration and regeneration, ultimately leading to a loss of available fibers. However, Zuchner and Vance report that only

mutations in the mitofusin 2 (MFN2) gene electrophysiologically manifest as a true axonal neuropathy by NCV measurements (Zuchner & Vance, 2006). MFN2 mutations cause the most common axonal form of CMTD. MFN2 is a mitochondrial protein, a dynamin-like GTPase spanning the outer membrane (Rojo et al., 2002). Complicating matters, mutations in GDAP1, as mentioned earlier as a cause of demyelinating CMT4A, can lead to myelinopathy, axonopathy, or both (mixed electrophysiological and histopathological features) depending on the affected individual (Niemann et al., 2005; Suter & Scherer, 2003). It is not surprising that there is an axonal form, AR-CMT2, since GDAP1 is expressed by both Schwann cells and neurons. It is not known how defects in mitochondrial proteins MFN2 and GDAP1 expressed by all cell types leads to axonal neuropathy, but the fact that neurons/axons are particularly sensitive to mitochondrial dysfunction/oxidative stress has been well-established and is exemplified by many neurological disorders including Parkinson's disease, Friedriech ataxia, several forms of hereditary spastic paraplegia, amyotrophic lateral sclerosis, and others (Bossy-Wetzel et al., 2003; Mandemakers et al., 2007). This is most likely due to the high energy consumption of neurons in generating action potentials and maintaining long projections rather than a differential role of mitochondria in various tissues.

Other axonal CMTDs include mutations in heat shock proteins 22 and 27, which underlie CMT2L and distal hereditary motor neuropathy, respectively (Evgrafov et al., 2004; Irobi et al., 2004). Proper trafficking of mitochondria, organelles, and vesicles from the cell body through the entire length of peripheral axons is crucial for nerve maintenance and function. Exemplifying this is the fact that mutations in trafficking proteins leads to axonal neuropathies. Dominant mutations in genes encoding for kinesin

family member 1B (KIF1B), a transport motor protein that binds to synaptic vesicles, underlies CMT2A (Zhao et al., 2001). Kif1B$^{+/-}$ mice, which express lower levels of synaptic vesicle proteins, develop a peripheral neuropathy (Suter & Scherer, 2003). CMT2B patients have mutations in RAB7 and show length dependent weakness and sensory loss so profound that it can lead to foot ulcerations requiring amputations (Auer-Grumbach et al., 2003; Verhoeven et al., 2003). Spinal motor and DRG neurons normally express RAB7, a Ras-related GTPase (Verhoeven et al., 2003), which explains why the loss affects both motor and sensory fibers. Although the glycyl transfer RNA synthetase (GARS) protein is expressed by all cell types, mutations in its gene cause two diseases that specifically target the nervous system, CMT2D and distal spinal muscular atrophy V (dSMAV), an allelic disorder. Oddly, unlike in other CMTDs, CMT2D patients exhibit an upper extremity neuropathy phenotype that affects specific muscles of the hand before the feet (Suter & Scherer, 2003; Zuchner & Vance, 2006). CMT2D patients appear clinically similar to dSMAV patients, except that they present with sensory symptoms (Zuchner & Vance, 2006).

Besides CMTD, other less common inherited peripheral neuropathies exist. Giant axonal neuropathy (GAN), a syndromic disorder that affects both the PNS and CNS, stems from mutations in the gene encoding gigaxonin, which is a microtubule-associated protein 1B binding protein (Ding et al., 2006). Disruption of gigaxonin disrupts all intermediate filaments, from hair to neurons. Peripheral axons over-accumulate neurofilaments, which leads to axonal swelling. Not all axons, however, are affected.

Underlying genetic causes for hereditary peripheral neuropathy are continuously being discovered and the proteins and pathomechanisms quite varied. For example, one

very recent finding is that mutations in the gene encoding a guanine nucleotide exchange factor for the Rho GTPase Cdc42, called Frabin/FDG4, cause CMT4H (Delague et al., 2007; Stendel et al., 2007). Although the underlying cause of either the tomaculum or thin myelin in patients' sural nerves are not known, overexpression of Frabin in Schwann cells led to morphological changes (i.e., filopodia and lamellipodia), so the pathophysiology may involve altered signaling that affects cell shape (Delague et al., 2007). The importance of Cdc42 was mentioned earlier for its role in axonal growth/extension, but since neurons express other GEFs (Murata et al., 2006), Frabin mutations lead to a demyelinating, not axonal, disease.

Models of hypomyelination

The following examples demonstrate that neuronal/axonal defects can lead to a Schwann cell phenotype of hypomyelination. Although these knockouts are physiological models that do not represent any known human disease, they illustrate other important mechanisms of peripheral nerve development. Michailov et al. analyzed the sciatic nerves of different genotypic Nrg1 and/or ErbB2 mouse mutants via electron microscopy and morphometric analysis to test the hypothesis that neuregulins can signal axon size to the Schwann cell through the glial ErbB receptor tyrosine kinases. Since the disruption of this signaling pathway during development alters myelin thickness, they concluded that Nrg1 does indeed signal a biochemical measure of axon caliber during myelination thereby controlling for appropriate myelin thickness: reduced Nrg1 expression leads to hypomyelination (conversely, neuronal overexpression of Nrg1 produces hypermyelination) (Michailov et al., 2004). Similar EM studies of peripheral nerve

development in two different models of Bace1-null mice revealed thin myelin in adult peripheral nerves. Myelin sheaths were also thin at younger ages in Bace1 knockout nerves due to delayed myelination compared to wild-type, indicating that the genetic deletion of Bace1, a neuronal beta-secretase that cleaves proteins, including Nrg1 and amyloid precursor protein, causes hypomyelination (Hu et al., 2006; Willem et al., 2006). Although the implication for Alzheimer's disease is very promising, blocking Bace1 may interfere with peripheral nerve maintenance as it does during development, so this should be further investigated. Thus, any signaling defect from the neuron to the Schwann cell can lead to delays in or aberrant myelination causing hypomyelination.

ACCPN

Peripheral neuropathy associated with agenesis of the corpus callosum (ACCPN) (OMIM 218000) is an autosomal recessive syndromic disorder affecting both the CNS and PNS. It is also called Andermann syndrome, named after the discoverer, Dr. Frederick Andermann, a Canadian neurologist who first described the disease in 1972. Peripheral neuropathy and mental retardation are the pathological hallmarks of the disorder and are often associated with variable agenesis of the corpus callosum, lack of reflexes, and adolescent-onset psychosis often referred to in the literature as "schizophrenia-like symptoms." The course of peripheral neuropathy, regardless of callosal status, begins with hypotonia during infancy, followed by delayed motor milestones, then wheelchair confinement in early adolescence (Dupre et al., 2003; Howard et al., 2002b). Mutations in *SLC12A6* (solute carrier 12A6; human KCC3 gene) resulting in truncated nonfunctional protein were identified in ACCPN patients by single-

strand conformation polymorphism analysis (Howard et al., 2002b). Although a very rare disorder worldwide, the prevalence of ACCPN is extremely high in two regions of Quebec, Canada—Saguenay-Lac-St-Jean (SLSJ) and Charlevoix counties—with incidence at birth at 1/2,117 and a carrier rate of 1/23 (Dupre et al., 2003; Howard et al., 2002a). The disorder follows migration patterns from France and within Canada; based on genealogical data, the 17th century French founders established themselves in Charlevoix and their descendants moved to SLSJ in the early 19th century (Dupre et al., 2003).

Patient data reveals the typical clinical onset and progression of the peripheral neuropathy, but little insight on the pathomechanism of the peripheral neuropathy itself. Nerve biopsies revealed demyelination and onion bulbs in some ACCPN patients while others showed signs of axon loss (Dupre et al., 2003). Thus, Dupre et al. raise the question of whether the Schwann cell or axon is the primary site of damage in ACCPN. The differences between French-Canadian patients is not likely due to different mutations since SSCP analysis revealed the same mutation in those tested (Howard et al., 2002b), but this cannot be discounted since not all biopsied patients were genotyped. Also, the qualitative nature of the histopathological analysis describing “tiny axons,” “massively enlarged axons”, “numerous onion bulb formations”, and “disproportionately thin myelin sheaths” does not tell us what the most predominant pathology is and gives no quantitative measure for comparison between patients at different ages to determine how the disease may evolve over time. Also, light microscopy is not the best tool for studying detailed nerve structures, and low magnification may lead to misinterpretations. The differences in histopathology in ACCPN patients may stem from the progressive and,

likely, changing nature of the disorder over age. The most recent analyses of nerve biopsies were from only a few children (ages 2-12) and autopsies from 22-33 year olds, which may not match as the neuropathology may change over time/age as in other peripheral neuropathies, such as CMTX and some forms of CMT1 discussed earlier, in which a demyelinating neuropathy ultimately progresses to axonal loss. Alternatively, it may be a mixed disorder consisting of both demyelination and axon degeneration. A review of patient motor nerve conduction velocities were also disparate, even when patients were grouped into similar ages, so the electrophysiology results were inconclusive and unable to shed light on the type of defect—primary demyelinating (myelinopathy) or axonal (axonopathy) (Dupre et al., 2003) as in the case of some CMTD forms. The peripheral neuropathy in ACCPN may be a mixed myelinopathy and axonopathy; this can only be determined histologically by EM. Although the clinical symptoms have been well-characterized (hypotonia, lack of reflexes, mental retardation, variable ACC, etc.), the dearth of information on the pathophysiology of the peripheral neuropathy called for a thorough analysis of defective sciatic nerves over age, which would also shed light on the function of KCC3. The KCC3-null mouse was created to study the physiology of KCC3, but is useful for yielding answers to the underlying pathogenesis of the disorder like other animal models of peripheral neuropathies.

Summary and Dissertation Goals

Although research on KCC3 has increased since it was first cloned in 1999, only the surface has been scratched. Many questions still remain about the physiological role of KCC3 in various tissues, including in the central and peripheral nervous systems. The

creation of the KCC3-null mouse by Dr. Eric Delpire is described in detail in the introduction of Chapter III. Their abnormal posture at ~2 weeks of age and eventual hind limb dragging, along with abnormalities of sciatic nerve upon histological analysis under light microscopy, pointed to peripheral neuropathy. There appeared to be no changes in the CNS of KCC3-null mice, and unlike ACCPN patients, all mice examined exhibited an intact corpus callosum. To complete the characterization of the mice, specific aim 1 was developed based on this preliminary data and the possibility that the KCC3-null mouse could be a model of ACCPN. Chapter III describes the results, and, indeed, we showed that the mice are relevant animal models of ACCPN. At the same time as the development of the knockout mouse, ACCPN patients and their families were being screened for mutations in the KCC3 gene by a Canadian research group headed by Dr. Guy Roleau, and their exciting results showed that all patients had mutations in KCC3.

Due to the 100% penetrance of peripheral neuropathy in ACCPN patients and available mouse model, my work focused on the pathophysiology of KCC3 loss in the PNS. The peripheral neuropathy was one of the more puzzling features of the disorder. The fact that KCC3 is expressed in the brain is compatible with mental retardation and psychosis due to the loss of cotransporter function, although the underlying reason is not yet known. However, the reported lack of KCC3 in adult rodent sciatic nerve did not correlate with sciatic nerve pathology and peripheral neuropathy. This dichotomy was addressed in specific aim 2. I describe the results in Chapter IV, showing that KCC3 is expressed by the sciatic nerve, but only in juvenile mice, not adult, with localization to Schwann cell bodies. Alternatively, there was the possibility that the peripheral neuropathy could stem from lack of function in spinal motor and/or DRG sensory

neurons where KCC3 was previously shown to be expressed (Boettger et al., 2003). Locomotor deficits can certainly stem from defects in brain and spinal cord as well as muscle. If KCC3 was not found in peripheral nerves, we would have likely pursued the peripheral neuropathy as a symptom of atypical spinal motor neuron disease since many forms, such as multifocal motor neuropathy, are characterized by defects in axon maintenance (Jablonka et al., 2004).

In an effort to understand the role of KCC3 in the peripheral nervous system through the pathophysiology underlying the neuropathy, we systematically evaluated sciatic nerves through morphometric analysis at different ages (specific aim 3). The case studies and literature reviews of ACCPN are based on electrophysiology and histology data from patients of a wide range of ages who were not followed over the course of the disease. Although the disorder is progressive as evidenced by patients' declining ability to walk, the initial defects and whether there were ongoing changes in the nerve with age was not known as there were no biopsies from infants and autopsy studies were performed only very recently. Likely because of the various ages of patients examined, sural biopsy reports described demyelination and onion bulbs (signs of demyelination) in some patients and signs of axon loss in others (Dupre et al., 2003). The advantage of a mouse model for this analysis is the ability to analyze sciatic nerves from age-matched cohorts (littermates) over time utilizing electron microscopy, a much more powerful tool than light microscopy. For detailed peripheral nerve studies, electron microscopy is indispensable for clearly distinguishing subcellular structures. We utilized EM to address several unanswered questions about this disorder: (1) whether the disease is developmental or neurodegenerative; (2) if it is a myelinopathy or axonopathy; and (3)

evidence for any underlying pathophysiology in structural changes. We addressed this in specific aim 3, utilizing EM and morphometric analysis to quantify changes in the KCC3 knockout compared to wild-type. The initial pathological defects of axonal and periaxonal swelling are described in Chapter V. Older adult knockout nerves, however, are characterized by Wallerian-like degeneration. Although we had originally hypothesized a myelin defect, we show that the disorder in our mouse model is not a myelinopathy, but involves the axon. Lastly, we compared sciatic-tibial nerve conduction velocities of wild-type, heterozygote, and homozygote knockout mice to determine whether the abnormalities lead to neurophysiological defects in nerve conduction and pain response (specific aim 4). The results of decreased nerve conduction velocity and sensitivity to noxious pain are discussed in Chapter VI.

In summary, the dissertation research verified the KCC3 knockout mouse as a relevant model of ACCPN. It is the first to demonstrate sciatic nerve expression of KCC3, which had continuously been questioned but never assessed. It is also the first morphometric analysis of the disorder and ultrastructural examination over age. This part of the study clarifies that the disorder is neurodegenerative, albeit very early onset anc clearly shows that it is not a primary myelinopathy (i.e., segmental demyelination), but an axonopathy. Changes in the adult KCC3 knockout nerve likely lead to their decreased nerve conduction velocities. The axonal enlargement and periaxonal fluid accumulation in young KCC3-null mice suggest a fluid-related dysfunction compatible with classic cotransporter function, pointing to the need of KCl regulation for the maintenance of the peripheral nerve most likely linked to cell volume control either from osmotic stress

and/or related to potassium buffering. Future experiments need to be completed to verify this hypothesis.

Specific Aims

Aim 1. Characterize locomotor and CNS behaviors of KCC3 knockout mice. *Hypothesis: Disruption of the KCC3 gene results in phenotypes resembling ACCPN patients.*

Specific Aim 2. Determine temporal and spatial expression of KCC3 in the sciatic nerve. *Hypothesis: KCC3 is expressed during sciatic nerve development by Schwann cells.*

Specific Aim 3. Conduct morphometric and ultrastructural analyses of KCC3-null sciatic nerves using EM. *Hypothesis: KCC3 loss in Schwann cells leads to myelin pathology.*

Specific Aim 4. Conduct nerve conduction and pain sensitivity studies in KCC3 knockout mice. *Hypothesis: Defects in KCC3$^{-/-}$ nerves lead to changes in nerve conduction and response to pain.*

CHAPTER III

BEHAVIORAL CHARACTERIZATION OF KCC3$^{-/-}$ MICE

Introduction

Of all of the major model organisms utilized for research—nematode worm, fruitfly, zebrafish, rat—the mouse is particularly advantageous for studying human biology and disease, not only because it is also a mammal with similar development, physiology, behavior, and diseases and shares homologs (99% of its genes) with humans, but also for targeted mutagenesis of genes by homologous recombination in a mammal. Mouse knockout technology has led to great scientific advances ever since it was first implemented in the late 1980s (Capecchi, 1989) Even before the advent of gene knockout technology, studies of genetic changes in mice were accomplished through research on natural, spontaneous mutants that still continue to be discovered and useful to this day. Most abnormal, spontaneous neuromuscular mutants found in the Jackson Laboratory colonies possess descriptive names, including tottering, staggerer, waddles, wobbler, wabbler lethal, awag (ages with abnormal gait), and shiverer (jaxmice.jax.org). Not all spontaneous mutations are detrimental; studies of the spontaneous mouse mutant called Wld^{s}, for Wallerian degeneration slowed, is a prime example of a mutation that confers a neuroprotective property, the remarkable slowing of Wallerian degeneration after axotomy or axonal degeneration in many neural diseases (Hoopfer et al., 2006).

With modern molecular biology techniques, the controlled creation of mouse mutants has led to valuable information on protein function and particularly disease

mechanisms. Knockout mice are undoubtedly a great scientific tool, especially in cases where there are no specific pharmacological inhibitors, such as for the individual cation chloride cotransporters. Embryonic lethality, however, can be an unpredictable result, and does not lead to information on protein function after development. This problem, however, can be overcome by generating conditional knockout mice, which provides temporal control of the gene knockout process. The creation of tissue- and cell-specific knockout mice is also becoming increasingly common and the combination of both strategies allows for temporal-spatial specificity. However, straight knockout mice, barring embryonic lethality, continue to be useful animal models for studying physiological, cellular, and molecular functions of a specific protein of interest. The general strategy is the replacement of an exon with an antibiotic selection marker, and, ideally, a reporter gene encoding for green fluorescent protein or beta-galactosidase as well as the negative selection marker thymidine kinase, which, with gancyclovir, allows for the death of embryonic stem (ES) cells containing random, non-homologous targeting vector insertions. The specific strategy needs to be carefully plotted to ensure that the restriction sites utilized for creating the construct are unique. Briefly, after using a probe to screen a genomic library to isolate a large region containing the exon of interest and inserting it into a vector, that exon can be disrupted by the insertion of a resistance gene cassette (i.e., neomycin) and a reporter gene. Although new methods have been developed, such as BAC clone recombination, the construct for our laboratory's KCC3 knockout mouse, detailed below, was modeled using the conventional strategy (Howard et al., 2002b).

The murine *Slc12a6* gene was disrupted by homologous recombination in ES cells. The targeting strategy included the removal of exon 3 and its replacement with a cassette containing a splice-acceptor site (en2), an internal ribosomal entry site (IRES), a beta-galactosidase−neomycin resistance (*LacZ−neoR*) gene fusion—encoding beta-galactosidase as the reporter gene and neomycin as a positive selection marker—and, finally, a polyadenylation signal (Figure 3-1). More specifically, a mouse genomic library (λ-FIXII) was screened using a portion of exon 3 (nucleotides 320−414) from mouse KCC3 cDNA. After the isolation of a 13.8-kb genomic clone containing the exon as well as ~11 kb upstream and ~2.5 kb downstream sequences, reconstruction for the recombination vector commenced with the insertion of fragment (4,200-bp SpeI−NotI), after restriction enzyme digest, into the vector pBluescript. The length of the left arm was increased—necessary for enhancing homologous recombination—by ligating a fragment (~3.9 kb AatII−SpeI) upstream to the new clone. The placement of a unique XhoI restriction site into exon 3 by PCR mutagenesis was a key strategic step as it allowed for the insertion of the en2−IRES−LacZ−neo−pA cassette through ligation of the cassette's SalI sites into the unique XhoI site created earlier (Figure 3-1) (Howard et al., 2002b).

Following standard techniques, ES cells were electroporated with linearized construct and grown on fibroblast feeder cells. Neomycin-resistant colonies (384 total), representing cells that took up the construct, were selected, expanded, and analyzed for presence of the mutated gene by Southern blot. Clones positive for the mutated gene (4) were further tested using internal and 5'-end probes (Figure 3-1). Ultimately, two ES cell clones were selected for injection into C57BL/6J blastocysts and resulted in chimeric

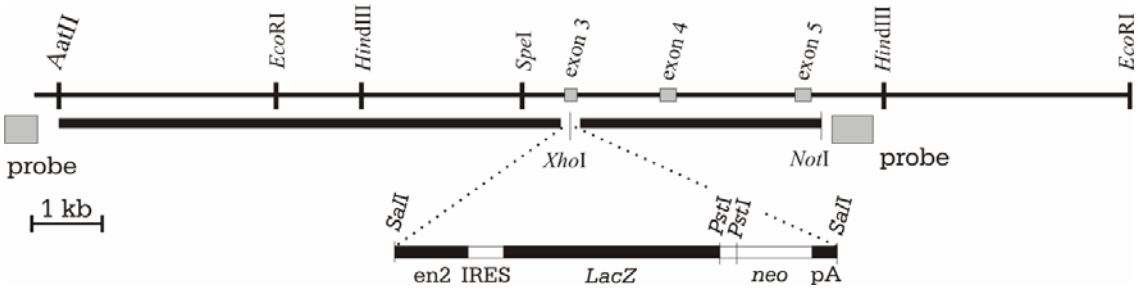

Figure 3-1. Targeting strategy for disruption of mouse *Slc12a6* gene

Structure of *Slc12a6* around exon 3 with the DNA fragment that was inserted into the gene. The cassette interrupting exon 3 includes an acceptor site (en2), internal ribosomal entry site (IRES), beta-galactosidase−neomycin resistance (*LacZ−neoR*) gene fusion, encoding the beta-galactosidase reporter gene and the positive selection marker neomycin, and polyadenylation signal. The 5' and 3' probes were designed for Southern blot analysis of ES-cell genomic DNA digested with *Hin*dIII, *Eco*RI and *Bam*HI. Figure from (Howard et al., 2002a).

mice (5) with more than 90% brown fur, demonstrating the large genetic contribution from ES cells for each clone. Males were mated with C57BL/6J females, and several successfully produced offspring at expected Mendelian ratios. All experiments used offspring of heterozygous breeding (F2 129svj/C57BL/6J mice). There were no overt differences in phenotype between the two clones (Howard et al., 2002b).

Absence of KCC3 protein expression in knockout mice was verified by Western blot analysis of brain microsomes. As expected, there was a significant reduction in KCC3 expression in heterozygous mice, but no detectable signal from homozygous knockout mouse brains. The beta-galactosidase gene (*LacZ*) downstream of the *Slc12a6* promoter, which should direct the synthesis of beta-galactosidase in cells that normally express KCC3, was functional as LacZ staining of knockout brain revealed intense color changes from beta-galactosidase enzymatic activity in neurons of the CA1 of the hippocampus, and to a lesser degree CA3 pyramidal cells, large cortical neurons, and cerebellar Purkinje cells, consistent with the pattern of KCC3 expression from immunostaining of brain sections with a KCC3 polyclonal antibody. All pups were weighed at two time points, but there were no differences in mass between the three genotypes at three weeks ($n = 132$, analysis of variance (ANOVA) $F_{2,129} = 2.42$, $P > 0.05$) or at eight weeks of age ($n = 39$, ANOVA $F_{5,33} = 11.97$, $P > 0.05$). KCC3-null mice were able to live a normal lifespan (Howard et al., 2002b).

Generally, knockout mice phenotyping involves a battery of standard tests. For example, the Irwin screen is a gross neurological assessment of basic sensory-motor performance by evaluating gross appearance (body weight and presence of whiskers, fur, and wounds); behavior in a novel environment (transfer of mice from their home cages

into a new, clean cage without bedding for evaluation of spontaneous activity, tremor, piloerection, tail elevation, urination, and defecation); and reflexes (touch escape, reaching reflex, and pinna reflex) (Irwin, 1968). Knockout mouse characterization is made easier, however, by knowledge of protein function, localization, and, if known, the equivalent human disease. However, hypotheses based on these known facts, should not be narrowly pursued. Astute home-cage observation is necessary, especially to develop hypotheses and tests for social and behavior phenotypes, which may not be expected. One interesting example of behavioral testing based on anecdotal evidence is the *Dvl1* (disheveled) knockout; although phenotypically unremarkable when observed alone, their longer whiskers and individual, instead of group, sleeping behavior propelled the research questions on social interaction and prepulse inhibition deficits (Lijam et al., 1997). Fortunately, most neuromuscular mutants demonstrate an easily observable phenotype, although the defect(s) may arise at different ages. $KCC3^{-/-}$ pups showed an early, distinct phenotype (Howard et al., 2002b), which gave direction on the behavioral assays to use. Also, our driving hypothesis, that KCC3-null mice are a model of ACCPN, provided a starting point. Before describing the results, I will introduce the testing paradigms used to characterize the $KCC3^{-/-}$ mice.

Neuromuscular deficits can result in a variety of abnormal behaviors, such as wobbly gait, muscle weakness, lack of coordination, and/or loss of balance. Since these problems can arise from defects in various regions—including different areas of the brain, spinal cord, peripheral nerve, neuromuscular junction and/or skeletal muscle fibers—similar symptoms can arise from very different defects. For example, lack of strength can stem from damage to the all of the above regions; imbalance from inner ear,

proprioceptive, or cerebellar abnormalities; and hind limb weakness or dragging from muscle, peripheral nerve, and/or spinal neuron defects. Thus, neuromuscular tests do not in themselves pinpoint the origin of the deficit. However, it allows for a starting point to evaluate and tease out the dysfunctions by quantifying performance against a control group (i.e., wild-type or no-drug). Also, these behavioral examinations are useful for behaviorally testing the progression of the neuromuscular defect through age and evaluating the efficacy of therapeutics designed to improve neuromuscular function without sacrificing the animal. One commonly used apparatus is the rotorod, on which mice must be able to maintain balance and remain walking on top of a rotating rod. This not only tests motor coordination, but also skill learning (i.e., wild-type mice improve during training). Performance on the wire-hang test is a measure of forelimb and grip strength as the mouse must have enough power to pull itself up to grab the wire with its hind paws and/or tail. The beam task measures balance and fine motor coordination. Any difficulty in these three tasks clearly point to neuromuscular problems, which can be teased out by other behavior tests and/or analyses of tissues.

Because sensorimotor gating is a phenomenon exhibited by all mammals and is disrupted in many neuropsychiatric diseases, it is frequently evaluated in animals to test hypotheses of CNS involvement in a disorder. Sensorimotor gating is the state-dependent regulation of transmission of sensory information to a motor system. It basically allows for the filtration of unnecessary information. Prepulse inhibition (PPI) of the startle response is one operational measure of sensorimotor gating. The startle reflex is a whole body response (Graham, 1975) that is attenuated in normal subjects when the startle-eliciting stimulus is preceded by ~10-500 milliseconds with a much weaker one, called

the prepulse. This prepulse-induced reduction of startle response magnitude is a natural behavior across species, from humans (Graham, 1975; Hsieh et al., 2006) to other mammals (Braff & Geyer, 1990; Swerdlow et al., 1999) and even marine mollusks (Mongeluzi et al., 1998; Nusbaum & Contreras, 2004), but is diminished in patients with schizophrenia, Huntington's disease, obsessive-compulsive disorder, and Tourette's syndrome—prepulses do not suppress the startle reflex to the normal extent (Braff et al., 1978; Braff et al., 2001; Braff et al., 2005; Hoenig et al., 2005; Munoz et al., 2003; Swerdlow et al., 1995; Swerdlow et al., 2007). Since drugs, such as dopamine agonists (e.g., amphetamine, apomorphine) and hallucinogens (e.g., LSD) can disrupt natural PPI in rodents (Metzger et al., 2007; Ouagazzal et al., 2001), and antipsychotic drugs can reverse these drug-induced PPI disruptions (Csomor et al., 2007; Kumari & Sharma, 2002; Metzger et al., 2007), there must be a neural correlate of PPI (i.e., the failure to inhibit).

The startle paradigm used by our laboratory to assess gating ability was the acoustic startle response, a reflex consisting of muscle contractions with changes in the sympathetic nervous system mediated by the brainstem in reaction to sudden noise, which most likely evolved as a protective mechanism against predators and other environmental threats (Yeomans et al., 2002). In the PPI of the acoustic startle response, a weak tone (prepulse stimulus) decreases the reflexive response (startle) produced by the second, more intense stimulus (pulse). Interestingly, the acoustic startle response can also be reduced by a non-startling tactile or visual stimulus before the pulse (Koch, 1999). We tested the startle response and PPI of KCC3-null mice because a deficit in PPI is an endophenotype of schizophrenia (Turetsky et al., 2007), and schizophrenia-like

symptoms, although variable, is one distinct CNS feature of ACCPN (Howard et al., 2002b). The deficits in attention and cognition in schizophrenic patients may be linked to sensorimotor gating problems so that irrelevant stimuli are not properly filtered out (Ludewig et al., 2005).

The open-field test assesses exploratory activity, anxiety in a novel environment and can also be repeated over time to evaluate habituation to the novel arena. Measurements generally consist of total distance traveled, amount of time spent in the periphery (thigmotaxis), time spent moving, number of times the animal rears, and average speed of movement. Both horizontal and vertical (rearing) activity can be assessed by the amount of beam breakage in each direction. Because mice naturally fear unknown open areas and exposure to bright lights, the center of the open field apparatus is an anxiogenic stimulus, so behavior in the chamber can be compared to evaluate anxiety levels between different genotypes or drug-treatments by timing thigmotaxis, or the tendency of the animal to stay close to the walls (time spent in periphery versus center) (Choleris et al., 2001).

Materials and Methods

All behavioral tests were carried out in the Vanderbilt Murine Neurobehavioral Laboratory of the Center for Molecular Neuroscience managed by Dr. Michael McDonald. Mice were acclimated to the testing location at least 12 h before the start of behavioral testing, except for startle response/pre-pulse inhibition for which they were allowed to acclimate at least 36 h before each testing.

Animals

KCC3$^{-/-}$ mice were generated by Dr. Eric Delpire through homologous recombination described above and in (Howard et al., 2002b). Mice were mated for more than 10 generations in the C57BL6 background and housed in a Vanderbilt University Medical Center animal facility with a 12 hour light-dark cycle and *ad libitum* food and water access. All animal procedures followed the National Institutes of Health guidelines on the use of animals and were approved by the Vanderbilt University Institutional Animal Care and Use Committee.

Genotyping

Wild-type, heterozygote, and homozygote mice were generated from KCC3$^{+/-}$ matings. DNA was isolated by clipping 1 mm of the tail from anesthetized mice, treating the tail clip with 200 µl of digestion solution (25 mM NaOH and 0.2 mM EDTA, pH ~12) for 20 min at 95°C, neutralizing the sample with 200 µl of a 40 mM Tris-HCl, pH 5 solution, and after mixing, centrifuging the digested tail tissue for 6 min at 14,000 rpm. Genotyping was performed through separate PCRs with 1 µl of tail DNA to amplify fragments specific to KCC3 control and mutant genes using the following primers:

(1) KCC3 control forward 5'-GAACTTTGTGTTGATTCCTTTGG-3'

(2) KCC3 control reverse 5'-TCTCCTAACTCCATCTCCAGGG-3'

(3) KCC3 mutant forward 5'-GAACTTTGTGTTGATTCCTTTGG-3'

(4) KCC3 mutant reverse 5'-TACAACACACACTCCAACCTCCG-3'

to generate a 371 bp product and a 290 bp product, respectively.

Rotorod

The ability to maintain motor coordination and balance on a rotating cylinder was measured with a standard rotorod apparatus (Model 7650, UGO Basile, Napoli, Italy). Mice were placed on the rotating drum (3.2 cm in diameter) and confined to a ~6 cm long section by gray plastic dividers. The latency at which mice fell off the rotating cylinder was recorded. Each mouse was tested with three trials per day over three days.

Wire-hang

The same wild-type and mutant mice were tested for their ability to hang from wire bars. Mice were allowed to hang on the bars with their forearms and their behavior was scored from 0-4 based on the rodent's ability to hang and pull up themselves up with their hind paws.

Beam

Mice were place at the center of a raised beam with a platform on either side. The latency to fall off the beam was measured with a stopwatch. However, mice that could successfully traverse the beam to one of platforms were assigned a score of 60.

Startle response and prepulse inhibition

Mice were placed in clear acrylic cylinders, which were attached to a platform in the startle chamber. Startle response and PPI of the acoustic startle response were

measured using four identical startle chambers (MED Associates). Each PPI session consisted of a 5-min acclimation period followed by 54 trials in 9 blocks of 6 trials each. Each six-trial block contained one startle trial (startle stimulus only), one null trial (no stimulus) and four prepulse trials (one trial at each of the four prepulse intensities, followed 100 ms later by the startle stimulus). The following experimental paradigm is depicted in Table 3.1: The startle stimulus was a 40-ms, 120-dB burst of white noise. The prepulse stimuli were 20-ms bursts of 70-, 76-, 82- or 88 dB white noise. The trials in which no stimulus was presented were used to measure baseline movement in the cylinders. The six trial types were presented in pseudo-random order such that each trial type was presented once within a block of six trials. The inter-trial interval ranged from 10−20 s with an average of 15 s. The startle response was recorded for 65 ms (sampling the response every 1 ms) starting with the onset of the startle stimulus. The maximal startle amplitude recorded during the 65 ms sampling window was used to calculate maximal startle for any given trial. PPI was calculated as the percent reduction in maximal startle on prepulse versus startle only trials. Experiments were conducted at the same time each day (900-1300) to eliminate effects of circadian rhythm. Mice that did not exhibit a startle response were not included in the analysis because it was impossible to show an inhibition of the startle response.

Open-field

Exploratory locomotor activity was measured using eight identical, commercially available open-field activity chambers (27 x 27) (MED Associates). Mice were placed in the monitors and allowed to explore freely over a period of 20-min. Each apparatus

contained 16 photocells in each horizontal direction and 16 photocells elevated 4.0 cm to measure rearing. Both horizontal and vertical activity was monitored by beam breakage that were recorded and analyzed automatically by MED Associates software. The horizontal beam breaks represent distance traveled while vertical beam breaks correspond to rearing.

Statistics

Comparison of three genotypes was made using repeated measures ANOVA followed by post-hoc Tukey tests. Unpaired t-tests were used for statistical analysis between two genotypes.

Results

Locomotor phenotype

Although heterozygous $KCC3^{+/-}$ mouse pups were indistinguishable in appearance and gross behavior from wild-type, $KCC3^{-/-}$ pups showed obvious locomotor abnormalities ~2 weeks of age. Their low posture on flat surfaces indicated rear limb weakness. Later neuromuscular deficits were obvious by observation and in video recordings of adult $KCC3^{-/-}$ mice crawling in an open field chamber. The control mice traveled in the cage without disrupting the corncob substrate, while mutant mice always dragged their hind limbs, generating wide tracks in the bedding.

Due to these locomotor defects observed in the $KCC3^{-/-}$ mice, all three genotypes were tested on the rotorod, beam, and wire-hang, which quantitate motor and coordination skills, balance and coordination, and grip strength, respectively, by

comparing the performance of mutant mice against that of wild-type. Mice were tested on a rotorod for three days with three trials per day, and their latency to fall was recorded. Data from the final day and session at both ages are represented in Figure 3-2A. $KCC3^{-/-}$ mice were clearly the worst performers on the rotorod test, falling shortly after being placed on the rod ($F_{2,35} = 28.9$, $P < 0.0001$); there was no significant difference in latency between wild-type and $KCC3^{+/-}$ mice. For the beam task, mice were placed on top of a narrow beam and given one minute to walk to a side platform, and the latency to fall was scored. Control and $KCC3^{+/-}$ mice were able to complete this task perfectly, but the $KCC3^{-/-}$ mice rapidly fell off the beam ($F_{2,35} = 89.6$, $P < 0.0001$) (Figure 3-2B). The wire-hang task involves gripping with the forelimbs to pull up the body so that the hind limbs (and tail) grab the wire. Wild-type and heterozygous mice scored perfectly, whereas the $KCC3^{-/-}$ mice performed poorly ($F_{2,35} = 77.5$, $P < 0.0001$) (Figure3-2C). For all these tasks, mice were tested at one month and four months of age, which are equivalent to human adolescence and adulthood, respectively. KCC3-/- mice showed no measurable decline in performance between these two ages (Figure 3-2A-C).

Sensorimotor gating and open-field

For startle reflex and PPI tests, we took great care to prevent anxiety in all test subjects because excessive anxiety-related movement or freezing behavior changes the startle response and its inhibition by prepulse. To minimize stress, we precoded their tails with stripes using permanent marker to easily identify the animals with minimal handling. Mice were transferred to the test site and housed at least two nights before the

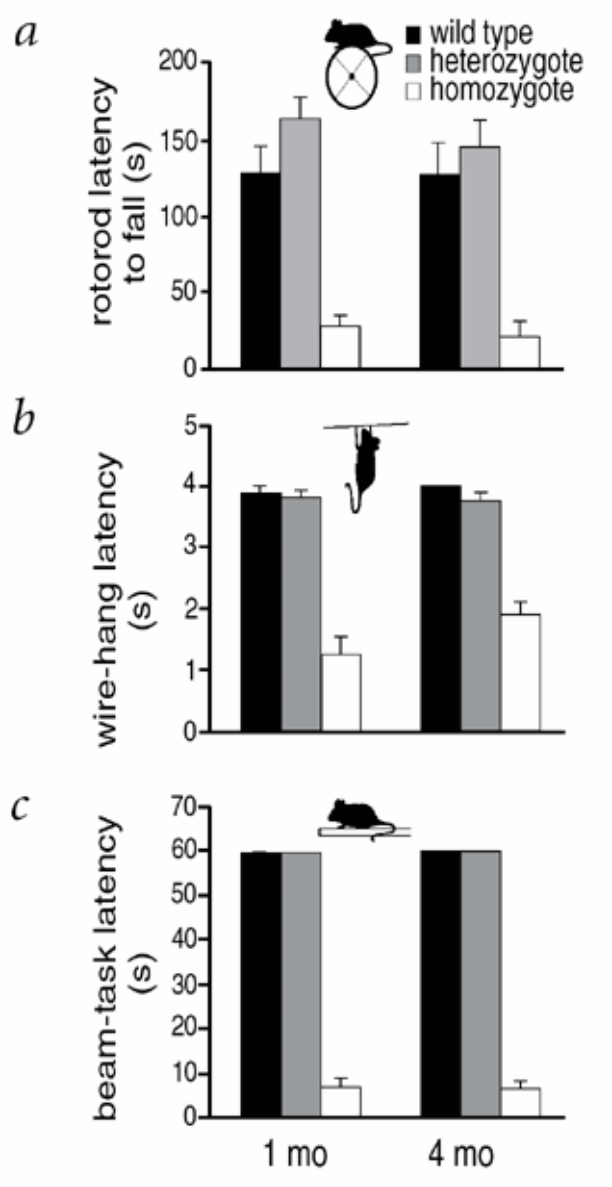

Figure 3-2. KCC3-null mice perform poorly on neuromuscular tests

KCC3 knockout mice perform poorly on (A) rotorod, (B) wire-hang, and (C) beam tests compared to their wild-type and heterozygote counterparts at both 1 month and 4 months of age.

testing session with the same white-noise background as the testing space for acclimation and to prevent behavior disturbances from the trauma of cage-transfer and moving. The startle chamber platforms were calibrated before each session and acrylic cylinders cleaned thoroughly with 70% ethanol between animals. Testing order was random.

Since the PPI test is based on inhibition of the startle reflex by a prepulse, we first demonstrated that there were no significant differences in startle response per se among the three genotypes or in their baseline movement when there was no acoustic stimulus (Figure 3-3A, B). Normally, there is greater suppression of the acoustic startle response (enhanced PPI) as the prepulse level increases; this occurred for all genotypes. However, $KCC3^{-/-}$ mice showed a significant deficit in PPI compared to the control and heterozygote knockout mice (Figure 3-3C). To assess exploratory behavior, locomotor activity was measured as the total distance traversed over four consecutive five-minute periods. The wild-type mice displayed strong exploratory behavior followed by habituation. In contrast, both heterozygous and homozygous knockout mice showed reduced exploratory activity. All three genotypes, however, spent equal time in the periphery (Figure 3-4).

Discussion

The KCC3 knockout as a model of ACCPN

Through the behavioral characterization of wild-type, heterozygous, and homozygous KCC3 knockout mice, we show that the peripheral and central nervous system deficits of KCC3-null mice match features of ACCPN. These shared symptoms not only show that the KCC3 knockout mouse is a good animal model of ACCPN but it

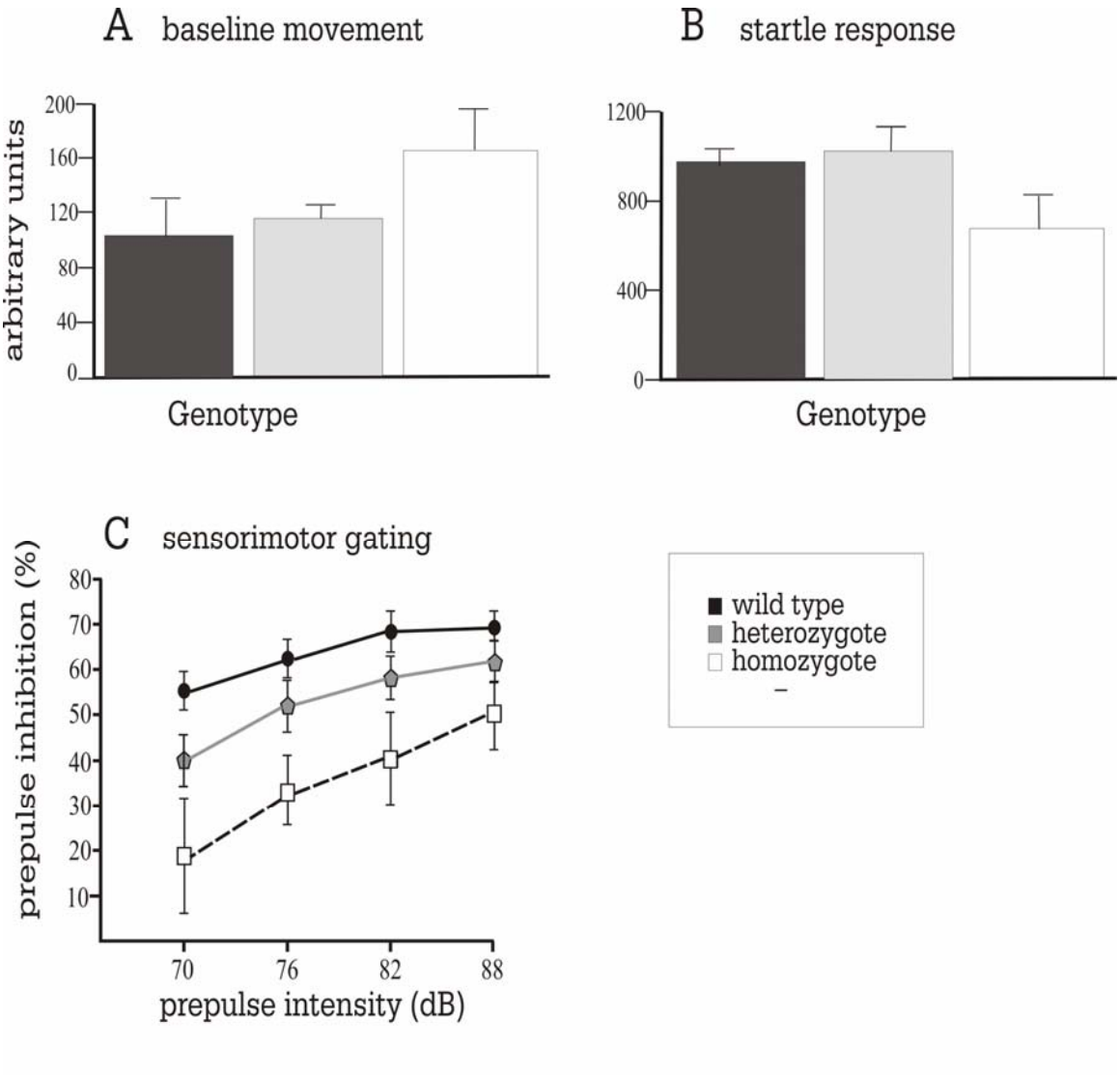

Figure 3-3. Startle response and PPI

(A) Baseline movement within the plastic holder (not stimulus) and (B) acoustic startle response (120 dB) were not different between genotypes. (C) Both homozygous and heterozygous KCC3 knockouts showed a significant deficit in PPI compared to wild-type, with KCC3-null mice exhibiting the most impairment. The PPI experiment was completed three times with similar results; the final trial is presented here.

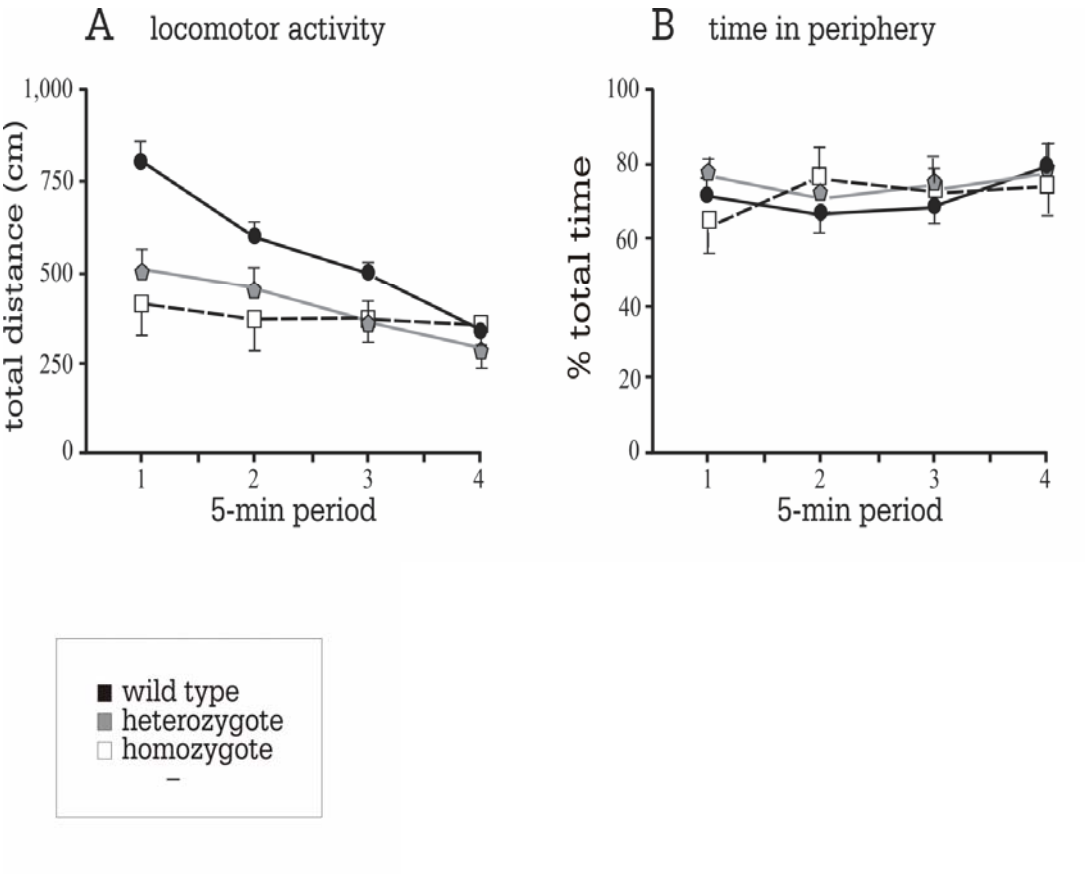

Figure 3-4. Reduced exploratory activity in open-field chamber
(A) Wild-type mice showed strong exploratory behavior followed by habituation while heterozygous and homozygous knockout mice showed reduced exploratory activity. (B) All three genotypes spent equal time in the periphery.

also underscores the importance of functional KCC3 in the entire nervous system. Although one species-related difference is the normal lifespan of $KCC3^{-/-}$ mice this is unrelated to the peripheral neuropathy as ACCPN patients commonly die in their thirties due to complications from respiratory infections, which have not been associated with KCC3 dysfunction (Howard et al., 2002a). Our mouse model of ACCPN can facilitate studies of disease progression from the beginning to the final stages, whereas human post-mortem tissue only allows end-stage studies. There has been a dearth of post-mortem studies of ACCPN patients because the causal relationship between KCC3 and ACCPN was not discovered until recently and no reported infant/toddler nerve biopsies. Therefore, KCC3 knockout mice offer new opportunities in studying the disorder in detail.

Neuromuscular defects

The neuromuscular defects in $KCC3^{-/-}$ mice were observable and upon testing, they performed poorly on the motor, balance, and strength tests compared to wild-type and heterozygous littermates. The fact that $KCC3^{+/-}$ mice performed just as well as wild-type (Figure 3-3) matches the human disease—carriers of one mutant allele do not develop peripheral neuropathy. However, the fact that heterozygous knockout mice showed impairments in CNS tests is intriguing as it suggests a gene dosage affect and that carriers of KCC3 mutations may have deficits.

The motor ability of mice younger than 2 weeks of age is impossible to assess because all young pups are uncoordinated with underdeveloped motor skills. However, the early onset weakness (low posture at ~2 weeks) in KCC3-null mice matches the early

onset hypotonia and peripheral neuropathy of ACCPN. Although the knockouts' hind limbs appeared to be more severely affected than the forearms by observation of their hind leg dragging, reduced grip strength indicates that the forelimbs are also weaker (Figure 3-3C). An alternative, more quantitatvie method of assessing forearm strength is through a grip strength meter; the mouse, grasping a ring connected to a force transducer, is slowly pulled away until its grip is broken and the force value at this point is a measure of maximal resistance. The wire suspension test, using a wire or wired grid, however, is a very simple way to assesses grip strength and endurance. Since the peripheral neuropathy is progressive in ACCPN, a decline in the rotorod and balance tests might be expected after 1 month of age, during re-testing at 4 months. One month in mouse age corresponds to human adolescence, which is typically when ACCPN patients become wheelchair-bound (Dupre et al., 2003). Perhaps, the reason why we could not tease out the age-related decline could be due to the particular ages chosen at three months apart. I expect mice tested at an even older age (> 6 months) would show a decline on all neuromuscular tasks that could reveal the progressive nature of the disorder, especially since very old mice (> 1 year) assume very awkward, splayed-leg positions even when sitting on a flat surface (Boettger et al., 2003). Besides lifespan, another species-related difference is the continuous ability of $KCC3^{-/-}$ mice to ambulate, albeit with low posture and leg dragging, while ACCPN patients become completely wheelchair dependent. This difference may be attributed to the longer limbs in humans, which require increased energy metabolism for peripheral nerve maintenance (e.g., anterograde/retrograde transport, action potential propagation, more myelin to maintain, etc.) and also the fact that mice place weight on all four legs, which decreases the physical stress on each limb. Most peripheral neuropathies

lead to more pronounced disability in patients' legs and hind limbs of animal models (see Chapter 2).

Other neuromuscular tests exist, but would not have shed new light on the KCC3-knockout's disabilities. For example, comparison of stride and stance measurements from paw print traces is a simple gait test (Bolino et al., 2004; de Medinaceli et al., 1982; Ding et al., 2006), and according to Jackson Laboratory, it can be a more reliable and sensitive method to detect mutants with subtle abnormalities (nmf.jax.org). Skeletal muscle endurance can be evaluated by changes in performance level with continuous forced treadmill exercise, which can pinpoint myopathies; for example, the mdx dystrophic mouse, a model of Duchenne muscular dystrophy, has less stamina than control mice due to muscle degeneration (Muntoni et al., 1993). Signs of cerebellar dysfunction, including swaying side-to-side, wide-stanced gait, and a loss of righting reflex (inability to right itself from a recumbent position) (nmf.jax.org) can all be scored. Since neuromuscular deficits are indicative of, but do not prove, either a motor neuron disease, peripheral neuropathy, and/or abnormal muscle innervation (neuromuscular junction) or structure, these need to be teased out with histopathology and/or electrophysiology to further test the hypothesis. It is important to note, however, that one initial defect can cascade into problems in other areas. For example, mice with the Schwann cell specific deletion of the beta-1 integrin gene develop muscular atrophy by one month in age even though the protein was only removed from Schwann cells; thus the initial defect of dysmyelination and diminished axonal sorting led to muscle wasting. Therefore, the disorder is a dysmyelinating peripheral neuropathy with secondary myopathy (Feltri et al., 2002).

Also, many demyelinating neuropathies progress into secondary axonal forms (see Chapter 2).

CNS deficits

The PPI deficits in KCC3-null mice is relevant to the schizophrenia-like symptoms—psychotic episodes, including hallucinations, paranoia, and persecutory fears—that many ACCPN patients develop. Both homozygous and heterozygous mutant mice exhibit a PPI deficit; the latter with an intermediate phenotype, suggesting a gene-dosage effect. The changes in PPI are not due to hearing loss because the three genotypes showed no significant differences in acoustic startle response measured at different intensities. Also, for all genotypes increasing the decibel level of the acoustic prepulses led to increases in PPI, which is normal and indicates that all the mice were able to hear the lower-decibel prepulse tones and distinguish between them, as well as the startle stimulus. The prepulse tone must be heard and processed in order to trigger any PPI of the auditory startle stimulus. Although Boettger et al. showed that KCC3-null mice become deaf, the process was age-related and auditory brainstem responses declined very slowly over the first year (Boettger et al., 2003). We were not aware of this phenotype, but based on the published plots of auditory threshold (in decibels) over age (Boettger et al., 2003), all $KCC3^{-/-}$ mice should clearly be able to hear the 120-dB startle noise and the prepulse intensities (70-, 76-, 82- and 88-dB) at the age we tested. However, if it were the case that the KCC3-null mice have a slightly reduced auditory capacity, this does not explain the statistically significant reduction of PPI in $KCC3^{+/-}$ animals.

As mentioned earlier, PPI is an operational measure of sensorimotor gating, and in humans, sensorimotor gating dysfunction is a feature of several psychiatric disorders, including schizophrenia, schizotypal personality disorder, obsessive-compulsive disorder, and Tourette syndrome (Braff et al., 2001) and, for schizophrenia patients and animal models of the disorder, can be reversed by antipsychotics (i.e., haliperodol, clozapine) (Csomor et al., 2007; Metzger et al., 2007), implicating neurotransmitter/receptor defects. However, psychosis, which ACCPN patients develop (Howard et al., 2002b), has also been linked to white matter deficits, not only for schizophrenia itself (Price et al., 2007), but also for psychosis that develops in Alzheimer disease (Lee et al., 2006) and metochromatic leukodystrophy (Black et al., 2003; Hyde et al., 1992). The psychosis reported for metochromatic leukodystrophy, a demyelinating disorder, and ACCPN are remarkably alike, including hallucinations and bizarre delusions as well as the age of onset. Alterations in neurotransmission, whether due to changes at the neurotransmitter/ receptor level or abnormalities in myelinated axon tracts, could possibly lead to similar symptoms, which would be analogous to the multiple genetic causes of peripheral neuropathy. Furthermore, the hypothesis that changes in white matter tracts are involved in schizophrenia is supported by neuroimaging as well as genetic studies (Kubicki et al., 2005; Segal et al., 2007). Clearly, new research points to mechanisms outside of the prevailing dopamine hypothesis of schizophrenia that can explain the various symptoms of the disorder.

The decreased exploratory behavior of knockout and heterozygous mice in the open-field chamber suggests a CNS phenotype that may be compatible to the mental retardation of ACCPN patients. It is unlikely that this exploratory difference in mice

results from anxiety, because mice of all three genotypes spent an equal amount of time at the center of the chamber, which is anxiogenic. Despite impairment when challenged on the rotorod and beam, the full knockouts were clearly able to ambulate, albeit abnormally, on flat surfaces. Also, locomotor deficits cannot explain the low exploratory behavior of heterozygous mice that performed as well as wild-type mice in neuromuscular tests. The lack of habituation in both the homozygous and heterozygous mutants suggests that they were not becoming familiar with the environment. Knockout models of Fragile-X syndrome, the most frequent form of hereditary mental retardation, also do not display habituation (Spencer et al., 2006; Van Dam et al., 2005), suggesting cognitive problems. There are other behavioral assays to better test rodent cognitive function, which can be pursued later with the interest in KCC3 expression in neurons of the hippocampus, a region for learning and memory (Boettger et al., 2003; Pearson et al., 2001). For example, spatial learning and memory can be tested in the water maze task developed by Morris et al. in which mice are trained to find a submerged platform in the water using spatial cues around the room, and the latency to find the hidden platform is recorded (Morris et al., 1982). In the dry version of this test called the Barnes maze, which relieves the stress and reliance on swimming ability, mice are motivated to find shelter in one of twenty holes. Just as in the Morris water maze, they are required to use spatial cues to find an escape location, which is the reinforcement (Bach et al., 1995; Seeger et al., 2004).

The open-field test does assess anxiety-related behavior based on the time spent in the center of the chamber (Crawley, 1985; Finn et al., 2003). The expectation that KCC3-null mice would spend more time at the periphery than in the center based their skittish

behavior upon handling was disproved by this test. However, there are other standard tests of fear/anxiety that could be used to test this hypothesis, including the elevated plus maze, which is a robust test of anxiety (Finn et al., 2003). It consists of four-arms, two open and two enclosed and the animals' behavior after placement in the center of the maze, including the frequency of entering and time spent in each arm, are recorded (Finn et al., 2003). The light-dark test in which rodents are first allowed to explore both a large, open, brightly lit chamber and the small, dark, closed chamber of the apparatus also tests anxiety with the number of transitions between the two chambers is the indicator (Bouwknecht & Paylor, 2002; Finn et al., 2003).

KCC3 knockout mice offer new opportunities in studying ACCPN and to understand the loss-of-function effect in the pathogenesis of the disorder as well as the biology of the cotransporter. The logical question is how the lack of KCC3 leads to the behavioral defects presented here. Although the CNS deficits were also intriguing, the fact that initial histological analysis revealed no defects deterred us from pursuing this avenue. The locomotor defects, however, is 100% penetrant in the mouse model and patients, which would likely decrease variability in experiments, and was accompanied by observable peripheral pathology. In that regard, I chose to focus my thesis project on the peripheral neuropathy component of ACCPN.

CHAPTER IV

PERIPHERAL NERVE EXPRESSION OF KCC3

Introduction

KCC3 is expressed in many tissues inside and outside of the nervous system. Initial Northern blot analyses by multiple groups revealed a broad tissue distribution of human KCC3 in kidney, brain, skeletal muscle, heart, placenta, lung, liver, and pancreas, with the highest levels in heart, brain, and kidney (Hiki et al., 1999; Mount et al., 1999). Western blot analysis performed on adult rodent tissues confirmed this broad expression pattern at the protein level (Pearson et al., 2001). Boettger et al. probed whole mice at P0 using *in situ* hybridization and detected KCC3 mRNA in the lung, kidney, and heart as well as nasal epithelium, trachea, esophagus, and stomach (Boettger et al., 2003). What many of these organs share in common is an abundance of epithelial tissues. Although the specific role(s) of KCC3 in epithelial tissues is not known, based on the function of other CCCs in transepithelial transport (i.e., reabsorption/secretion), one can hypothesize that KCC3 participates in ion/fluid secretion like the cystic fibrosis transmembrane conductance regulator (CFTR). If the thermodynamics shift away from physiological conditions, KCC3 could become an influx pathway, like KCC4 in the inner ear.

The importance of KCC3 expression in the nervous system is underlined by the severe CNS and PNS deficits from its loss of function in both mouse and human (Boettger et al., 2003; Dupre et al., 2003; Howard et al., 2002b). Northern and Western blot analyses revealed mRNA and protein expression, respectively, in rodent brain

(Pearson et al., 2001) as did *in situ* hybridization at P0 (Boettger et al., 2002). Specific areas of the brain that were KCC3-positive by immunoblot included the cerebral cortex, hippocampus, diencephalon, brainstem, and cerebellum (Pearson et al., 2001). Immunostaining results from two different anti-KCC3 polyclonal antibodies and LacZ staining of KCC3-null brain tissue from two different knockout models yielded positive signal in hippocampal neurons (Boettger et al., 2003; Pearson et al., 2001). Colorimetric changes were especially strong in CA1 pyramidal neurons compared to CA3 neurons (Boettger et al., 2003; Pearson et al., 2001). The antibodies also stained cerebellar Purkinje cells and large neurons of the cortex and brainstem (Boettger et al., 2003; Pearson et al., 2001). The anti-KCC3 antibody also strongly labeled the base of the choroid plexus epithelium (Pearson et al., 2001). The basolateral membrane of the choroid plexus faces the vasculature, which implicates KCC3 in K^+ reabsorption. The K^+ concentration of cerebrospinal fluid (CSF) secreted by the choroid plexus must be tightly regulated (Jones & Keep, 1987) and this could be mediated by KCC3 for ion reabsorption with NKCC1 coupled to KCC4 on the apical side (Karadsheh et al., 2004). In immunostaining experiments, unlike KCC2, which always is preferentially localized to the plasma membrane (Hubner et al., 2001; Zhu et al., 2005), KCC3 was detected intracellularly as well as on the plasmalemma (Boettger et al., 2003; Pearson et al., 2001). The intracellular localization of KCC3 suggests that the cotransporter may regulate ion movement in internal structures such as the endoplasmic reticulum (ER) and/or Golgi. On the other hand, KCC3 clearly functions at the cellular level, so intracellular KCC3 could represent a pool of proteins not yet trafficked to the plasma membrane. These hypotheses need to be tested in future experiments.

Probes for whole-mount *in situ* hybridization also detected KCC3 mRNA in the spinal cord and DRG in mouse pups at P0 (Boettger et al., 2003). Pearson et al. demonstrated by Western blot that the spinal cord expressed KCC3 at high levels, the DRG showed low expression, while adult peripheral nerves revealed no immunoreactivity (Pearson et al., 2001). In agreement, Boettger et al. also showed that adult sciatic nerves do not express KCC3 (Boettger et al., 2003). Spinal cord white matter tracts were also positive for KCC3 by immunoblotting (Pearson et al., 2001). Other white matter tracts, such as the lateral lemniscus, the main auditory tract located in the brainstem, showed intense KCC3 labeling that colocalized with antibody against 2',3'-cyclic nucleotide 3'-phosphodiesterase (CNPase), an oligodendrocyte-specific marker. There is some controversy, though, about the specific spinal cord localization of KCC3 since Boettger et al.'s antibody was only reactive in grey matter in spinal cord and brain (Boettger et al., 2003). Although this matched their results from their LacZ staining experiments of KCC3-null embryos (E14) and pups (P0), the tissues were from different ages (Boettger et al., 2003).

In the PNS, myelinated axon bundles are not referred to as tracts, but as nerves. The largest peripheral nerve is the sciatic nerve, which carries both motor and sensory fibers. Previous reports indicating the lack of KCC3 expression in sciatic nerves (Boettger et al., 2003; Pearson et al., 2001) appeared inconsistent with the peripheral nerve pathology of $KCC3^{-/-}$ mice and ACCPN patients (Boettger et al., 2003; Dupre et al., 2003; Howard et al., 2002b). To explore this discrepancy, we investigated the expression of KCC3 in peripheral nerves at earlier ages. In order to test our hypothesis

that KCC3 is expressed in the peripheral nerve, we developed primers for RT-PCR and a new anti-KCC3 antibody for Western blot analysis and immunostaining.

Materials and Methods

Animals and genotyping

Animal generation, mating, and genotyping have been described in the previous chapter (Chapter 3).

Semi-quantitative RT-PCR

Total RNA from freshly dissected sciatic nerves and brain (positive control) was extracted using an RNeasy Mini Kit (Qiagen, Valencia, CA) according to manufacturer's instructions, and treated with RQ1 RNase-free DNase (Promega, Madison, WI) to prevent false positive results. Reverse transcription was performed using total RNA, random hexamers as primers, dNTPs, DTT, and Superscript II reverse transcriptase (Invitrogen, Carlsbad, CA). For PCR amplification oligonucleotide primer pairs specific to mouse KCC3 cDNA were synthesized as well as for mouse beta-actin cDNA as a positive control and internal standard:

(1) KCC3 forward 5'-AGCTCAAGGCAGGAAAGGGA-3'

(2) KCC3 reverse 5'-TTGTGTTTCAT GCCTCCGAGG-3'

(3) Actin forward 5'-GTGGGCCGCCCTAGGCACCA-3'

(4) Actin reverse 5'-GATGTCAACGTCACACTTCATGATG-3'

to produce a 765 bp product and 560 bp product, respectively.

Antibody generation

The first 132-amino acids of the C-terminal of mouse KCC3a were fused to GST using the vector pGEX-T (Pharmacia, Piscataway, NJ). The fusion protein was grown in *E. coli* and purified with glutathione-conjugated sepharose beads. Polyclonal antibodies were produced in two New Zealand white rabbits after subcutaneous injections of the GST-peptide (Covance, Denver, PA). Antiserum from one rabbit with high titer was affinity purified by linking the peptide to Affi-gel 15 support (BioRad, Hercules, CA) by incubating the immune serum for two days at 4°C with the Affi-gel-peptide complex. After washing in 5X phosphate-buffered saline (PBS) 5x, specific antibodies were eluted with 0.1 M sodium citrate (pH 2.5), neutralized with 1 M Tris (pH. 8.8) and dialysed in 1X PBS overnight at 4°C. The purified antibody was concentrated by centrifugation in a 30kDa cut-off Centriplus column (Amicon, Beverly, MA), aliquoted, and stored at -20°C. The purified antibody was tested by immunoblot on mouse brain microsomes and lysates from wild-type and KCC3$^{-/-}$ mice. Because the antibody nonspecifically detected a large band (~300 kDa) in both wild-type and knockout, the antibody was further purified using the technique described above with a shorter fragment (amino acids 1-44) of the antigenic GST-peptide to remove nonspecific binding while still detecting the ~155 kDa KCC3 protein band.

Microsomal protein isolation and Western blot analysis

Sciatic nerves and brains were dissected from euthanized mice and homogenized in a sucrose buffer (0.32 M sucrose, 5 mM Tris-HCl, pH 7.5, 2 mM EDTA) with a Teflon pestle. We obtained microsomal protein through successive centrifugations at 3000 g, 10,000 g and 100,000 g. Following resuspension of the high-speed pellet in a 5 mM Tris–HCl, pH 7.5/2 mM EDTA buffer, we determined protein concentrations using the Bradford assay (BioRad, Hercules, CA). Protein samples from microsomes were denatured in SDS-PAGE loading buffer at 75°C for 20 min and separated on a 9% polyacrylamide gel. After the proteins were electroblot-transferred from the gels onto polyvinylidine fluoride membranes (BioRad), the membranes were incubated for 2 h at room temperature (RT) in blocking solution made up of 5% non-fat dry milk in Tris-buffered saline with Tween 20 (TBST). Membranes were then incubated with primary antibody at 1:1000 dilution in blocking solution at 4°C overnight. Following TBST washes (3 h), membranes were incubated in horseradish peroxidase-conjugated anti-rabbit secondary antibody in blocking solution (1:4000; Jackson Immunoresearch, West Grove, PA) for 1 h at RT, and then rinsed for 2 h in TBST. Protein bands detected by antibody were visualized by chemiluminescence using ECL Plus (Amersham Biosciences, Arlington Heights, IL).

Schwann cell cultures

Primary rat Schwann cell cultures were prepared following the method of Yeiser et al. (Yeiser et al., 2004). Sciatic nerves were dissected from P2-P3 rat pups, and following enzymatic digestion with 0.3% collagenase (37°C for 15 min) and 0.25%

trypsin (37°C for 15 min). The trypsin reaction was halted with DMEM with 10% FBS. After applying rat Schwann cell media (DMEM containing 10% FBS, 100 U/ml penicillin, and 100 µg/ml streptomycin), Schwann cells were dissociated by trituration, and pipetted into poly-L-lysine (Sigma, St. Louis, MO) coated 6-well plates. The following day, cultures were treated with Ara-C to remove fibroblasts.

Immunohistochemistry

Dissected spinal cord and dorsal root ganglia from P14 mice were fixed overnight at 4°C in fresh 4% paraformaldehyde, then cryoprotected in 30% sucrose in PBS. The following day, tissues were embedded in Tissue-Tek OCT compound (Sakura Finetek, Torrance, CA), frozen, sectioned into 12 µm thick slices on a Leica cryostat, and thaw mounted onto Superfrost Plus slides (Fisher Scientific, Pittsburg, PA). After drying, sections were washed in PBS, permeabilized with 1% SDS in PBS, blocked for 1 h in 1% BSA/5% goat serum in PBS, and then incubated overnight with purified polyclonal KCC3 antibodies (see above) in blocking solution (1:200) at 4°C. Antibody-treated sections were washed in PBS and incubated in Cy3-conjugated mouse anti-rabbit antibody (1:800) for one hour at RT. Following PBS washes, sections were mounted in VectaShield (Vector Laboratories, Burlingame, CA), coverslipped, and sealed. Teased sciatic nerves from P8 $KCC3^{+/+}$ and $KCC3^{-/-}$ pups were immunostained as described by Boyle et al (Boyle et al., 2001), but with anti-KCC3 antibody (1:200) and Cy3-conjugated goat anti-rabbit secondary antibody (1:800). Fluorescence signal was visualized using a Carl Zeiss LMS 510 META confocal microscope.

Results

KCC3 transcript in sciatic nerves, Schwann cells, and DRG

Although previous reports indicated a lack of KCC3 expression in sciatic nerves (Boettger et al., 2003; Pearson et al., 2001), there remained the possibility that KCC3 is expressed by peripheral nerves at earlier ages and that the sciatic and sural nerve pathology of $KCC3^{-/-}$ mice and ACCPN patients, respectively (Howard et al., 2002b), stemmed from a lack of KCC3 function during development. In fact, there are several proteins that are upregulated early in life in the peripheral nerve, then diminish or disappear altogether. For example, the voltage-gated sodium channel Nav1.2 is expressed by peripheral nerve axons during development at P1 and P2.5, but by P7 is replaced by Nav1.6 (Baker, 2002; Rios et al., 2003). Myelinating Schwann cells lose the p75 neurotrophin receptor after development and, later, it is only upregulated after injury (Song et al., 2006). Based on the early onset of the neuromuscular problems in KCC3-null mice (~2 weeks) that corresponds to ACCPN patients who all develop symptoms during infancy/toddlerhood, we hypothesized that KCC3 is expressed postnatally during peripheral nerve development. To test our hypothesis, we first designed primers and utilized RT-PCR to investigate KCC3 expression in the sciatic nerve at different ages since only adult, E14, and P0 were previously assessed (Boettger et al., 2003; Pearson et al., 2001). The sciatic nerve was used as a prototypical peripheral nerve model, not only because it is the largest and most amenable to clean dissection without bleeding, but also because it is most relevant to the peripheral neuropathy as its branches innervates the legs. We extracted RNA from sciatic nerves of P2, P5, P14, and adult mice for semi-quantitative RT-PCR. KCC3 mRNA was present at ages P2 through P14 while KCC3

transcript was undetectable in adult sciatic nerve (Figure 4-1A). Sciatic nerves from age P7, P10, and P12 were also positive for KCC3 transcript (data not shown). The lack of KCC3 in adult sciatic nerves is in agreement with previous reports.

To investigate whether the Schwann cell component of the peripheral nerve expresses KCC3, we established primary Schwann cell cultures from P3 rat pup sciatic nerves, and performed RT-PCR with RNA extracted from these cells. Cultured Schwann cells were positive for KCC3 transcript (Figure 4-1B). It has been previously shown that both PNS and CNS neurons express KCC3 (Boettger et al., 2003; Pearson et al., 2001), so as expected, RT-PCR results confirmed that rat DRG were positive for KCC3 mRNA (Figure 4-1C).

KCC3 protein expression in sciatic nerves

After developing and purifying a new KCC3 antibody, we were able to further test our hypothesis that the peripheral nerves express KCC3 protein during development. Since KCC3 is a membrane-bound protein, we isolated microsome fractions from freshly dissected sciatic nerves to enrich for membrane proteins from both plasma and intracellular membranes. Microsomal proteins were separated on SDS-polyacrylamide gels and immunoblotted using the polyclonal anti-KCC3 antibody. No band was apparent for adult sciatic nerves, but P4 sciatic nerve was positive for KCC3 protein, while the ~155 kDa band was barely detectable at P15 (Figure 4-1D). These results confirmed the RT-PCR data.

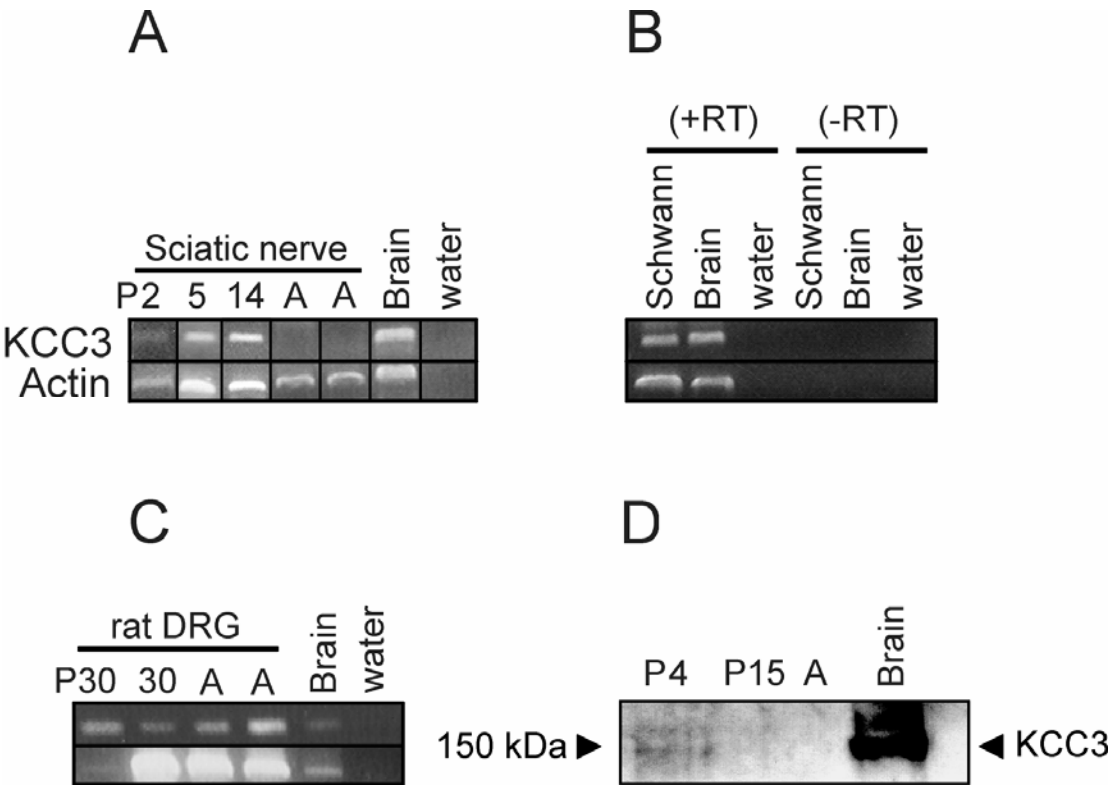

Figure 4-1. KCC3 is detected in sciatic nerves by semiquantitative RT-PCR and Western blot analysis

(A) Sciatic nerves from mouse pups (P2, P5, P14) but not adult are positive for KCC3 transcript. Mouse brain mRNA is used as positive control for KCC3, and actin primers are used as positive control for the PCR. Reactions with water (no cDNA) are negative. (B-C) KCC3 transcript is identified in rat cultured Schwann cells and rat DRG. Reactions without reverse transcriptase enzyme (-RT) are negative, indicating no DNA contamination. (D) Immunoblotting shows KCC3 protein expression in microsomes isolated from sciatic nerves at age P4, which are barely perceptible at P15, and undetectable in adult. Each lane was loaded with 35 µg microsomal protein, except for mouse brain positive control with 70 µg microsomal protein.

To determine whether axons and/or Schwann cells express KCC3, we designed an anti-KCC3 antibody. After purification and testing for specificity, we utilized it to immunostain teased sciatic nerve fibers. Using confocal microscopy, we found that in teased fibers from P8 wild-type mice, KCC3 signal localized to Schwann cell bodies, appearing like beads on a string (Figure 4-2A, B). Secondary antibody yielded no signal (Figure 4-2C) although Schwann cell bodies could be distinguished as rounded protrusions along the fibers (4-2D). At higher magnification we found that the staining was predominantly perinuclear (Figures 4-2E, F). Optical sections through Schwann cells and axons showed signal on Schwann cell body membranes and perinuclear regions, but not within nuclei, axons, and not along the axolemma. Only Schwann cell bodies exhibited strong staining, and KCC3 was not detected in specific subcellular regions of myelin or axon such as Schmidt-Lanterman incisures, nodes, juxtaparanodes, or paranodes. For immunostaining experiments, tissues from $KCC3^{-/-}$ littermates served as negative controls. $KCC3^{-/-}$ sciatic nerves (Figure 4-2G, H), which were processed at the same time, exhibited no staining. KCC3 staining of DRG neurons, which were identified morphologically, was localized both to the plasma membrane and intracellularly (Figure 4-2I, J). As expected, KCC3 is expressed by the cell bodies of peripheral axons since KCC3 has been shown to be expressed in both spinal motor and DRG neurons throughout early development and into adulthood (Boettger et al., 2003).

Discussion

Although previous studies reported lack of KCC3 expression in E14, P0, and adult sciatic nerve (Boettger et al., 2003; Pearson et al., 2001), we show here that KCC3

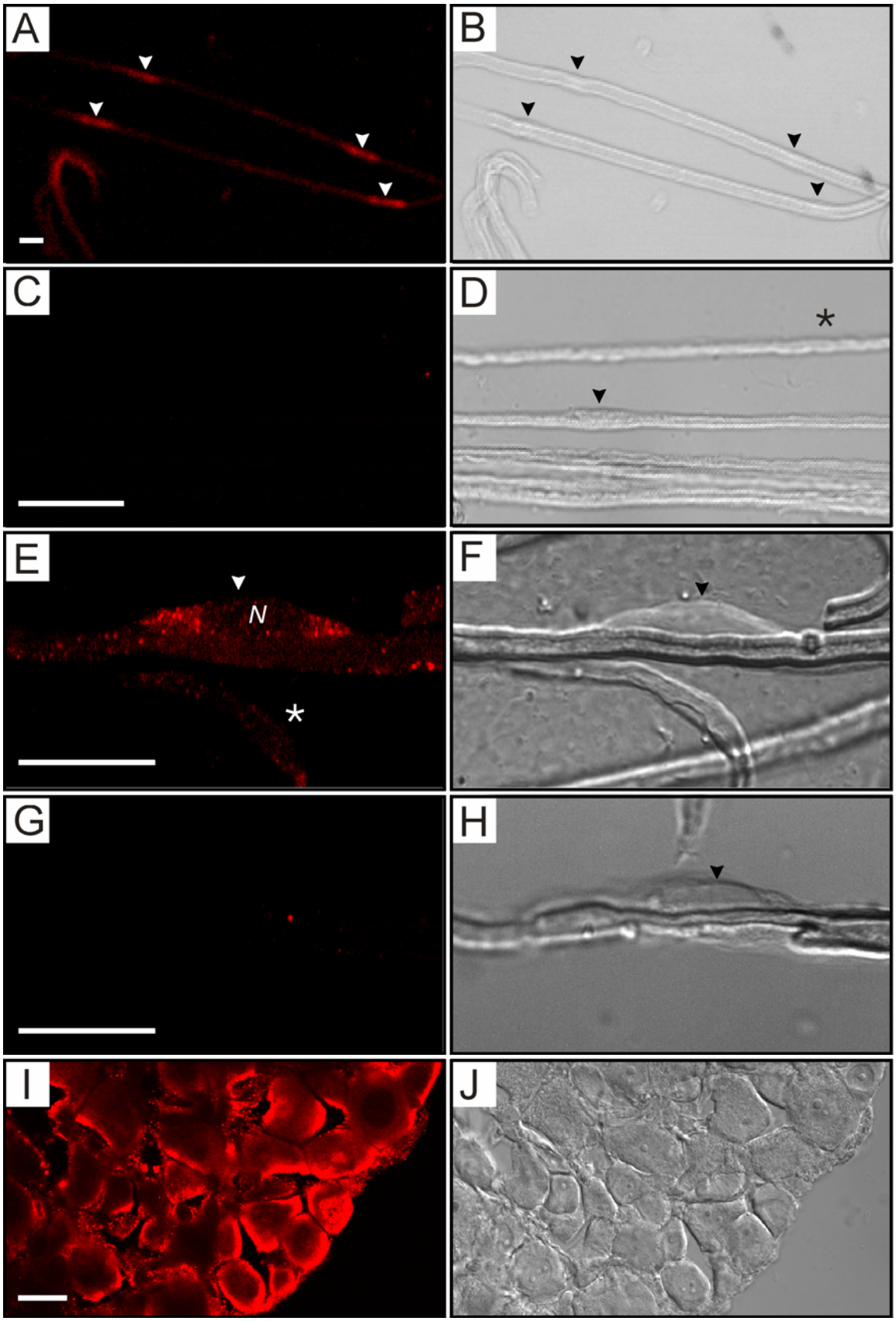
A
B
C
D
E
N
F
G
H
I
J

Figure 4-2. **Positive immunolabeling of Schwann cells and DRG neurons**

(A) KCC3 immunostaining (red) of teased sciatic nerve fibers from wild-type mice at P8 shows punctate staining of Schwann cell bodies (arrowheads). (B) In the corresponding DIC image, arrowheads point to Schwann cell bodies, which appear as rounded protrusions along the fiber exterior. (C) Control panel, immunostaining with Cy3 secondary antibody alone, gives no signal. (D) Corresponding DIC image with arrowhead pointing to a Schwann cell body. (E) At higher magnification, the immunofluorescence shows a predominantly perinuclear distribution in the Schwann cell body. N = nucleus. This image reflects one plane of the confocal Z-stack. The asterisk denotes a Schwann cell body lying in a different plane. (F) Corresponding DIC image. (G) Control panel, immunostaining of $KCC3^{-/-}$ fibers show absence of signal. (H) Corresponding DIC image. (I) Cryosectioned DRG (12 µm) shows strong KCC3 signal in sensory neurons. (J) The corresponding DIC image displays distinctive morphology of individual neurons. Scale bars = 20 µm.

is expressed in sciatic nerves of juvenile mice and by Schwann cells. We also confirmed its expression in sensory neurons. Although we did not detect KCC3 staining in axons, we cannot rule out axonal expression since it may be at levels below detection sensitivity of our methods. Only immuno-gold electron microscopy would provide enough resolution to immuno-localize KCC3 protein at low levels. In addition to membrane staining, our results demonstrated intracellular localization of KCC3, which matches other immunostaining results in multiple cell types and non-heterologous systems (i.e., *Xenopus* oocytes) (Boettger et al., 2003; Howard et al., 2002b; Mercado et al., 2005; Pearson et al., 2001). One question that arises from the consistent intracellular staining of KCC3 is whether it functions in organelles. Multiple types of ion channels function in intracellular compartments, such as the well-studied Ca^{2+} channels of the endoplasmic/sarcoplasmic reticulum. Also, mitochondria express ion channels (e.g., K^+, Ca^{2+}) and exchangers (e.g., Na^+/Ca^{2+}, K^+/H^+) for ion homeostasis and proton accumulation (Bernardi, 1999). Also, the chloride channels CLC3-7 all localize to lysosomes to acidify vesicles either by acting as an electrogenic Cl^-/H^+exchanger or through an unknown mechanism, and their disruption leads to lysosomal diseases (Jentsch et al., 2005; Poet et al., 2006). KCC3 expression by various organelles can be established through immuno-gold EM and double immunostaining with specific markers for each compartment. Although it is possible that KCC3 acts at the endoplasmic reticulum (ER) or Golgi levels, this has not been investigated since KCC3 is certainly active on the plasma membrane under stimulating conditions (Hiki et al., 1999; Mount et al., 1999; Race et al., 1999) and lack of KCC3 impairs RVD at the cellular level (Boettger et al., 2003). All membrane proteins traffick through the ER and Golgi for

processing though. Whether cellular stress recruits KCC3 to the plasma membrane is a hypothesis that needs to be explored. This can be achieved through studies in heterologous systems, like *Xenopus* oocytes, utilizing fluorescently tagged KCC3 for microscopy and immunoblotting, or through biotinylation experiments.

In the peripheral nerves, regulation of ions is crucial for action potential conductance, resting membrane potential, and numerous signaling pathways. Both axons and myelinating Schwann cells, cultured and *in vivo*, express Na^+, K^+, Ca^{2+}, and Cl^- channels (Baker, 2002). Of particular interest to us is the regulation of potassium ions by Schwann cells since that may give us a clue to why KCC3 is expressed by Schwann cells as well as a larger understanding of potassium control. Although the Na-K ATPase maintains the differential Na^+ and K^+ gradients in Schwann cells (Kofuji & Newman, 2004), K^+ channels are necessary for the maintenance of the resting membrane potential, and experiments support that Schwann cell K^+ channels siphon potassium ions released from the internode into the periaxonal space after action potentials (Baker, 2002; Kofuji & Newman, 2004; Konishi, 1990). At least two K^+ channel sub-types, Kir and Kv1, are positioned in locations—Schwann cell microvilli and paranodal loops—that could serve in an uptake and spatial buffer circuit (Baker, 2002). In fact, Kir channels possess the biophysical property of increased conductance with increasing extracellular potassium concentrations, which supports such a role (Kofuji & Newman, 2004). Ransom et al., however, demonstrated in the optic nerve that the glial Na-K ATPase is responsible for the K^+ uptake since blocking Ba^{2+}-sensitive K^+ channels and NKCC had no effect (Ransom et al., 2000). Despite the controversy over the specific mechanism, excess K^+ is indeed cleared from the periaxonal space by glia (Frankenhaeuser & Hodgkin, 1956;

Ransom et al., 2000). Although gap junctions, which are formed by connexin proteins in myelinating Schwann cells, are not ion channels or transporters, they serve as conduits for ions and small molecules. Based on the localization of Cx32 and the periaxonal swelling that develops in Cx32-null peripheral fibers, the current model relates the fluid accumulation to defects in the uptake and transport of K^+ ions, and thus fluid, from the periaxonal space through incisures, similar to the model for Cx32/47 mutants (Baker, 2002; Kofuji & Newman, 2004; Menichella et al., 2006; Scherer et al., 1998). It seems logical to surmise that after uptake by the Na-K ATPase, K^+ channels, and possibly NKCC1, K^+ is carried through SLIs via Cx32 gap junctions since this path of uncompacted myelin is a route to the cell body for storage or release. Although theoretically, KCC3 can act as an uptake pathway under favorable thermodynamic settings, its normal function and localization supports a possible role in ion/fluid extrusion from the Schwann cell. Three possible roles of Schwann cell KCC3, based on its localization, include RVD counteracting ionic/osmotic stress, volume regulation related to cell motility and proliferation, and/or extrusion of cytoplasm during myelin compaction.

It is intriguing that KCC3 expression in the sciatic nerve is high at young ages and disappears by adulthood since the opposite occurs in the brain with the highest levels in adult tissue (Pearson et al., 2001). The temporal expression pattern suggests that the cotransporter may be involved in peripheral nerve development. From its early expression, which overlaps with the onset of the myelination process, it is tempting to hypothesize that KCC3 plays a role in Schwann cell development and/or the myelination process itself. As an ion/fluid extrusion mechanism, we proposed that KCC3 may play a

role in myelin compaction, although there are other possibilities related to cell volume regulation, including Schwann cell motility and proliferation. If our proposal that KCC3 plays a role in myelin compaction were correct, we would expect to find defects in compact myelin in KCC3-null sciatic nerves, such as splitting between lamellae and demyelination due myelin sheath instability. Problems in Schwann cell motility and proliferation would lead to hypomyelination. Our hypothesis that the peripheral neuropathy is a myelinopathy due to Schwann cell defects needed to be tested through electron microscopy and morphometric analysis.

CHAPTER V

MORPHOMETRICAL AND ULTRASTRUCTURAL ANALYSIS OF KCC3$^{-/-}$ SCIATIC NERVE

Introduction

Thin myelin sheaths in adult vertebrate peripheral nerves, particularly around large axons, often suggests a defect Schwann cell development, myelin ensheathing and/or compaction process that causes sheaths to be abnormally thin, or hypomyelinated (Hu et al., 2006; Michailov et al., 2004; Runker et al., 2004; Warner et al., 1996; Willem et al., 2006). Preliminary analysis of toluidene blue stained KCC3 knockout sciatic nerve cross sections by light microscopy revealed large axons with thin myelin sheaths and myelin debris. Therefore, we hypothesized that KCC3 expressed by Schwann cells is involved in the myelination process. A role in myelin compaction appeared to be an attractive proposal since cytoplasm extrusion is part of the compaction process. It may work alongside with P0, a structural/adhesion molecule, which is thought to actively promote compaction. In fact, some mutations in *mpz* led to hypomyelination (see Chapter 2). Based on our hypothesis of primary Schwann cell involvement, I predicted that KCC3 knockout nerves would exhibit myelin abnormalities.

Besides congenital defects, thin myelin in adult nerves is also characteristic of regenerating axons after damage (Smith et al., 1982). However, regenerating axons are small in diameter, and preliminary light microscopy analysis of KCC3-null sciatic nerves revealed large axons with thin myelin sheaths (Figure 5-1). Taken together with the early

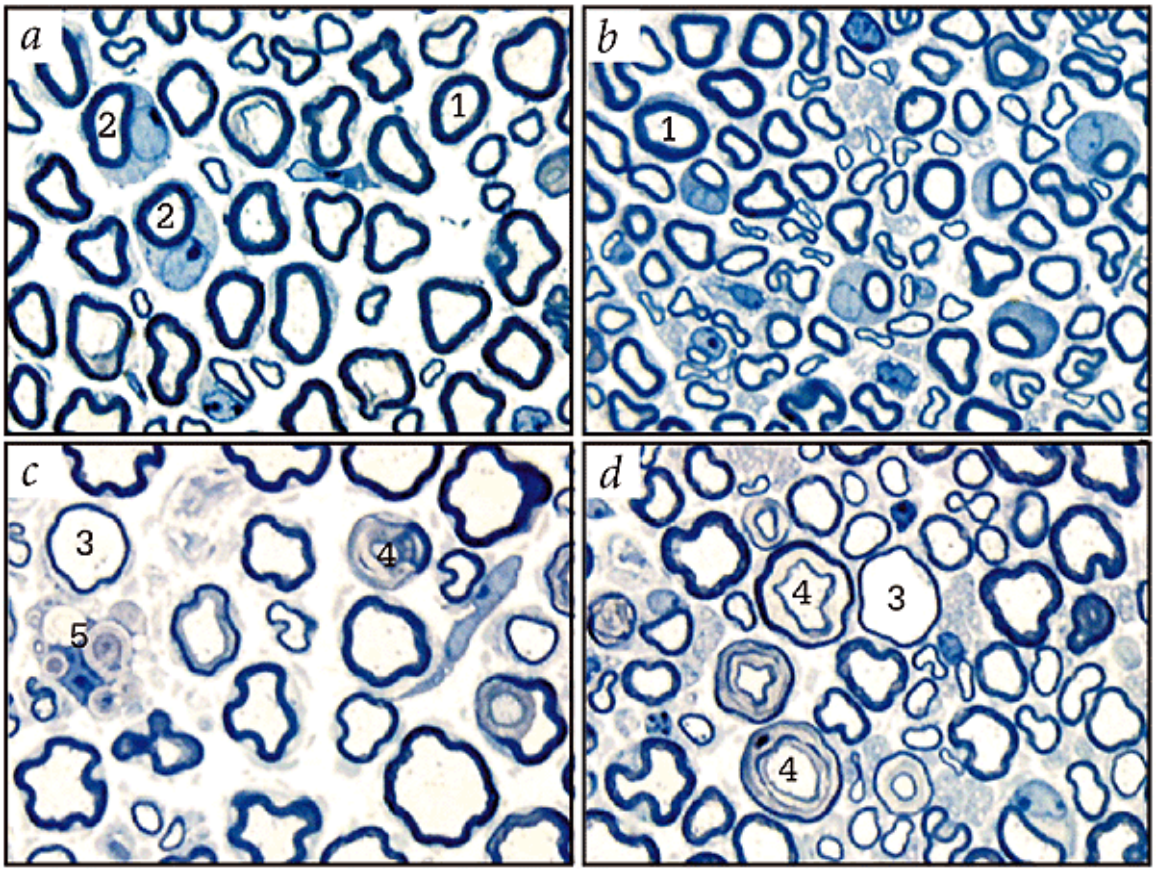

Figure 5-1. Thin myelin sheaths and myelin deposits in KCC3-null sciatic nerves

Thick sections (1 micron) of adult sciatic nerve from wildtype (A,B) and KCC3 homozygous mutant (C, D) mice. In wildtype mice, large axons exhibit a thick myelin coating (1). Note sections cut randomly through Schwann cells (2). In KCC3-null mice, however, the larger axons have a thinner myelin layer (3) than for wild-type axons of similar size. Although control nerves also display ring-like structures (4) the mutant showed many more. In the knockout, there are numerous myelin deposits, indicating degeneration (5). Three mice of each genotype were analyzed and yielded similar morphologies.

expression of KCC3 in sciatic nerves and early onset neuromuscular deficits in ACCPN patients and our mouse model, we hypothesized that the lack of KCC3 in peripheral nerves during postnatal development leads to hypomyelination. Adult KCC3-null nerves also contained myelin debris, likely in macrophages (Figure 5-1), that could be indicative of unstable myelin, so we believed that a reasonable alternative to our hypothesis of ACCPN/KCC3-null peripheral nerve pathology could be demyelination due to sheath instability. There were few redundant basal lamina, definitely not in layers, and not prominent in the light micrographs, but this observation would have to be confirmed through EM.

Based on the early KCC3 expression by Schwann cells during development and our preliminary data of $KCC3^{-/-}$ sciatic nerve pathology, we asked if KCC3 is involved in the myelination process: segregation of axons, ensheathement, myelin formation, and myelin compaction. To determine the role of KCC3 in peripheral nerve growth and maintenance and follow the pathogenesis of $KCC3^{-/-}$ sciatic nerves, we quantitatively compared these processes in $KCC3^{-/-}$ and wild-type mice by utilizing electron microscopy to conduct morphometric and ultrastructural analyses. Since Rozsa et al.'s 1950 report "The electron microscopy of sectioned nerve" in *Science*, EM has been utilized for analyzing the development and pathology of peripheral nerves and central tracts (Rozsa et al., 1950). Even in the most recent studies on peripheral neuropathy, EM has been utilized for neuropathological analysis to study the disorders (Chow et al., 2007; Stendel et al., 2007). In cross-section, myelin appears as a multilamellar structure circling axons, and software, such as ImageJ, can semi-automatically measure the area of an axon (area within the myelin sheath) and fiber (area of axon plus the myelin sheath) since the high

contrast from osmium tetroxide staining allows the software to distinguish myelin, stained black, from other regions. From this data we extrapolated diameters under the assumption that the fiber cross-sections were exact circles. The high magnification and resolution of EM allowed us to the compare ultrastructure of axons and unequivocally distinguish different cell types—including fibroblasts, Schwann cells, neutrophils, and macrophages—and organelles (mainly nuclei and mitochondria). Schwann cells are not only distinguished by their morphology and association with axons, but also by basal lamina, which only Schwann cells secrete. Peripheral nerve cells and their sub-structures cannot be easily distinguished with light microscopy. Although morphometric analysis can be conducted at the light microscope level after staining with a myelin contrast agent, such as toluidene blue, ultrastructural analyses are less accurate.

Using EM to analyze nerves at different ages can help distinguish the onset, pathogenesis, and type of neuropathy, which ultimately can help in developing appropriate therapies. For example, the pathology of CMT1B-affected peripheral nerves (quadriceps nerve) from adult mutant mice included many abnormal profiles, including thin myelin, tomacula (hypermyelination with myelin infoldings) as well as naked axons. However, by following the development of the peripheral nerve from P4 into adulthood, Runker et al. showed that the disorder actually begins as a dysmyelinating neuropathy (Runker et al., 2004). As explained in Chapter 2, many demyelinating diseases develop into axonal neuropathies; these changes have been elucidated by analyzing nerves from animal models and human patients, mainly through EM. Thus, it is critical to follow the pathogenesis of the disorder from early ages, not only to help determine the initial role of

the protein of interest and the primary pathology, but also to help develop treatments at different stages of the disease.

Materials and Methods

Animals

Animal generation, mating, and genotyping have been described in Chapter 3.

Transmission Electron Microscopy (TEM)

Deeply anesthetized adult mice were perfused intercardiacally with 0.1M sodium cacodylate buffer followed by 2.5% glutaraldehyde in sodium cacodylate. Sciatic nerves were dissected and post-fixed in fresh glutaraldehyde, then processed by the Vanderbilt EM Core. Nerves were washed in 0.1M sodium cacodylate buffer, post-fixed in 1% osmium tetroxide for 1 h, rinsed with sodium cacodylate buffer 3x 5 min, then dehydrated through an ethanol series (50% 5 min, 75% 15 min, 95% 2x 15 min, 100% 3x 20 min). Resin (1/2 propylene oxide-1/2 Spurr) was placed in a vacuum oven (18 psi) overnight, then changed into fresh Spurr and returned to the vacuum oven for 2 h. Samples were embedded in Spurr resin and incubated at 60°C for 24-48 h. Thick sections (500 nm) were examined after toluidine blue staining. For TEM, ultra-thin sections (80 nm) were placed on copper grids (Electron Microscopy Science, Hatfield, PA), and stained with uranyl acetate and lead citrate. Samples were viewed using a Philips CM-12 transmission electron microscope at 80kV. Photomicrographs for morphometric analysis were taken at 2650 magnification, by systematically covering adjacent but non-overlapping fields.

Morphometric analysis

Using TEM photomicrographs at 2650 magnification, we measured the diameters of sciatic nerve axons and fibers (axon and myelin sheath) using the free image analysis software ImageJ (NIH, http://rsb.info.nih.gov/ij/). Photomicrograph frames that were only partially filled with fascicle, wrinkled, or damaged were excluded from the analysis. Images were thresholded to allow the software to digitally trace inside the myelin sheath to measure axon area and outside the myelin sheath to measure the area of the entire fiber. Diameters were extrapolated from areas under the assumption that fibers were perfect circles, and G ratios (axon diameter/fiber diameter) were calculated. The numbers of myelinated, unmyelinated, and partially myelinated axons were also tallied. Periaxonal/intramyelinic fluid accumulation was also counted. At P8 and P30, proximal (location where the nerve exits the spinal cord) and distal (the bifurcation into separate tibial and peroneal components at the knee) sciatic nerve regions were morphometrically evaluated.

Statistics

Comparisons between two genotypes in the evaluation of morphometric data (for axon diameter and G ratio means) from $KCC3^{+/+}$ and $KCC3^{-/-}$ mice at P3 and 7-8 months were made using unpaired t-tests. Group statistical differences for morphometric data for proximal and distal $KCC3^{+/+}$ and $KCC3^{-/-}$ sciatic nerves at P8 and P30 were analyzed using one-way analysis of variance (ANOVA) followed by multiple comparison using the Tukey post test. We used GraphPad Prizm software (GraphPad Software Inc., San Diego, CA) for all of our statistical analyses. $P < 0.05$ was considered significant.

Results

Mutant mice initiate myelination correctly but axons are enlarged

At P3, just after the onset of myelination, $KCC3^{-/-}$ Schwann cells had essentially correctly segregated all large-caliber axons in a 1:1 relationship, and myelination was proceeding as in $KCC3^{+/+}$ littermates (Figure 5-2A, B). $KCC3^{-/-}$ nerve cross-sections appeared normal and undistinguishable from those of wild-type in EM photomicrographs, although the average axon diameter was larger for $KCC3^{-/-}$ mice (Table 5-1, Figure 5-2C, D). The increased mean diameters of $KCC3^{-/-}$ axons were due to a shift in the entire population of axons, which is graphically indicated by the histogram shift to the right (Figure 5-2C). There was no significant difference between mean G ratios at this age (Table 5-1) and G ratio scatter plots did not indicate hypomyelination (Figure 5-2D). On G ratio-axon diameter scatterplots, general hypomyelination would be represented as an upward shift of the entire regression line (Hu et al., 2006; Michailov et al., 2004), which is an increase in the y-intercept value without intersection of the regression lines being compared.

Possible explanations for increased axonal caliber between littermates include advanced development or swelling. To check whether sciatic nerve development was proceeding faster in $KCC3^{-/-}$ mice, we tallied the numbers of completely myelinated, partially myelinated, and segregated but unmyelinated axons (axons in Remak bundles were not counted), since a more mature nerve should have a higher ratio of myelinated axons. We found no difference between the two genotypes (Figure 5-2E), thus conclude that nerve development is not expedited, but rather, $KCC3^{-/-}$ axons are larger due to swelling. Equivalent densities of myelinated and total axons between wild-type and

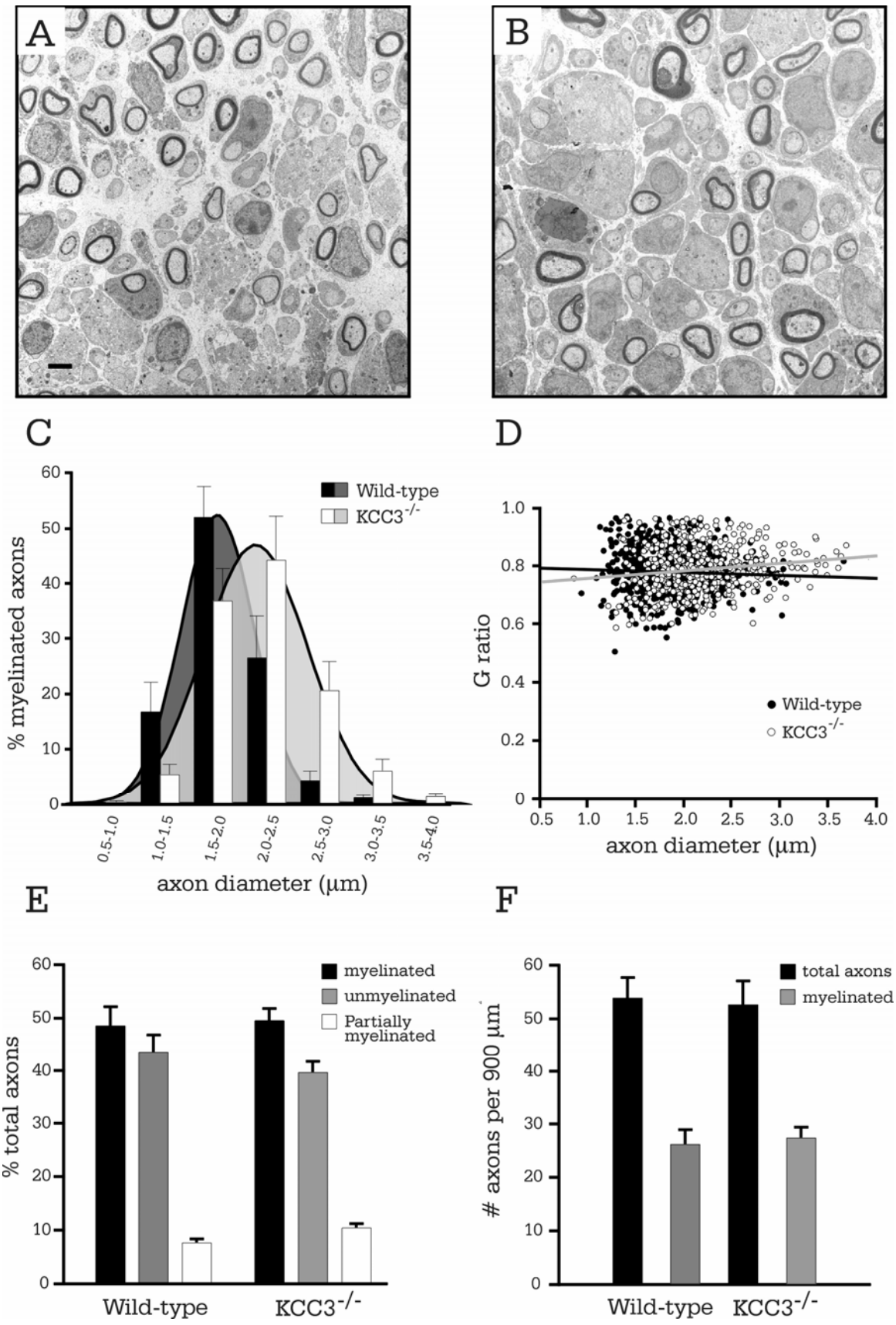
A
B
C
% myelinated axons
Wild-type
KCC3-/-
0.5-1.0
1.0-1.5
1.5-2.0
2.0-2.5
2.5-3.0
3.0-3.5
3.5-4.0
axon diameter (μm)
D
G ratio
Wild-type
KCC3-/-
axon diameter (μm)
E
% total axons
myelinated
unmyelinated
Partially myelinated
Wild-type
KCC3-/-
F
axons per 900 μm
total axons
myelinated
Wild-type
KCC3-/-

Figure 5-2. Normal myelination in P3 KCC3$^{-/-}$ sciatic nerves but axons are enlarged

(A) Electron micrograph of P3 KCC3$^{+/+}$ and (B) KCC3$^{-/-}$ fibers are undistinguishable. Scale bar = 2μm. (C) Histogram analysis of axon diameter distributions reveals a shift to larger calibers for KCC3$^{-/-}$ axons. (D) G ratios are plotted as a function of axon diameter for both wild-type and KCC3$^{-/-}$ fibers. Note the increased size of the KCC3$^{-/-}$ axon population. (E) The percentage of myelinated, partially myelinated, and segregated unmyelinated (excluding Remak bundles) axons do not differ between wild-type and KCC3$^{-/-}$ mice. (F) The number of myelinated axons and total axons per unit area (axonal densities) are also equivalent between the two genotypes. (N = 4 per genotype)

Table 5-1. Morphometric data of KCC3 sciatic nerves

	N	Total myelinated fibers	Axon diameter (um)	G ratio	% periax. fluid
P3					
KCC3+/+	4	600	1.87 ± 0.09	0.774 ± 0.008	0
KCC3-/-	4	467	2.19 ± 0.09	0.783 ± 0.021	0.22
P value			0.0395 (s)	0.713 (ns)	
P8 Proximal					
KCC3+/+	7	1752	2.00 ± 0.34	0.699 ± 0.005	0
KCC3-/-	4	1131	2.24 ± 0.64	0.689 ± 0.007	1.23 ± 0.48
P value			< 0.05 (s)	> 0.05 (ns)	
P8 Distal					
KCC3+/+	4	1296	1.81 ± 0.07	0.665 ± 0.008	0
KCC3-/-	4	1128	2.18 ± 0.09	0.701 ± 0.007	2.55 ± 0.67
P value			< 0.05 (s)	< 0.05 (s)	
P30 Proximal					
KCC3+/+	3	1227	2.89 ± 0.10	0.645 ± 0.0020	0
KCC3-/-	3	710	3.93 ± 0.31	0.697 ± 0.0038	4.57 ± 2.3
P value			<0.05 (s)	<0.001 (s)	
P30 Distal					
KCC3+/+	3	2456	3.25 ± 0.13	0.651 ± 0.0012	0
KCC3-/-	3	1898	3.18 ± 0.23	0.675 ±0.0018	5.53 ± 3.8
P value			>0.05 (ns)	<0.001 (s)	
7-8 months					
KCC3+/+	2	498	3.86 ± 0.86	0.65 ± 0.0056	0
KCC3-/-	2	473	3.93 ± 0.10	0.67 ± 0.0097	1.14 ± 0.46
P value			0.61 (ns)	0.17 (ns)	

(ns) not significant; (s) significant

KCC3$^{-/-}$ sciatic nerves (Figure 5-2F) indicated that axon migration and numbers were normal. KCC3 is not necessary for Schwann cell migration, axon segregation, or initiation of myelination either, as this was occurring as in wild-type, although we cannot rule out subtle changes in KCC3$^{-/-}$ nerves.

KCC3$^{-/-}$ fibers accumulate fluid

We analyzed P8 sciatic nerves at two regions: (1) the location where the nerve emanates from the spinal cord, which we labeled as proximal (Figure 5-3A, B); and (2) the bifurcation into separate tibial and peroneal components at the knee, which we labeled as distal (Figure 5-3C, D). The most striking ultrastructural finding was the presence of significantly enlarged fibers in mutant nerves (Figure 5-3D). Examination of electron micrographs revealed that these enlarged fibers were not due to enlarged axons, but rather, to the widening of the periaxonal space that is electron-transparent and presumably fluid-filled. The denser neurofilament and microtubule packing in affected fibers may be due to degeneration or compression. Myelinated fibers of both distal and proximal sciatic nerve were affected (2.55 ± 0.67% and 1.23 ± 0.48 %, respectively) (see Table 5-1). We observed different degrees of severity or stages of fluid filling in the periaxonal space (Figures 5-3E-H) while intramyelinic fluid (data not shown) was rare. Some affected fibers contained myelin debris (Figure 5-3E, G). Clearly the periaxonal space has expanded beyond its normal spacing of 12 to 14 nm (Trapp et al., 1984). The fluid in the periaxonal space separated the axolemma from the Schwann cell, but surprisingly, the myelin remained intact and accommodated the fluid build-up. Although internal myelin figures and debris were found in both wild-type and mutant fibers (Figure

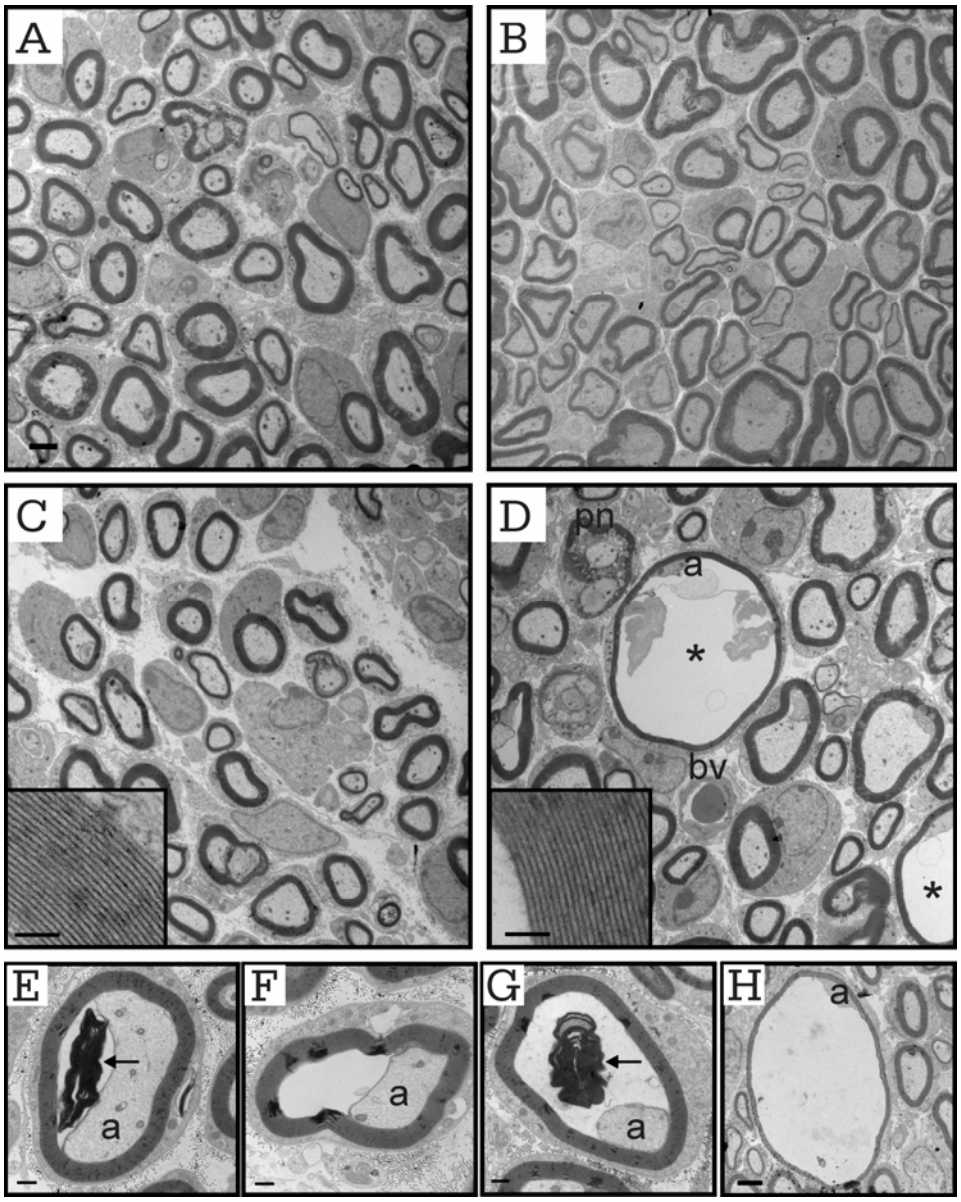

Figure 5-3. P8 KCC3$^{-/-}$ fibers exhibit abnormal periaxonal fluid accumulation

Electron micrographs of proximal sciatic nerve from wild-type (A) and mutant (B) mice. Electron micrographs of distal sciatic nerves of wild-type (C) and KCC3$^{-/-}$ (D) mice. Scale bar = 2 m. Myelin compaction in mutant fibers (D, inset) is undistinguishable from that of wild-type (C, inset, scale bar = 500 nm). (D) Fibers with periaxonal fluid accumulation appear only in KCC3$^{-/-}$ nerves (asterisk). Note that even though the axon is still attached to the Schwann cell, it has lost most of its glial contacts. (E-H) Varying stages or degrees of severity of the abnormal fluid accumulation, which appear as an electron transparent region, in distal KCC3$^{-/-}$ sciatic nerve fibers. Scale bar = 500 nm. Note the presence of myelin debris (arrows) in the periaxonal space (E, G). These abnormal profiles were never seen in wild-type sciatic nerves. a = axon; pn = paranodes; bv = blood vessel.

5-3E), control nerves never showed periaxonal or intramyelinic fluid accumulation. Ultrastructurally, there were no visible defects in compact myelin in mutant mice, indicating normal compaction as in wild-type (Figure 5-3C, D).

Although most KCC3$^{-/-}$ fibers surrounding those with periaxonal swelling appeared qualitatively normal, our morphometry results indicate a subtle but significant defect. Mean axon diameters were larger for KCC3$^{-/-}$ axons compared to wild-type in both regions (Table 5-1). The general enlargement of the entire population of KCC3$^{-/-}$ axons indicated by the histogram shift and G ratio-axon diameter scatterplot was less prominent in proximal (Figure 5-4A, B) than in distal nerve (Figure 5-4C, D). The higher mean G ratio of distal KCC3$^{-/-}$ fibers than in wild-type (Table 1) is reflected by the steeper G ratio scatter plot regression slope (Figure 5-4D). Since KCC3$^{-/-}$ axons at this age are of larger calibers as a population, there is no hypomyelination *per se,* even though the mean G ratio is higher, because the appearance of thin myelin stems from the fact that axon enlargement skews G ratios to higher values. However, mean G ratios were similar between mutant and wild-type fibers in proximal sciatic nerve. Note that fibers with periaxonal fluid swelling were not included in any G ratio plots, histograms, or calculations for mean axon diameters and G ratios since we were investigating underlying pathologies in KCC3$^{-/-}$ fibers with normal appearances.

KCC3$^{-/-}$ young adult nerves

At P30, sciatic nerve fibers or mutant mice continued to exhibit increased axon diameters and periaxonal fluid pathologies, unlike wild-type fibers (Figure 5-5A-D). We observed a few signs of myelin deterioration in knockout nerves, such as myelin-laden macrophages,

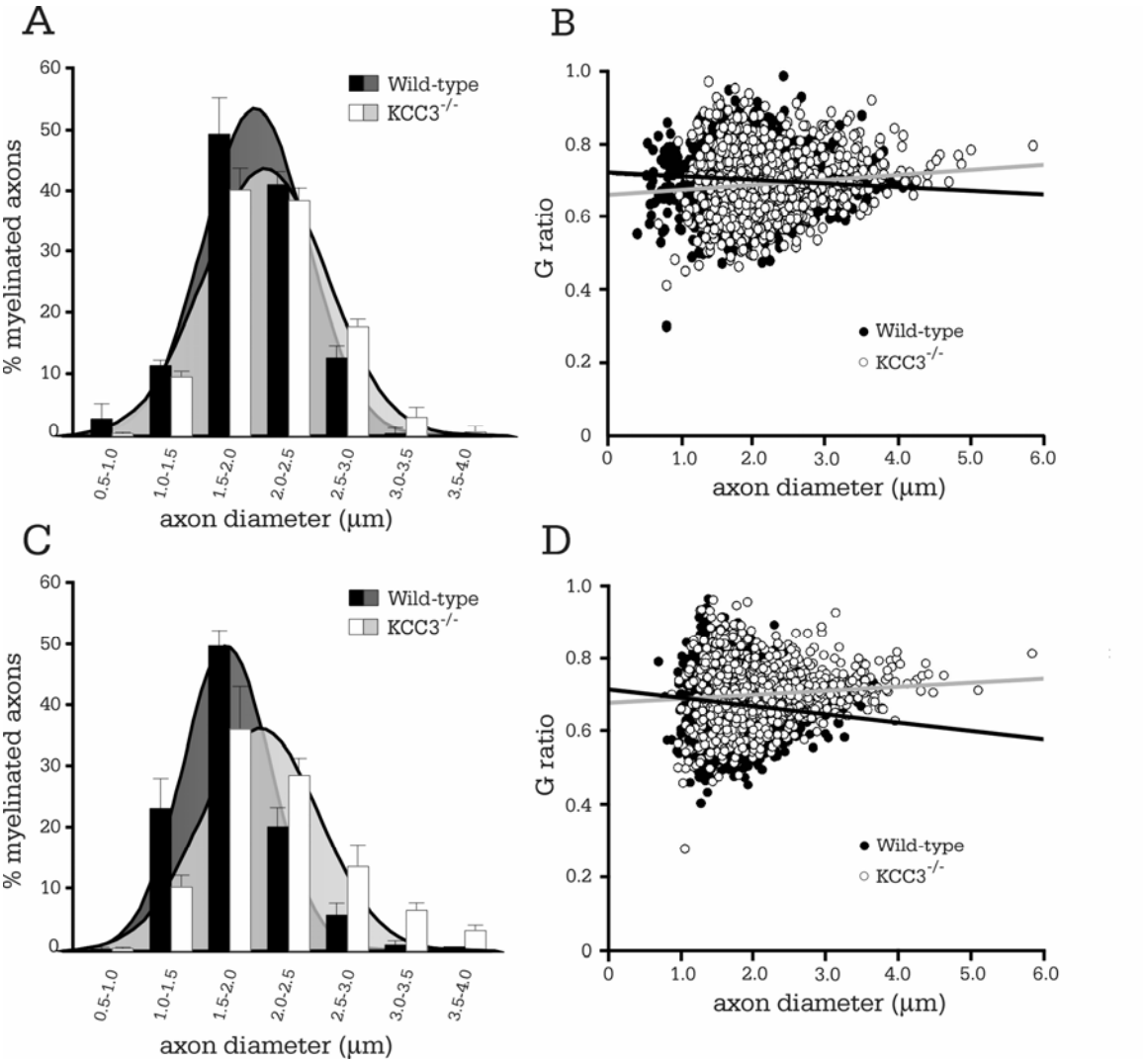

Figure 5-4. Increased axon diameters in P8 KCC3$^{-/-}$ fibers

(A) Histogram analysis of proximal sciatic nerve. Note the subtle but statistically significant (see Table 5-1) shift in axon diameter size. (B) G ratio scatter plot of proximal sciatic nerve. (C) Histogram analysis of distal sciatic nerve reveals an obvious shift in axon diameter for the mutant fibers. (D) Comparison of G ratio scatter plot regressions shows decreased myelin thickness in distal KCC3$^{-/-}$ sciatic nerve fibers. Fluid filled fibers were excluded from all graphs. (distal KCC3$^{+/+}$ N = 7; distal KCC3$^{-/-}$ N = 4; proximal KCC3$^{+/+}$ N = 4; proximal KCC3$^{-/-}$ N = 4)

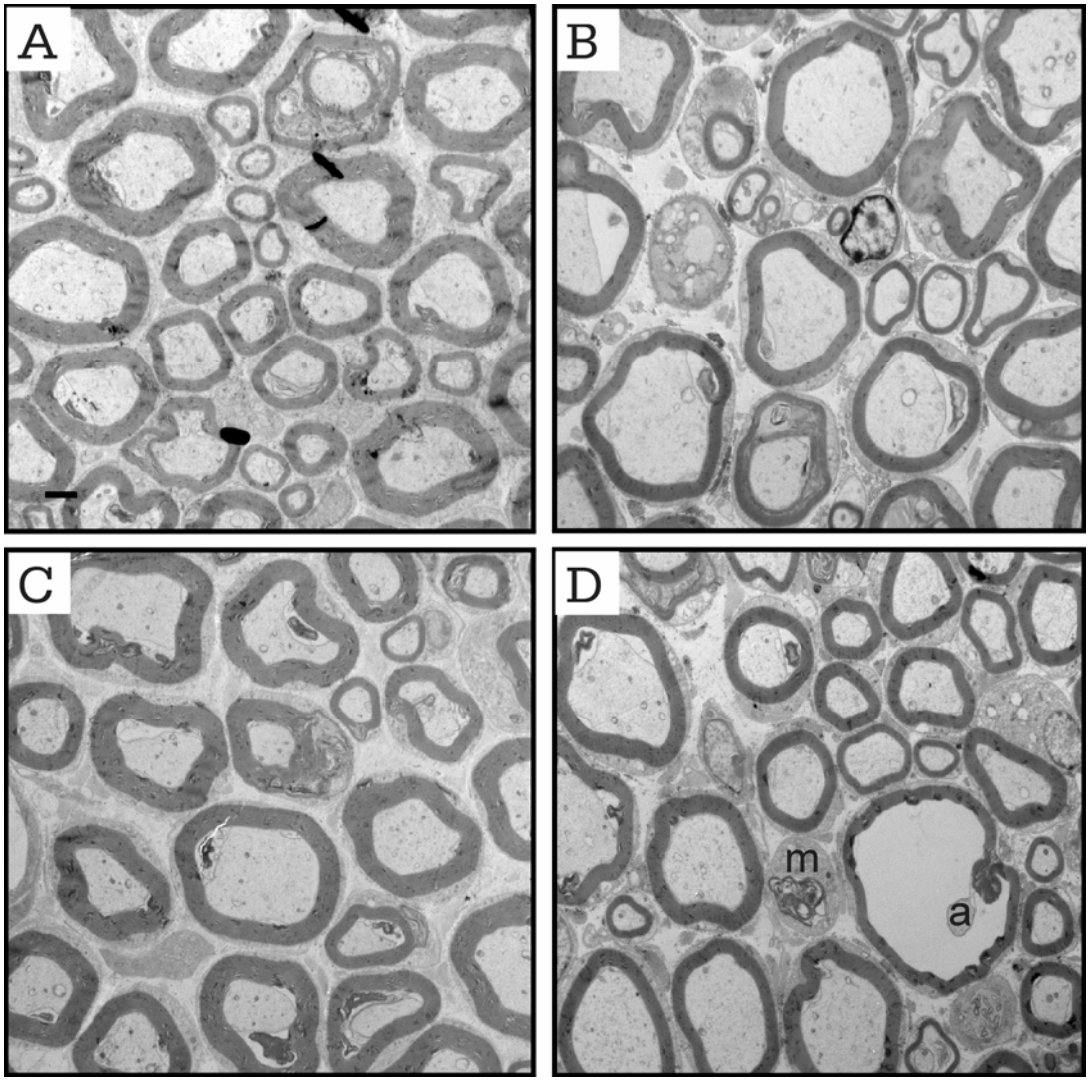

Figure 5-5. Abnormal fluid accumulation in P30 KCC3$^{-/-}$ fibers

(A) Wild-type proximal; (B) KCC3$^{-/-}$ proximal; (C) Wild-type distal; (D) KCC3$^{-/-}$ distal sciatic nerve electron micrograph. (D) Periaxonal fluid accumulation in KCC3$^{-/-}$ fibers, never seen in wild-type fibers, leads to a loss of axon (a) contact with the Schwann cell. The myelin-laden macrophage (m) indicates myelin breakdown. Scale bar = 2 µm.

but the myelin sheaths around enlarged periaxonal spaces were intact with normal ultrastructure (Figure 5-5D).

The greater mean proximal axon diameter for KCC3$^{-/-}$ compared to wild-type (Table 5-1) is represented by the shift to the right of the entire mutant axon size distribution (Figure 5-6A). G ratio scatterplots indicate a reduction of myelin thickness for axon size in proximal KCC3$^{-/-}$ sciatic nerve, which is represented by the steeper regression line for KCC3$^{-/-}$ (Figure 5-6B). Like at P8, axon enlargement skews G ratios to higher values. Unexpectedly, the histograms for distal sciatic nerve of the two genotypes overlapped (Figure 5-6C) and mean axon calibers were not significantly different (Table 5-1). Despite this, the mean G ratio is higher for distal KCC3$^{-/-}$ fibers than for wild-type (Table 5-1), indicated by the steeper regression line in the G ratio-axon diameter scatterplots for KCC3$^{-/-}$ (Figure 5-6D). Periaxonal fluid accumulation remained the most prominent abnormality in KCC3$^{-/-}$ sciatic nerves (5.53 ± 3.8 % distally; 4.57 ± 2.3 % of proximally) although with large variability between nerves.

Neurodegeneration in older murine adult sciatic nerves

Previously, we had described defects such as thin myelin sheaths and myelin debris in transverse toluidene blue stained sections of KCC3$^{-/-}$ adult sciatic nerve (Howard et al., 2002b). In this study, electron microscopy showed normal architecture of fibers in wild-type sciatic nerve sections (Figure 5-7A) and degeneration in the knockout (Figure 5-7B-E). The dying-back of axons after injury, or Wallerian degeneration, is followed by sprouting of new axons through the neural tube in the PNS (Hoopfer et al., 2006; King, 1999), which KCC3$^{-/-}$ sciatic nerves exhibit. Indeed, 11.24±1.84% of total

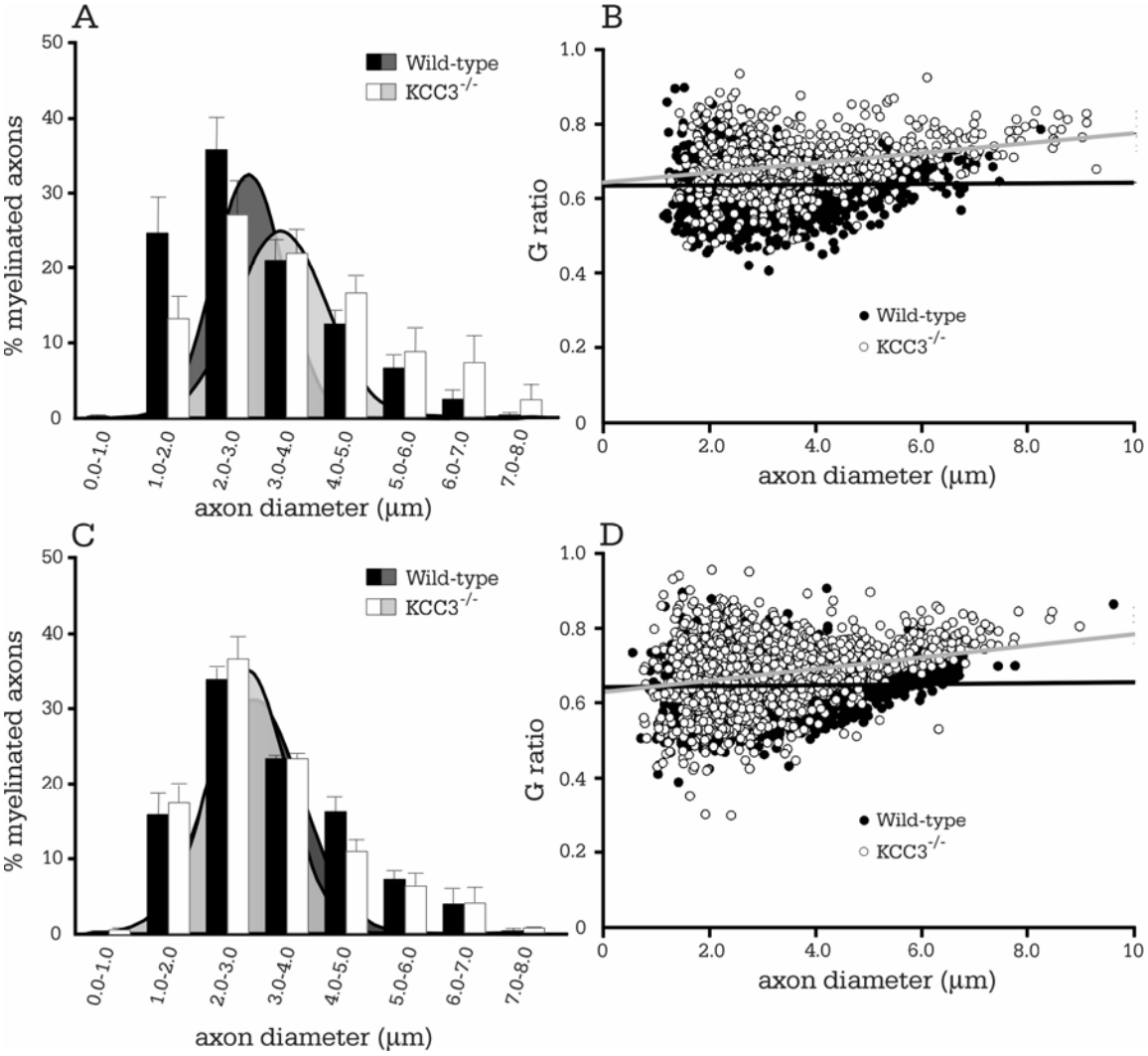

Figure 5-6. Proximal P30 KCC3$^{-/-}$ fibers are enlarged

(A) Histogram analysis of axon diameters reveal a population enlargement for proximal mutant fibers, indicating general swelling of axons. (B) Comparison of G ratio scatter plot regressions demonstrates the subtle reduction in myelin thickness in distal KCC3$^{-/-}$ sciatic nerve fibers. Fluid filled fibers were excluded from the plot. (C) Surprisingly, histogram plots of wild-type and mutant axon diameters overlapped, while (D) G ratio regression slope remained skewed for thinner myelin in mutant fibers.

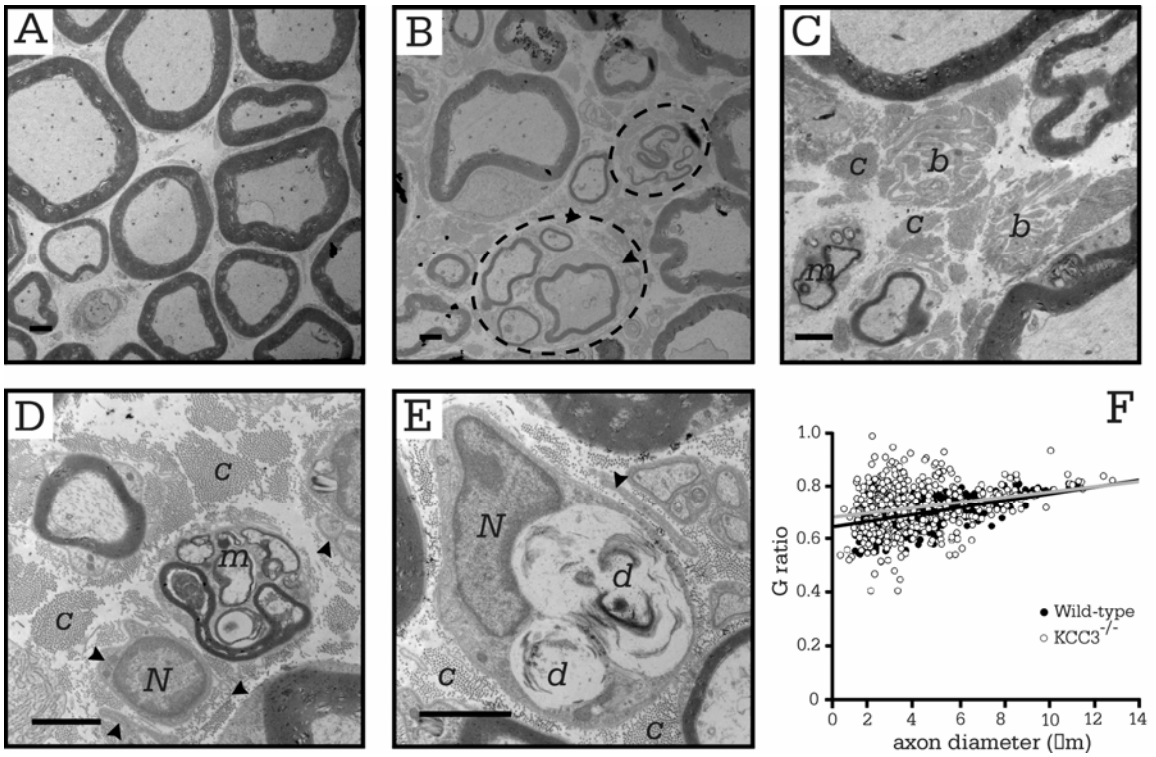

Figure 5-7. Axonal defects and myelin debris in adult KCC3$^{-/-}$ sciatic nerves

(A) Electron micrograph of wild-type sciatic nerve fibers with myelinated axons. (B-E) Electron micrographs of KCC3$^{-/-}$ nerve fibers showing macrophage invasion (m), bands of Büngner (b), signs of axon degeneration (d). Dashed ovals = regenerating clusters. Note the abundance of collagen fibers (c) and a few redundant basal lamina (arrowheads) but no onion bulbs.

myelinated axons was in regenerating clusters. The thinly myelinated axons that lie in regenerating clusters are evidence of axon degeneration followed by regrowth (Figure 5-7B). The most prominent abnormality in the knockout, however, was the presence of bands of Büngner (Figure 5-7C), which were not observed in wild-type sciatic nerve sections. Denervation leaves behind the Büngner bands, which are arrays of Schwann cell processes that provide substrate for regenerating axons (Hoopfer et al., 2006; King, 1999). Large quantities of collagen pockets (Figure 5-7D) are associated with axon loss (King, 1999). We also observed myelin and lipid debris within scavenging macrophages (Figure 5-7D-E). Myelinating Schwann cells were differentiated from macrophages by the presence of basal lamina, which macrophages do not produce. Macrophages, however, can invade a Schwann cell or neural tube (King, 1999), but when this was suspected, we re-examined the region at even higher magnification with EM. We observed a few layers of basal lamina surrounding some myelinated axons, (Figure 5-7B, D-E), which are Schwann cell remnants that indicate continuous Schwann cell activity of cell death and remyelination; these are considered pseudo-onion bulbs and cannot distinguishable from axonal loss and sprouting or demyelination (King, 1999). We did not, however, observe at least two Schwann cell processes at different distances from the fiber, a definition of an onion bulb (King, 1999), in either genotype. There was no difference in G ratio scatter plots between the two genotypes (Figure 5-7F). In older knockout animals, the frequency of periaxonal/intramyelinic fluid accumulation was 1.14 ± 0.46% (Table 5-1). The clear evidence of axon loss at 7-8 months old was not at all apparent at early postnatal ages or even at P30.

Discussion

KCC3 loss leads to a neurodegenerative, not developmental, disorder

The early expression of KCC3 led to our original hypothesis that the cotransporter is involved in peripheral nerve development. However, based on the normal Schwann cell:axon segregation and initiation of myelination, and equivalent axon densities between the two genotypes, KCC3 does not appear to regulate axon migration or myelination. The ultrastructurally normal compact myelin at all ages in KCC3-null mice supports normal development and confirms that KCC3 is not necessary for the dehydration process during myelin compaction. The periaxonal fluid defects appear to be linked to axonal atrophy, and eventually sciatic nerves of older adult KCC3-null mice succumb to Wallerian-like degeneration, which I discuss in detail below. Axonal atrophy does not necessarily mean that axons are undergoing degeneration, but massive accumulation of organelles, which indicate defects in axonal transport, along with atrophy clearly signifies degeneration (King, 1999), which we did not observe. However, the axonal atrophy may be a prelude to the degeneration found in older, 7-8 month old knockout sciatic nerves. We can conclude that KCC3 loss causes a neurodegenerative disorder in the PNS, not a developmental disorder, albeit with initial defects emerging at very early ages. Although we are not certain whether the periaxonal fluid accumulation or axonal enlargement contributes more to the Wallerian-like degeneration, the fact that Cx32-null fibers, which exhibit similar periaxonal fluid defects but maintain normal axons for three months, eventually undergo axonal degeneration (Scherer et al., 1998) supports periaxonal swelling as the predominant factor.

Periaxonal swelling

The most dramatic and characteristic feature of all KCC3$^{-/-}$ sciatic nerves, never observed in wild-type, is the periaxonal fluid accumulation. The focal swellings are distributed along the length of the myelinated fiber, but never take up the entire length of the axon. This could partly be due to the physical barriers at the paranodes that limit the periaxonal space to outside the internode, while there is no periaxonal space at paranodal and nodal regions. The periaxonal swelling is not an artifact of fixation or tissue-processing since the defect was only found in the knockout even though all genotypes of one age group were processed in parallel. The fact that fibers with periaxonal swelling were surrounded by well-intact myelin without holes or separation between lamellae support that the abnormality is related to genotype since myelin is especially sensitive to poor fixation (King, 1999). Only a minority of fibers (at most 5%) exhibited periaxonal swelling, suggesting that only a small subset is affected. However, the defect was undercounted since we had analyzed cross-sections while the swelling itself was focal. The possibility that only a subset of myelinating Schwann cells express KCC3 is unlikely, based on our immunostaining results (Chapter 3). The analysis of ultra-thin cross sections ignores a huge area of the sciatic nerve, so periaxonal swellings in different fibers above and below the thin plane would never be counted through our method. The fact that periaxonal swelling occurs at both proximal and distal nerve regions supports that the defect is not isolated to one area, but occurs throughout the length of the nerve. However, not all internodes exhibit periaxonal swelling. This suggests that not all Schwann cells face stress conditions that lead to KCC3 activation.

One reason why periaxonal swelling does not occur at all internodes could be differential exposure to a stressful microenvironment that triggers cell swelling and thus KCC3 activation. Schwann cells unexposed to stress would not need to activate RVD mechanisms such as KCC3. Microenvironmental changes may take place outside of the Schwann cell body, extracellularly and/or in the periaxonal space; for example, local changes in extracellular ion concentrations could initiate cell swelling. Based on the fact that KCC3 is quiescent until activated by cell swelling, it is logical to ask what physiological stressors exist that could lead to swelling and thus KCC3 activation. A common experimental method to activate KCC3 is simply exposing cells to hypo-osmotic media. Are there situations in which cells in an organism encounter hyposmolality? Pathological conditions, such as congestive heart failure, kidney disease, and cirrhosis of the liver, can cause hyponatremia, which leads to hyposomotic environments due to abnormally low sodium levels (Pasantes-Morales et al., 2000). Severe hyponatremia affects the brain by shifting water into neurons and glia. Initially, hyponatremia should cause cell swelling, activating KCC3 and other ion-extruding mechanisms. But hyponatremia alone is not correlated with neural defects. The danger actually lies in the rapid correction of a pateint's hyponatremia, or other serum hyposmolality, and can cause osmotic demyelination disorder, also known as central and extrapontine myelinolysis (Brown, 2000; Kleinschmidt-Demasters et al., 2006). Why some regions of the nervous system are more sensitive than others to osmotic insults is not known. This type of myelinolysis, however, exemplifies the extreme sensitivity of myelinating glia to abrupt osmotic changes. There are, however, no reports relating the effects of hyponatremia reversal on peripheral nerve function and histology. The only

case studies associating neuropathy with hyponatremia are on various porphyrias, which are disorders of heme biosynthesis (Gordon, 1999), but this is not a cause-and-effect situation; porphyrias can produce hyponatremia through decreased vasopressin release (Gordon, 1999) and can lead to neuropathy (Albers & Fink, 2004).

One process that is known to change the microenvironment adjacent to the Schwnan cell is axonal activity, which leads to the accumulation of K^+ ions in the periaxonal space. Due to the normally low baseline concentration of extracellular K^+ and limited volume in the periaxonal space and CNS extracellular space, even a small release of K^+ ions can considerably increase the periaxonal/extracellular K^+ concentration. The fact that higher nerve activity causes a rise in periaxonal K^+ was first shown by Frankenhauser and Hodgkin who demonstrated in squid giant fibers that a longer train of impulses results in more K^+ release than a shorter train; for example, a 125 impulse/second train for 200 milliseconds released more than five times the K^+ than a 50 impulse/second train (Frankenhaeuser & Hodgkin, 1956). They also showed that the excess periaxonal K^+ eventually disappeared along an exponential curve with a rate constant of 30-100 milliseconds (Frankenhaeuser & Hodgkin, 1956). The results of a more recent study assessing K^+ accumulation and clearance with ion sensitive microelectrodes demonstrated similar results for the optic nerve, revealing a double exponential curve for K^+ clearance, one slope predicted to represent strong, initial glial Na-K ATPase activity and another likely characterizing the late-onset activity of the axonal Na-K pump; blocking glial K^+ channels with Ba^{2+}, however, did not change the rate of K^+ clearance (Ransom et al., 2000). Pharmacological inhibition of adaxonal K^+ channels is questionable though since they are hidden under the myelin sheath, which is

difficult for compounds to access. Alberti et al. have shown that the Na-K pump is distributed evenly on the axolemma and irregularly on and within the myelin sheath in peripheral nerve by EM detection of nitrophenol granules, a product of the Na-K ATPase component K-*p*NPPasse (Alberti et al., 2007). This localization pattern supports a role for the NA-K pump in K^+ uptake buffering in the peripheral nerve, which can be tested through nerve activity experiments in the sciatic nerve with and without oubain, a Na-K ATPase inhibitor. As discussed in the previous chapter, the localization of KCC3 does not support a role for the uptake of K^+ and Cl^- into the Schwann cell, i.e., uptake buffering. Then KCC3 may play a role in spatial buffering of potassium. Does the intake of excess K^+ from the periaxonal space by the Na-K ATPase and possibly K^+ channels and NKCC lead to glial swelling that can activate KCC3? High extracellular potassium levels do drive K^+ into cells, causing swelling (Kofuji & Newman, 2004). Ransom et al. have demonstrated activity-dependent shrinkage of the extracellular space (ECS), which can be interpreted as glial swelling, of up to 20% in mature optic nerves (Ransom et al., 1985). ECS shrinkage/glial swelling from nerve activity is reversible, and can be prevented by the application of 10mM furosemide (Ransom et al., 1985), most likely through the inhibition of NKCC1, although this high concentration would also block KCCs and stimulate the Na-K ATPase. There was no mention of whether furosemide affected the process of ECS expansion/glial shrinkage back to normal, pre-tetanic sizes. It would be interesting to test whether activity-dependent Schwann cell swelling occurs and if it is sufficient to activate KCC3 flux; for example, nerve-activity related flux experiments can be performed after preloading tissues or myelinated axon cultures with $^{86}Rb^+$. High extracellular K^+ is also depolarizing. In the hippocampus, rises in the

concentration of extracellular K^+ depressed high-frequency synaptic transmission (Meeks & Mennerick, 2004). High extracellular K^+ can cause neuropathy through chronic depolarization of axons, which patients with hyperkalemia often develop (Kiernan et al., 2002), and caused conduction block in rats (Martin & Decima, 2003).

Fluid trapped in the periaxonal space appears to be a defect involving the Schwann cell's inability to extrude ions/fluid, ultimately disrupting axon-glial contacts necessary for the maintenance and survival of both. Of the numerous studies of knockout mice with disruptions of PNS proteins there are two types of defects leading to abnormal periaxonal enlargement from fluid accumulation: (1) loss of proteins mediating axon-glial contacts, such as MAG (Trapp et al., 1984) and (2) inactivation/mutations of proteins involved in ion movement, such as Cx32 (Anzini et al., 1997; Scherer et al., 1998). The mutant Syrian hamster with hind leg paralysis also exhibits periaxonal swelling in peripheral nerve fibers, but the underlying mechanism is not known (Hirano & Dembitzer, 1981). Poisoning by *Phoneutria* spider venom, which causes repetitive nerve firing, also leads to periaxonal fluid build-up like those in KCC3-null fibers (Cruz-Hofling et al., 1985) The periaxonal defects in $Cx32^{-/Y}$ and $Cx32^{-/-}$ peripheral nerves are remarkably similar to that of $KCC3^{-/-}$ fibers. From their ultrastructural studies of Cx32-null fibers of both sciatic and femoral nerves, Scherer et al. described axonal separation from the inner surface of the Schwann cell and "electron-lucent" regions. They also observed that the axons that had separated from their myelin sheaths had more tightly packed neurofilaments (Scherer et al., 1998) like the increased cytoskeletal density in affected $KCC3^{-/-}$ fibers. At older ages (5-12 months), similar to KCC3-null sciatic nerves, regenerating clusters of tight groups of small axons with thin myelin as well as

denervated Schwann cells, appearing as intact Schwann cell myelin surrounding an empty hole, were observed in Cx32-null nerves (Scherer et al., 1998). Although we rarely observed intramyelinic fluid accumulation in KCC3 knockout fibers, there were several examples of myelin splitting with fluid build-up in the photomicrographs of Cx32-null nerves. The fluid and axonal defects were not quantitated, so we cannot compare the extent of those abnormalities between the two knockouts, but qualitatively, they appeared similar. Like in the KCC3 knockouts, it is obvious that not all myelinated fibers were affected in Cx32-null nerves; I counted only 1-2% in the photomicrographs featured for 5 months in age. The intramyelinic fluid build-up in the Cx32-null fibers may be due to the localization of Cx32 to incisures (Scherer et al., 1995). Without functional gap junctions, fluid that has been taken up the Schwann cell on the adaxonal side may accumulate in the incisures, eventually splitting the myelin to accommodate excess fluid. In fact, Scherer et al. reported that some incisures, under EM, appeared to be larger than normal under cross-section (Scherer et al., 1998). Furthermore, since gap junctions are made up of two interacting connexons, they can also be considered to be adhesion molecules. The loss of a highly expressed adhesion molecule in SLIs may also contribute to myelin splitting and larger incisures. Although incisures in KCC3$^{-/-}$ did not qualitatively appear larger than that of wild-type, morphometric analysis may have revealed differences between genotypes. I did not, however, measure and compare the size of knockout and wild-type incisures because they are very irregular structures with indistinct borders and may appear to take up the entire circumference of myelin in some cases or only partially, depending on the sectioning since they are spiral structures. I would not expect

significant fluid accumulation in KCC3$^{-/-}$ incisures since their gap junctions most likely function normally to move ions and fluid in either direction.

Unlike in KCC3$^{-/-}$ nerves, demyelination was a large component of the defects in Cx32-null nerves, beginning as denuded and remyelinated large-caliber axons at 3 months and progressing to thickly-layered onion bulbs surrounding large, remyelinated axons at 5-12 months (Scherer et al., 1998). This striking difference between the two knockouts may be due to the multiple functions of gap junctions in glial cells. The periaxonal swelling supports a role for spatial buffering of K^+ ions after nerve activity, as originally mentioned by Anzini et al. (Anzini et al., 1997). The demyelination, however, may be due to the lack of nutritional/trophic and/or signaling molecules to and/or from the cell body from other Schwann cell regions due to gap junctional defects impairing the passageway through myelin and between paranodes. Because KCC3 only moves K^+ and Cl^- ions, but not small molecules, only the periaxonal fluid accumulation defect occurs. Besides demyelination, another prominent difference in Cx32-null mice is the late age of onset of the described defects. Our KCC3-null mice exhibited periaxonal fluid defects at an early age (P8), while Cx32$^{-/-}$ mice showed no peripheral nerve irregularities at P5, 4 weeks, and 7 weeks in age, with fiber abnormalities emerging at 3 months (Anzini et al., 1997; Scherer et al., 1998). In adult rodent peripheral nerves, immunostaining experiments revealed Schwann cell Cx32 expression at incisures, paranodes, and, like MAG, on the entire circumference of the adaxonal membrane, which was believed to represent the mesaxon; this expression pattern strongly supports a role in serving as a passageway from the region facing the periaxonal space to the cell body and vice versa (Scherer et al., 1995). The late-onset of the nerve defects, however, brings up the

question of whether another connexin exists at earlier ages (< 7 weeks) and is later replaced by Cx32. Although Northern blots revealed that mRNA levels increased from P5 up to P33, Cx32 was undetectable in incisures by immunostaining at P6, and was found only on mesaxons. Either Cx32 is not necessary at early ages because the myelin is thinner during development, another Cx gap junction exists, or perhaps the defects were not obvious in young nerves without quantitative morphometric analyses. The fluid accumulation in Cx32-null peripheral nerves, however, demonstrates the importance of an ion/fluid clearance pathway in Schwann cells. Although the Cx32 model supports a defect in transport of ions/fluid *through* the Schwann cell, KCC3's localization supports a role in the extrusion of ions/fluid *from* the Schwann cell body.

Similar periaxonal fluid accumulation was observed in CNS fibers of Cx47-null mice, while Cx32/Cx47-null mice displayed a more severe phenotype (Menichella et al., 2003; Menichella et al., 2006; Odermatt et al., 2003). Intriguingly, the severity of periaxonal swelling, as measured by the number of swollen fibers and degree of enlargement, increased with repetitive nerve activity (Menichella et al., 2006), which, like the Cx32 knockout, links the ion buffering capacity of glial cells with fluid homeostasis. Kir4.1 knockout mice also exhibited similar enlargements in brain and spinal cord white matter, establishing it as a candidate for K^+ buffering as well (Djukic et al., 2007; Menichella et al., 2006; Neusch et al., 2001). Similarly, the genetic ablation of CLC-2, which is normally expressed by oligodendrocytes, led to intramyelinic and periaxonal fluid accumulation, particularly affecting fiber tracts of the cerebellum, corpus callosum, internal capsule, brainstem, and spinal cord (Blanz et al., 2007). In RVD, the efflux of K^+ and Cl^- is electrically balanced through KCCs as well as by concomitant ion

extrusion through K^+ and Cl^- channels (Okada et al., 2001). For potassium buffering to be electrically silent, a similar type of balance must occur. Although the CLC-2 chloride channel participates in RVD, as mentioned in Chapter 1, Blanz et al. propose that the fluid defects in the knockout result from lack of spatial ion buffering, hypothesizing that both Cl^- uptake and efflux through CLC-2 is necessary to neutralize the electrical currents associated with bulk K^+ entry and exit through glial cells (Blanz et al., 2007). The punctate CLC-2 staining on the cell bodies of cerebellar oligodendrocytes (Blanz et al., 2007), however, do not support a model of buffering ions from the periaxonal space, i.e., uptake buffering. Based on its localization, a role for CLC-2 in neutralizing outward potassium currents from oligodendrocytes as part of spatial buffering is more credible. There was no speculation, though, on whether cellular stresses inherent to myelinated axon development might lead to such fluid defects because of RVD-deficiency from CLC-2 loss. CLC-2 is not expressed by Schwann cells, so the PNS was unaffected in the knockouts; it will be interested to see if genetic ablation of an equivalent chloride channel expressed by Schwann cells leads to a similar phenotype. Indeed, Schwann cells express chloride channels (Baker, 2002), and one may play a role similar to oligodendroglial CLC-2. The above CNS models with analogous periaxonal fluid phenotypes could be relevant to $KCC3^{-/-}$ fibers. Although potassium buffering has been studied much more in the CNS than in the PNS, a similar mechanism could be occurring in peripheral nerves since repetitive firing of action potentials similarly elevates peripheral periaxonal K^+ concentrations. One main difference in the CNS is that astrocytes, which are directly linked to the capillaries through their end-feet, also participate in K^+ buffering (Djukic et al., 2007; Kucheryavykh et al., 2007). KCC3 could also be involved in spatial K^+

buffering by releasing excess potassium ions after the uptake buffering of K^+ from the periaxonal space through other mechanisms, e.g., Na-K ATPase, K^+ channels, NKCC1. Supporting my argument are the numerous proposed models, which pose that excess K^+ entering the cell should be released by the glial cell body through the K^+ channels with the concomitant entry and extrusion of Cl^- through chloride channels (Baker, 2002; Blanz et al., 2007; Konishi, 1990; Wilson & Chiu, 1990). Indeed, my proposed function of KCC3 is ideal since its ion efflux is inherently electroneutral. Increasing nerve activity should increase the severity of periaxonal fluid build-up in KCC3- and Cx32-null sciatic nerves, either by the number of periaxonal expansions or their size. In fact, tetanic nerve activation from *Phoneutria* spider venom alone leads to periaxonal swelling in peripheral nerves (Cruz-Hofling et al., 1985). KCC3 requires activation by cell swelling. Cell swelling caused by the uptake of K^+ with Cl^- could activate KCC3.

The movement of ions into and out of a single cell through different ion channels and transporters is not unusual, and, in fact, is the major role of ion channels and CCCs in epithelial transport in which the influx of salts by, for example, in TALH kidney cells through NKCC2 is balanced by the efflux of sodium, potassium, and chloride toward the bloodstream through CLC-K/barttin, KCCs, and the Na-K ATPase (Jentsch, 2005; Jentsch et al., 2005). As mentioned in Chapter 2, the Schwann cell is considered to be analogous to epithelial cells due to its polarity. The analogy is quite fitting when considering the proposed pathways of glial K^+ and Cl^- uptake, spatial buffering (gap junctions), and concomitant K^+ release with Cl^-. Also supporting the epithelial cell-like nature of the Schwann cell are its gap junctions that form a passage through, and thus connect, the layers of myelin to the cell body, much like the classical role of gap

junctions in linking epithelial cells together to form a route for ions and small molecules between cells.

Evidence of axonal swelling

By following the course of the disorder morphometrically, we also showed evidence for axonal swelling preceding the neurodegeneration in adult KCC3$^{-/-}$ mice. Not only was axonal swelling demonstrated by the increased mean diameters of KCC3$^{-/-}$ axons, but histogram analyses of axon diameters at ages P3, P8, and P30 also showed that axons that appeared normal (i.e., without periaxonal fluid accumulation) are enlarged as a population. Even at P3 when periaxonal swelling is not observed, KCC3$^{-/-}$ axons are swollen, with the mean radius increased by 17%. This represents a 37% difference in surface area and volume if the axons are considered cylinders of the same length (Table 5-2). Unlike other disorders featuring axonal swelling, such as giant axonal neuropathy (GAN patients and gigaxonin-null mice) and Charcot Marie Tooth disease 2E, which both involve excessive neurofilament accumulation (Ding et al., 2006; Fabrizi et al., 2004; Fabrizi et al., 2007; Yang et al., 2007b), KCC3$^{-/-}$ fibers show decreased cytoskeletal density compared to wild-type, supporting fluid accumulation. The fluid accumulation leads to a 25% and 45% increase in surface area/volume in proximal and distal sciatic nerve, respectively, at P8, and 85% increase in P30 KCC3$^{-/-}$ sciatic nerve. These dramatic enlargements are not seen in 7-8 month old knockout sciatic nerves in which there was no statistical difference in axon diameters and calculations show, likewise, a neglible 3.7% difference in surface area/volume (Table 3). This axonal

Table 5-2. Changes in axon size.

	Axon diameter (um)	Axon radius (um)	% increase KCC3-null axon radius	Surface area (SA) (um^2)	% increase KCC3-null SA (and volume)
P3					
KCC3+/+	1.87 ± 0.09	0.935	17.1	2.74	37.2
KCC3-/-	2.19 ± 0.09	1.095		3.77	
P value	0.0395 (s)				
P8 Proximal					
KCC3+/+	2.00 ± 0.34	1	12	3.14	25.4
KCC3-/-	2.24 ± 0.64	1.12		3.94	
P value	< 0.05 (s)				
P8 Distal					
KCC3+/+	1.81 ± 0.07	0.905	20.4	2.57	45.1
KCC3-/-	2.18 ± 0.09	1.09		3.73	
P value	< 0.05 (s)				
P30 Proximal					
KCC3+/+	2.89 ± 0.10	1.445	36.0	6.56	84.9
KCC3-/-	3.93 ± 0.31	1.965		12.13	
P value	<0.05 (s)				
P30 Distal					
KCC3+/+	3.25 ± 0.13	1.625	-2.2	8.30	-4.3
KCC3-/-	3.18 ± 0.23	1.59		7.94	
P value	>0.05 (ns)				
7-8 months					
KCC3+/+	3.86 ± 0.86	1.93	1.8	11.70	3.7
KCC3-/-	3.93 ± 0.10	1.965		12.13	
P value	0.61 (ns)				

(ns) not significant; (s) significant. Measurements were made for axon diameters. Radius and surface area were calculated from the mean axon diameter values.

swelling skews the G ratio to higher values giving the appearance that the axon is hypomyelinated.

Axonal swelling in KCC3$^{-/-}$ nerves was unexpected since cotransporter expression was not detected on the axolemma. However, we cannot rule out axonal expression at levels below our detection sensitivity. The question remains whether an axon is capable of volume control completely independent of its cell body or if it relies on the soma, even to some degree, for volume regulation. Also, whether volume changes in the cell body affect the axon is also unclear. A combination of both axon-autonomous and soma-dependent cell volume changes likely occurs. An axon reaching meters away from its cell body lies in an absolutely different environment, and it makes little sense if the axon could not combat osmotic threats that are not perceived by its soma. On the other hand, since the axonal space is contiguous to the cell body, volume regulation defects in the soma, as observed in hippocampal KCC3$^{-/-}$ neurons (Boettger et al., 2003), could impact axonal volume. Indeed, KCC3 is expressed in both spinal motor and DRG neurons throughout development and into adulthood (Boettger et al., 2003).

The majority of previous volume regulation studies were conducted in cells without extensions, like *Xenopus* oocytes, or just focused on cell bodies without consideration of dendrites or axons. Neurites, however, can be considered tube-like extensions of cells. The behavior of neurites, such as axons, in hypotonicity, appears to differ from that of cell bodies. Time-lapse videomicroscopy of cultured goldfish retinal ganglion cell axons revealed that hypotonic shock caused swellings, or varicosities, along their lengths, but the axons recover within ten minutes through RVD mechanisms (Edmonds & Koenig, 1990). The intermittent varicosities were not glial swellings since

the axons were unmyelinated. It would be interesting to perform similar videomicroscopy experiments with cultured DRG neurons to look for furosemide-sensitive RVD, which would indicate a KCC, followed by RT-PCR or Western blots to confirm expression of KCC1, 3, and/or 4. The experimental set-up of Edmonds and Koenig, however, did not separate axons from cell bodies; both were exposed to hypotonic solution (Edmonds & Koenig, 1990). Therefore, they did not prove that the swelling and RVD they observed were completely axon-autonomous. They did not measure or describe rates of volume change to the cell bodies. It is curious though that the swelling they observed was not uniform along the axon, but appeared as beads. This may reflect the flexibility of the cytoskeleton in certain areas, such as the internode, compared to the node where a defined network of cytoskeletal elements, including ankyrin and spectrin, bolts down Nav channels. Pullarkat et al. also observed beading in hypotonically shocked chick embryo axons and PC12 neurites and attributed this phenomenon to the "gel-like dynamics" of the cytoplasm, cytoskeleton, and plasma membrane from which they based their physical and mathematical models (Pullarkat et al., 2006). This beading may be due the physical properties of the axon, but in our model, we were not able to distinguish axonal beading from periaxonal fluid swelling in teased fibers. In KCC3-null fibers with periaxonal swellings, however, which were not included in axon diameter histograms, the axons appeared to be atrophied, not swollen, like $Cx32^{-/-}$ axons adjacent to periaxonal fluid (Scherer et al., 1998).

A more meaningful experiment to answer the question of whether the axon regulates volume independently and how much influence changes in soma volume has on axonal size would entail the compartmentalization of neurons and axons. A three-

chamber culture system, where DRG neurons plated in the center compartment are allowed to grow their axons into the adjacent compartments, which are separated and sealed by silicon-grease, has been successfully utilized in Wallerian degeneration studies and advantageous since the axons grow in parallel (Guertin et al., 2005), would be a desirable set-up for neuron and axon volume experiments. For another type of experiment, since hypotonic stress is a method to load dyes and contrast agents into cells (Edmonds & Koenig, 1990; Johnson et al., 1998), an adaptation of this method may allow us to test which types of cells or sizes of axons are more reactive to osmotic stress at different osmolalities by measuring uptake of agents through optical imaging techniques.

Since CCCs are activated by changes in osmolarity, most studies utilize hypotonicity to activate KCCs and hypertonicity to activate NKCCs, a method that utilizes osmotic pressure changes to drive fluid movement. However, when considering cell and axonal swelling, several factors need to be considered, including membrane tension, membrane permeability, osmotic pressure, hydrostatic pressure, and hydraulic pressure. A cell body is not analogous to a fixed sphere just as an axon cannot be considered a rigid tube. Swelling stretches the plasma membrane up to a point, akin to blowing a balloon, but continued swelling does not necessarily lead to rupture because membrane can be continuously added to the cell surface. This elastic property of cells in response to forces (Bao & Suresh, 2003) is exemplified by the accommodation of periaxonal swelling in KCC3-null fibers by the myelin sheath and the increases in surface area/volume of $KCC3^{-/-}$ sciatic nerve axons. Although cells/axons are incredibly flexible, physical barriers can block continued expansion, such as other cells/axons as well as their structural links to the ECM. Beyond a certain point, cell death may occur, possibly from

the disruption of metabolism or other processes (King, 1999). Cell volume and membrane regulation also relate to the stability of cell shape, which depends on the rate of swelling or shrinkage. For example, axons that undergo sudden shrinkage may obtain an irregular non-circular shape from infoldings of “extra” membrane and swollen axons may have show increased circularity by cross-section, but this would be less obvious.

Water molecules are not actively transported, but rather, they passively follow actively transported solutes. Therefore, water movement requires the driving force of osmotic gradients. However, besides osmotic pressure, there is another transmembrane driving force that moves water out of the cell/axon—hydrostatic pressure (Mathias, 1985; Vargas, 1968). In fact, the fluid dynamics of a bulk solution across and within membranes, including axons, are the basis of diffusion tensor imaging (Madi et al., 2005; Sato et al., 2001). The osmotic pressure difference, of course, depends on the difference in intra- and extra-cellular ion/osmolyte concentrations. Hydrostatic pressure is the pressure exerted by (non-moving) fluid. Studies of CCCs in volume regulation are generally based on osmotic pressure differences. In an experiment testing only hydrostatic pressure as the driving force, when the internal pressure of a squid giant axon was raised by perfusing fluid into it, axonal swelling occurred, lasting 10-15 minutes. But after this time period, axon volume remained constant and volume flux out of the axon increased linearly with increasing hydrostatic pressure (Vargas, 1968). The post-swelling efflux phenomenon was explained by the widening of channels or pores on the axolemma (Vargas, 1968), which we now know is due to the activation of volume-sensitive ion channels and cotransporters. Continuous perfusion, or fluid-filling an axon without or with limited efflux mechanisms would increase its volume, as demonstrated in the squid

giant axon. This could explain the increase in volume of KCC3$^{-/-}$ fibers (percent change compared to wild-type) from P3 to P30. However, the squid giant axon could recover from swelling, likely due to RVD, while KCC3$^{-/-}$ fibers did not. One question that arises is whether hydrostatic pressure is a large component in the swelling of KCC3-null axons. This would necessitate a source of fluid perfusing into the axon as in the squid giant axon perfusion experiment. Thus, a related question is about the origin of the fluid that causes KCC3$^{-/-}$ axons to expand. Does the fluid enter at the node following the influx of sodium ions during an action potential or from the periaxonal space? Or is it "overflow" from the cell bodies that lack KCC3? If fluid is continuously flowing into the soma, but its plasma membrane, after expansion to a final point acts as a wall, the force transmitted by the wall cannot compress excess liquid, so it exerts force, pushing the fluid through the axon. Thus the hydraulic pressure, pressure from moving liquid, can force the fluid through the axons. The fluid pressure would be evenly distributed in a tube made of homogeneous material. Since the walls of an axon are flexible, the axon will enlarge if an efflux pathway on the axolemma is blocked or missing.

The property of the cell membrane describing the ability of fluid to move through the membrane is its hydraulic conductivity, or filtration coefficient, which can be determined by measuring the rate of cellular swelling/shrinking in response to osmotic pressure changes by diluting or concentrating the external solution (Vargas, 1968). KCC3 and volume-sensitive ion channels and aquaporins all contribute to the hydraulic conductivity. KCC3-null spinal and DRG neurons most likely have an altered filtration coefficient, as demonstrated for hippocampal neurons (Boettger et al., 2003). But why does the filtration coefficient, and thus the volume relaxation rate, appear to return to

normal in distal sciatic axons at P30 while the proximal sciatic nerve axons remain abnormally enlarged? This is extremely puzzling since it is highly unlikely that a compensatory protein mediating ion efflux, such as KCC4, is upregulated by the axon from the distal to proximal direction. If KCC4 appeared along the entire axon, but was not expressed by the soma, the cell body would still have RVD defects, and thus continued swelling. When the soma reaches a point where it no longer expands, then the fluid should become evenly distributed through the axon, if the axon is considered a flexible tube. In my example in which an axon developed a compensatory efflux pathway along its entire length, water should exit through those pathways both proximally and distally equally since fluid exerts equal pressure in all directions. For example, water exerts equal pressure to all sides of a hose. Even when the hose is blocked at one end and connected to spigot with water running in at the other end, the hose may slightly expand, but equally along its length. The only situation where a bulge would occur is at a weak point in the hose (e.g., thinner or different material). Therefore the great increase in volume in P30 proximal sciatic nerve, but not distally, may be explained by a weakness in that particular region. The axon, however, is not a simple hose, and its properties may likely be closer to gel-like dynamics rather than fluid dynamics (Pullarkat et al., 2006) an investigation that is beyond the scope of this work. An alternative explanation is that axons regulate volume autonomously and that proximal axons encounter more ionic/osmotic stress in their environment than do distal axons. For example, dorsal and ventral spinal roots are bathed in CSF while their axons in the periphery are not. However, I analyzed sciatic nerve from outside of the spinal cord, so this is not likely. As described earlier, a multi-chamber culture system is needed to test the osmoregulation

properties of the cell body and axon, and the results may help explain the changes we measured in KCC3-null axons.

Intriguingly, in older mice, when cotransporter transcript and protein become undetectable in wild-type mice, the axon diameter histograms for $KCC3^{-/-}$ and wild-type nerves overlap, which seems to indicate recovery from axonal swelling. Another puzzling finding was the overlap of axon diameter histograms for wild-type and $KCC3^{-/-}$ at P30 only in distal sciatic nerve fiber while proximal nerves were still enlarged as a population. Since KCC3 is still expressed by cell bodies in the wild-type P30 spinal cord and DRG, it seems logical that its loss would lead to continued swelling of neurons at that age, unless there was compensation by another mechanism. This “recovery” in axonal diameter could originate from the expression of another volume-activated transport mechanism in neurons/axons. In fact, we have previously shown expression of KCC4 in adult sciatic nerve (Figure 5-8). It seems improbable, however, that KCC4 expression/function moves from distal to proximal. One explanation is that many of the distal fibers are beginning to atrophy. The combination of axon atrophy and degeneration with regeneration of axonal sprouts may give the appearance that $KCC3^{-/-}$ axons are within normal size ranges when in fact they may be abnormal. If KCC3-/- axons at 7-8 months is indeed swollen, this can be assessed by comparing neurofilament density between knockout and wild-type axons. There would be less neurofilament density in axons enlarged by fluid.

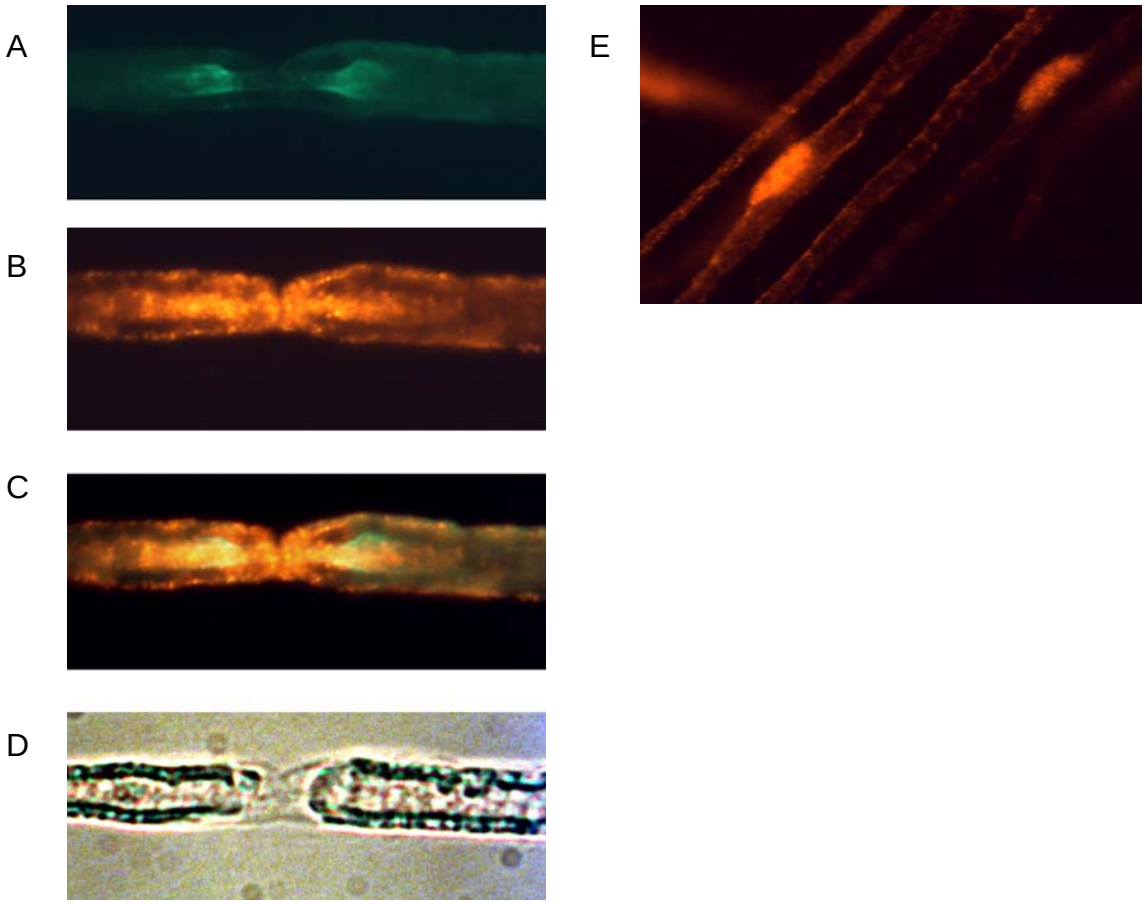

Figure 5-8. Axonal KCC4 expression in teased sciatic nerve

(A) Potassium channels are localized to the axonal juxtaparnodes as shown by Kv1.2 staining (FITC in green). (B) KCC4 also localizes to the axon at discrete regions. (C) Overlay of Kv1.2 and KCC4 immunostaining show that KCC4 is localized to the juxtaparanode as well as at the paranode. (D) In the DIC image, the myelin sheaths are distinguishable by its darker contrast. (E) KCC4 also distinctly stains Schwann cell bodies.

Wallerian-like degeneration without segmental demyelination indicates axonopathy

In older adult knockout sciatic nerves (7-8 months), regenerating clusters and bands of Büngner, which were only observed in KCC3$^{-/-}$ sciatic nerves, were the key evidence of axon loss, as in Wallerian degeneration followed by attempts at re-growth. Wallerian degeneration describes the process of axon degeneration in transected nerves, which includes axonal degeneration, disintegration of fibers distal to the transection, phagocytosis of myelin secondary to axonal loss, and remodeling of the basal lamina (King, 1999). In the PNS, this can be followed by regrowth and remyelination. When there is no crush or transection injury, the similar features seen in neurodegenerative diseases are described as "Wallerian-like" degeneration. KCC3$^{-/-}$ sciatic nerves lacked a main feature of segmental demyelination—onion bulbs (King, 1999)—disproving our original hypothesis. We cannot entirely eliminate the possibility of segmental demyelination since onion bulb formation depends on the rate of Schwann cell death and remyelination as well as the age the process began. One can argue that the demyelination/remyelination process was occurring too slowly in KCC3$^{-/-}$ sciatic nerves to be detected, but the fact that regenerating clusters and bands of Büngner, not redundant basal lamina, were the most striking features strongly supports Wallerian-like degeneration with regrowth. Under light microscopy, bands of Büngner appeared as onion bulb structures, but EM disproved this. Denuded axons are another feature of segmental demyelination (King, 1999), but in the case of KCC3$^{-/-}$ fibers, only small-diameter axons were unmyelinated and they were located in regenerating clusters; thus, we did not consider them to be demyelinated. EM photomicrographs show collapsed

myelin and myelin debris in macrophages in KCC3-null sciatic nerves, which are typical in Wallerian degeneration (Hoopfer et al., 2006; King, 1999).

Does this Wallerian-like degeneration stem from the KCC3 knockout's early periaxonal swelling defects? Like in nerves poisoned with *Phoneutria* spider venom (Cruz-Hofling et al., 1985) and Cx32-null mice (Scherer et al., 1998), axons of KCC3-null fibers adjacent to periaxonal swellings exhibited denser cytoskeletal packing, which indicates axonal atrophy. Anzini et al. proposed that in Cx32-null mice, the periaxonal fluid may have originated from the axon, eventually leading to shrinkage (Anzini et al., 1997), but this is highly unlikely since Cx32 is not expressed by neurons/axons, only Schwann cells (Scherer et al., 1995). The atrophy found in all three models with peripheral periaxonal swelling may be due to physical compression from the fluid. Most likely, however, it represents a stage of degeneration after loss of contact with the Schwann cell (King, 1999). Extensive collagen pockets, like those observed in older adult $KCC3^{-/-}$ nerves (Figure 5-7D), are also associated with axonal loss (King, 1999). Adolescent mice (P30) histologically do not show axonal degeneration (or demyelination); however, they also perform poorly on standard motor and balance tests (Chapter 3). This indicates that the earlier sciatic nerve defects of axonal enlargement and periaxonal swelling can already impair motor and balance functions.

To summarize this chapter, in order to understand how disruption of KCC3 function leads to neurodegeneration in peripheral nerves, we conducted a detailed morphometric analysis of $KCC3^{-/-}$ and $KCC3^{+/+}$ sciatic nerves for quantitative and ultrastructural comparisons and found that axonal and periaxonal swellings are the pathological hallmarks at early ages into adolescence, while Wallerian-like degeneration

characterizes older KCC3$^{-/-}$ adult nerves. Axonal and periaxonal swelling in KCC3-null fibers point to role of KCC3 in ion/fluid regulation. Future experiments need to address whether KCC3-null spinal and DRG neurons, as well as their axons, and peripheral Schwann cells are defective in volume regulation compared to wild-type cells as shown for renal tubules and hippocampal neurons (Boettger et al., 2003), and whether the volume regulation is related to spatial potassium buffering.

CHAPTER VI

PERIPHERAL MOTOR AND SENSORY DEFICITS IN KCC3$^{-/-}$ MICE

Introduction

Targeted disruption of the KCC3 gene in mice led to abnormal axon and periaxonal ultrastructure at early ages followed by neurodegeneration of peripheral nerves of old adult KCC3$^{-/-}$ mice. Locomotor and strength tests clearly demonstrated their neuromuscular problems at the behavioral level, which were consistent with sciatic nerve histopathology. However, since abnormalities in the brain, spinal cord, peripheral nerve and/or muscle can all manifest as peripheral deficits, electrophysiological diagnosis clinically aids in the determining the severity of the conduction deficit. It is also used to determine whether the peripheral neuropathy is due to demyelination or axonopathy as discussed in Chapter 2. In humans, motor NCVs below 38 m/s indicates demyelination while decreased amplitude with relatively normal NCVs with supports axonal neuropathy, as in CMT2 (Harding & Thomas, 1980; Suter & Scherer, 2003; Zuchner & Vance, 2006). However, a mixture is possible, depending on the myelin histopathology and/or axonal abnormalities or loss (Zuchner & Vance, 2006). Unfortunately the nerve conduction results from ACCPN patients were inconsistent. Dupre et al. reviewed electrophysiological studies of 48 ACCPN patients (0 to 35 years old) who were all evaluated by the same neurologist over the last twenty years. The median motor nerve conduction velocities were separated in ranges by age, but the NCVs showed a wide rage of variability: 16-57 m/s (mean 33 m/s) for ages 0-2 years; 26-45 m/s (mean 34 m/s) for

ages 2 to 15; and 11-39 m/s (mean 23 m/s) for ages 15 to 35 the (Dupre et al., 2003). These differences could stem from the grouping of a wide age ranges, but the reason for the discrepancy is not known and the authors point out that it is difficult to classify the neuropathy of ACCPN as primarily axonal or demyelinating. Some patients may be more severely affected than others due to compounding environmental factors, such as poor nutrition or injury. Although unlikely due to their common French-Canadian background, some patients may have different mutations in KCC3, which increases the severity of the disease.

Neurologists frequently utilize EMG for nerve conduction to evaluate nerve disorders. Despite the opportunities for genetic testing, nerve conduction velocity is still a parameter for diagnosing CMTD and other peripheral neuropathies (Zuchner & Vance, 2006). EMG is a technique for recording muscle fiber responses. The instrumentation, an electromyograph, detects changes in the electrical potential generated by electrode-targeted muscle fibers during contraction and at rest. The resulting electromyogram is the waveform of the compound muscle action potential (CMAP). Stimulation of the innervating peripheral nerve can contract muscle fibers. When a peripheral nerve is stimulated at the threshold for activation, either voluntarily or with current input through an electrode, the compound action potential (CAP) travels down the nerve bundle, and eventually the signal, mediated by the neurotransmitter acetylcholine, is passed through the neuromuscular junction (NMJ) to muscle fibers. The NMJ is the synapse between the axon and motoneuron's motor end plate, which is a highly excitable region of muscle fiber membrane responsible for initiating muscle contraction. Before reaching the NMJ, motor axons split into many unmyelinated terminal branches that end just adjacent to the

sarcolemma. At the terminal boutons, or varicosities, of the motor axons, synaptic vesicles loaded with acethylcholine are ready to fuse to the axolemma and release neurotransmitter (exocytosis). Vesicular release depends on sufficient calcium influx for the depolarization of the axon terminal resulting in an end-plate potential that normally triggers muscle depolarization and contraction. Certain toxins, perhaps most famously botulinum toxin A, affect cholinergic junctions presynaptically, causing paralysis and respiratory failure; internalized botulinum toxin, for example, blocks vesicular exocytosis. Acetylcholine released into the NMJ binds to nicotinic acetycholine receptors, which are ligand-gated ion channels permeable to cations.

The difference between muscle and peripheral nerve defects can be teased out using EMG. A mouse model of Friedriech ataxia, the neuron-specific frataxin-knockout, dragged its hind limbs. These mutants developed a progressive movement disorder that included gait abnormality. However, motor velocity was relatively normal in the knockout animals. In contrast, the absence of H band response, representing sensorimotor reflexes, after sciatic nerve stimulation indicates that the large myelinated proprioceptive sensory neurons are functionally defective. The peripheral nerve deficiency is therefore restricted to large myelinated sensory neurons, characteristic of Freidriech ataxia (Puccio & Koenig, 2002).

We utilized EMG for nerve conduction studies of KCC3-null sciatic nerves to assess whether the defects described in Chapter IV led to neurophysiological changes. We evaluated motor NCV of the sciatic-tibial nerves since they innervate the hind leg, the region of interest, by stimulating at the knee using needle electrodes, then injecting current at the sciatic notch. CMAPs were recorded at the foot muscles. Assessing motor

nerve conduction and pain threshold can help evaluate the functional integrity of nerves underlying those modalities.

Materials and Methods

Animals

Animal generation, mating, and genotyping have been described in Chapter 3.

EMG and nerve conduction

Mice were anesthetized under constant oxygen and isoflurane flow using a vaporizer, and body temperature was maintained using a warming pad. Sciatic-tibial motor NCV was determined by first stimulating distally at the knee using bipolar Nicolet 0.4 mm platinum subdermal needle electrodes (Viasys Healthcare, Yorba Linda, CA) at supramaximal stimulation, and then at the sciatic notch. Compound muscle action potentials were recorded at the foot muscles with bipolar needle electrodes and data acquired using a Nicolet VikingQuest Portable System (Viasys Healthcare) with stimulus duration at 0.02 ms, range 25mA. Electrodes were cleaned with 70% alcohol between animals. Latencies and traces were analyzed using the VikingQuest software. Latencies were measured from stimulus onset to maximum negative peak. Sciatic-tibial NCVs were calculated using the distances between the two points of stimulation along the nerve divided by the resultant latencies.

Hot plate assay

Mice were transferred to the testing room and allowed to acclimate for 1 h before testing. Nociception threshold was measured for each mouse using a hot plate (model 35D; IITC Corporation, Woodland Hills, CA) that was maintained at 52°C. The mouse was confined to the surface of the hot plate by a clear acrylic cylinder (15 cm in diameter and 12.5 cm high). To measure pain threshold, the latency to respond with either hind paw licking, shaking/fluttering, or jumping was measured with a stop watch. The mouse was then immediately removed from the hot plate and returned to its cage. Each animal was tested twice, with a one week interval between the two sessions.

Results

Motor nerve conduction velocity is reduced in KCC3-null mice

To test whether the morphological abnormalities in the adult knockout mouse result in a change in nerve conduction velocity (NCV), we measured CMAPS at the foot muscle after stimulation at the knee and sciatic notch to determine sciatic-tibial conduction velocities. Since we were not directly measuring the CAP, we first calculated the conduction and muscle response rate after stimulation at the knee for the tibial component, and then moved the stimulating electrode to the sciatic notch. This way we could subtract out the time for neuromuscular junction/muscle response, in case there were defects in knockout, and calculated a conduction velocity for the nerve itself. The sciatic nerve is a mixed motor-sensory nerve, but since the output of nerve stimulation was muscle response (CMAP), we were solely evaluating motor fibers, which are all large-caliber, myelinated nerve fibers. We found that motor NCVs were significantly

reduced in KCC3$^{-/-}$ mice, compared to heterozygote knockout and wild-type mice (Figure 6-1B).

Decreased pain perception in KCC3-null mice

We utilized the standard hot plate test to evaluate pain threshold in KCC3$^{-/-}$ mice. Since the knockout mice have weak hind limbs, they may not be able to lick their hind paws as easily as wild-type mice, so we included shaking, fluttering, lifting of hind paws, and jumping as nociceptive withdrawal reflexes for both genotypes. Although KCC3$^{-/-}$ mice rarely licked their hind paws on this test, they were able to display the other discomfort responses, even jumping. KCC3 knockout mice exhibited impaired pain perception on the 52°C plate assay as demonstrated by their longer response latencies (Figure 6-1C). Noxious pain signals, such as 52°C temperature, are carried by unmyelinated fibers, so the sensory defect of KCC3$^{-/-}$ mice point to possible changes in unmyelinated fibers.

Discussion

Here our goal was to measure the impact of the morphological changes in the sciatic nerve of older KCC3-null adult mice, described in Chapter V, on its neurophysiological properties. NCV of KCC3$^{-/-}$ sciatic nerve was statistically slower than in wild-type and the knockouts also exhibited a decreased sensitivity to pain. The two main underlying causes of decreased compound nerve conduction velocity are a loss and/or decreased thickness of the myelin sheath, a loss of myelinated axons, or a combination of both, all which need to be verified histologically. Thin sheaths, or

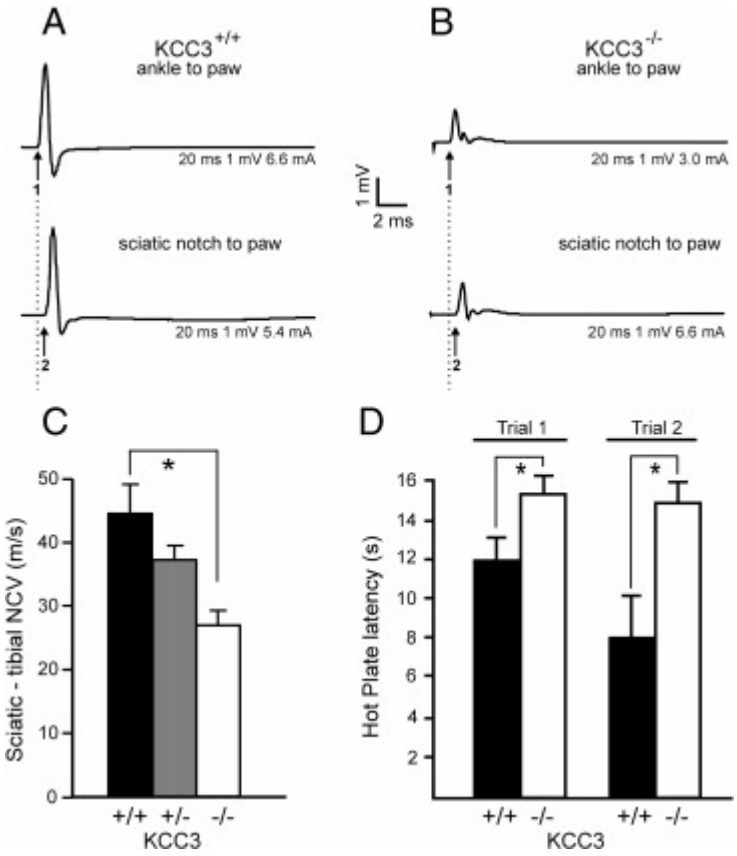

Figure 6-1. Decreased motor conduction velocities and pain sensitivity in KCC3-null mice

Electromyograph traces from representative wild-type (A) and KCC3$^{-/-}$ (B) sciatic nerves. The top trace represents the compound muscle action potential (CMAP) measured at the foot muscles after stimulation at the ipsilateral knee, while the lower trace represents the CMAP measured at the same foot muscles (recording electrodes were not moved) after stimulation at the sciatic notch. Numbers 1 and 2 mark the onset of the CMAP. (C) Conduction velocity is significantly decreased in sciatic nerve from KCC3$^{-/-}$ mice. (D) KCC3$^{-/-}$ mice show increased latencies for pain response on the 52^{o}C hot plate. Two trials were conducted, one week apart, yielding similar results. Asterisks indicate statistical difference with $P < 0.001$.

hypomyelination, can usually be determined by calculating G ratios, and demyelination can be assessed by microscopy on cross-sectioned nerve samples by the presence of onion bulb formations and large, naked axons. The mean G ratio of fibers of older adult $KCC3^{-/-}$ sciatic nerves was not significantly different compared to wild-type. Also, there was no evidence of onion bulbs and large, unmyelinated axons in knockout sciatic nerves, but rather regenerating clusters, an excessive amount of collagen pockets, and bands of Büngner, which are all evidence of axon loss (King, 1999). The loss of axons in adult KCC3-null sciatic nerves is compatible with decreased sciatic motor NCV. Since we measured CMAPs, a muscle response, we were evaluating large-diameter, myelinated motor axons. Therefore, the decrease in NCV in $KCC3^{-/-}$ mice indicates the specific loss of large motor fibers. Indeed, there is axonal loss in $KCC3^{-/-}$ sciatic nerves as 11.24 ± 1.84% of total myelinated axons counted were in regenerating clusters. This count does not include sprouting axons that have not yet been myelinated, so there is actually more axon regrowth than that percentage reflects. Axonal sprouts, however, even if myelinated and reach their targets, have consecutively short internodes (King, 1999), which slows axon conduction velocities.

Although slowed NCV is considered an indication of hypo- or de-myelination, subtle but statistically significant decreases in NCV have been reported for axonopathies. Animal models of some axonal neuropathies, such as superoxide dismutase knockout mice, had slowed motor conduction due to axonal loss (Flood et al., 1999). The motor NCVs of MAG knockouts, which exhibited axonal degeneration but normal myelin in their peripheral nerves, were also slowed compared to wild-type (Weiss et al., 2001). On the other hand, an extremely dramatic decrease in NCV, would be more compatible with

dys- or de-myelination. For example, in a mouse model of CMT1B with dysmyelinating neuropathy, mean motor nerve conduction velocity dropped from 40.2 ± 2.9 m/s to 2.0 ± 0.3 m/s (Runker et al., 2004). Compared to this, the slowed motor NCV in KCC3-null mice are mild.

The waveform of the CMAP can also give clues to the defect. For example, nerve conduction block is demonstrated by the lack of F-waves, which is normally a small peak following the CMAP. When the sciatic or tibial nerve is stimulated, the foot muscles respond; however, an impulse can travel back up the nerve to stimulate the neurons, which is basically the volleying of stimulation, so the F-wave reflects a second nerve activation. Full or partial conduction block prevents the signal from volleying up and down the nerve (Thaisetthawatkul et al., 2002). We could not elicit F-waves in the wild-type, which may require a different frequency of stimulation, so we did not pursue these in the knockouts. H band responses represent large myelinated proprioceptive sensory neurons (Puccio & Koenig, 2002), but this was beyond my technical abilities. Using our method, amplitudes are not comparable between animals because of the varying distances of the stimulation electrode from the nerve. An accurate way to assess amplitudes would be to surgically open the sciatic notch and directly stimulate the nerve with electrodes.

The significantly higher pain threshold measured in $KCC3^{-/-}$ mice compared to wild-type on the hot-plate test matches the clinical findings of sensory neuropathy in ACCPN patients. The failure to elicit reflexes in patients is a common finding, which also indicates sensory defects. Abnormalities in both ventral and dorsal roots of $KCC3^{-/-}$ mice indicate the involvement of both motor and sensory fibers (Boettger et al., 2003). In the sciatic nerve, however, large, myelinated proprioceptive fibers cannot be distinguished

from motor fibers, so we do not know if one is preferentially affected. Since noxious pain is transduced via unmyelinated fibers, this supports the finding of sensory fiber involvement in the loss of sensitivity in the knockout. Although we did not observe any obvious abnormalities in the Remak bundles of the sciatic nerve, whether or not unmyelinated axons also undergo swelling is unknown and could be evaluated by morphometric analysis. However, as the hot-plate-evoked-pain response occurs through a supraspinal pathway, conduction and/or processing of pain sensory information can occur at multiple levels, including the CNS. Therefore, the pain phenotype could also originate from outside the peripheral nervous system.

We cannot exclude CNS abnormalities as one component of the locomotor problems of ACCPN patients and $KCC3^{-/-}$ knockout mice. Slower conduction of somatosensory evoked potentials (SSEPs) in the spinal cord would indicate such a problem. I would expect decreased conduction of SSEPs in affected spinal cord due to swelling defects of similar appearance in spinal cord white matter (data not shown).

CHAPTER VII

FINAL CONCLUSIONS AND FUTURE DIRECTIONS

Summary

The behavioral characterization of $KCC3^{-/-}$ mice revealed peripheral and central deficits highlighting the importance of the cotransporter in the nervous system despite its widespread expression. Although the KCC3-null mouse is biologically interesting in itself for the study of the role of the cotransporter, concomitant studies by collaborators revealing that KCC3 is mutant in the neurological disorder ACCPN was exciting as the $KCC3^{-/-}$ mouse proved to be an accurate disease model since the human mutations led to nonfunctional protein. Since the peripheral neuropathy is fully penetrant in patients and mice, we focused on this aspect of the disorder. Outside of the clinical symptoms, literature on ACCPN was devoid of information except for a small number of sural nerve biopsies at different ages, while authors puzzled over the sciatic nerve defects and the lack of expression in that tissue. Therefore, we pursued further investigation on how the loss of KCC3 leads to neuromuscular defects in order to determine a role of the cotransporter in the PNS. We showed that KCC3 is indeed expressed by sciatic nerves at early postnatal ages and that the protein localizes to Schwann cell bodies. We hypothesized that the lack of KCC3 in Schwann cells leads to hypomyelination and myelin degeneration based on results of previous histology experiments. An alternative would be that the neuropathy could stem from the lack of KCC3 in the spinal motor and/or DRG sensory neurons as several spinal motor diseases can lead to peripheral

deficits and histopathology. However, in the case of our KCC3-knockout mice, morphometric and ultrastructural analyses show that both neuron/axon and Schwann cell are involved in the disorder, with the lack of neuronal KCC3 leading to axonal swelling and KCC3 loss in Schwann cells causing periaxonal swelling. These defects subside in adult nerve when KCC3 is undetectable, which instead, show signs of neurodegeneration, specifically Wallerian-like degeneration of axon loss and regrowth. The loss of large axons reduces nerve conduction velocities in $KCC3^{-/-}$ mice compared to wild-type. They are also less sensitive to noxious temperatures, which points to a sensory defect. Both types of abnormalities likely underlie the peripheral neuropathy of ACCPN since the fluid-related swelling (without any signs of neurodegeneration) occurs in early ages when locomotor problems arise. The neuromuscular problems continue into adulthood while the histopathology changes. Although axon development is normal, at least in quantity, reflected by equal numbers in mutant and wild-type nerve, the adult-onset Wallerian-like degeneration in KCC3-null sciatic nerve points to ACCPN as an axonal neuropathy. Based on the swelling pathologies, we propose that KCC3 plays a role in volume and ion/fluid regulation, which matches the classical function of KCCs. KCC3 is essential for the maintenance and normal function of peripheral nerves.

KCC3 function

Volume regulation

The results of the morphometric analysis presented here points to swelling of axons as an initial abnormality in KCC3-null sciatic nerves, supporting a problem in cell volume regulation. Although immunostaining did not reveal KCC3 protein at the

axolemma, KCC3 is expressed by motor and sensory neurons and its loss there could affect its extensions. Impaired regulatory volume decrease (RVD) after hypotonic challenge has been demonstrated for KCC3 deficient hippocampal neurons (Boettger et al., 2003). To test the hypothesis that the ability to maintain volume is lost in motor and sensory neurons, similar experiments need to be performed on cultured DRG and spinal cord neurons. Briefly, after video monitoring of cells in culture before and after perfusion with hypotonic solution, cells can be measured from individual frames at different time intervals using software such as Image J, and volumes extrapolated. I expect that KCC3 deficient cells would exhibit an extremely slowed response. Such a result would functionally support the morphometric data. Although hypotonicity is used to activate KCC3 in experiments, other cellular stressors should also be tested in a similar manner, including hypoxic, excitotoxic, and hyponatremic conditions.

Potassium buffering/ion transport

The fact that KCC3 localized to the Schwann cell body and not to the adaxonal membrane may lead to skepticism to the suggestion that it is involved in potassium buffering especially since KCCs are extrusion, not uptake, mechanisms. Na-K ATPase, potassium channels, and gap junctions are all potassium uptake mechanisms into the Schwann cell (Dyer, 2000). As discussed in detail in Chapter V, KCC3 may be involved in spatial buffering of potassium. In epithelial cells, ions taken up on one side of the cell are released to another. In the CNS, potassium uptake into the oligodendrocyte and release into junctionally connected astrocytes requires gap junctions (Menichella et al., 2003; Menichella et al., 2006). In the PNS, once potassium ions radially move through

Cx32 gap junctions connecting the myelin layers to the Schwann cell body, KCC3 could serve as a release mechanism, which would be followed by fluid movement. The Schwann cell's capacity for RVD can be evaluated *in vitro* in as described for neurons above. In this current study, unlike for axons, it was not possible to measure Schwann cell diameters for morphometric analysis from EM photomicrographs since it was rare to section through a cell body and impossible to tell if the slice was taken at the center (larger) or edges (smaller).

Immunostaining experiments showed that KCC3 is located mostly perinuclearly, so there is the possibility that KCC3 protein is recruited to the plasma membrane in activating conditions (i.e., hypotonic stress). This could be tested by perfusion of cultured Schwann cells in hyposmotic solution followed by fixation and immunostaining. Transfecting cells with GFP-KCC3 would allow for live cell imaging during hypotonic stress and recovery.

KCC3 may play different roles in the neuron and Schwann cell, such as volume regulation in the neuron and transepithelial-like ion/fluid transport (i.e., spatial buffering triggered by cell swelling) in the Schwann cell. Schwann cells have been likened to epithelial cells as they are both polarized. Any ion movement from the basolateral to apical side would require uptake of ions into the Schwann cell followed by extrusion by the cell body (Figure 7-1). Although other proteins, based on their localization, are likely the main players in potassium uptake buffering, the blockade or loss of KCC3 could cause a backup of ions/fluid resulting in excessive fluid in the periaxonal space. We could perform similar experiments that were conducted by Menichella et al. (Menichella et al., 2003; Menichella et al., 2006), such as continuously overstimulating the sciatic

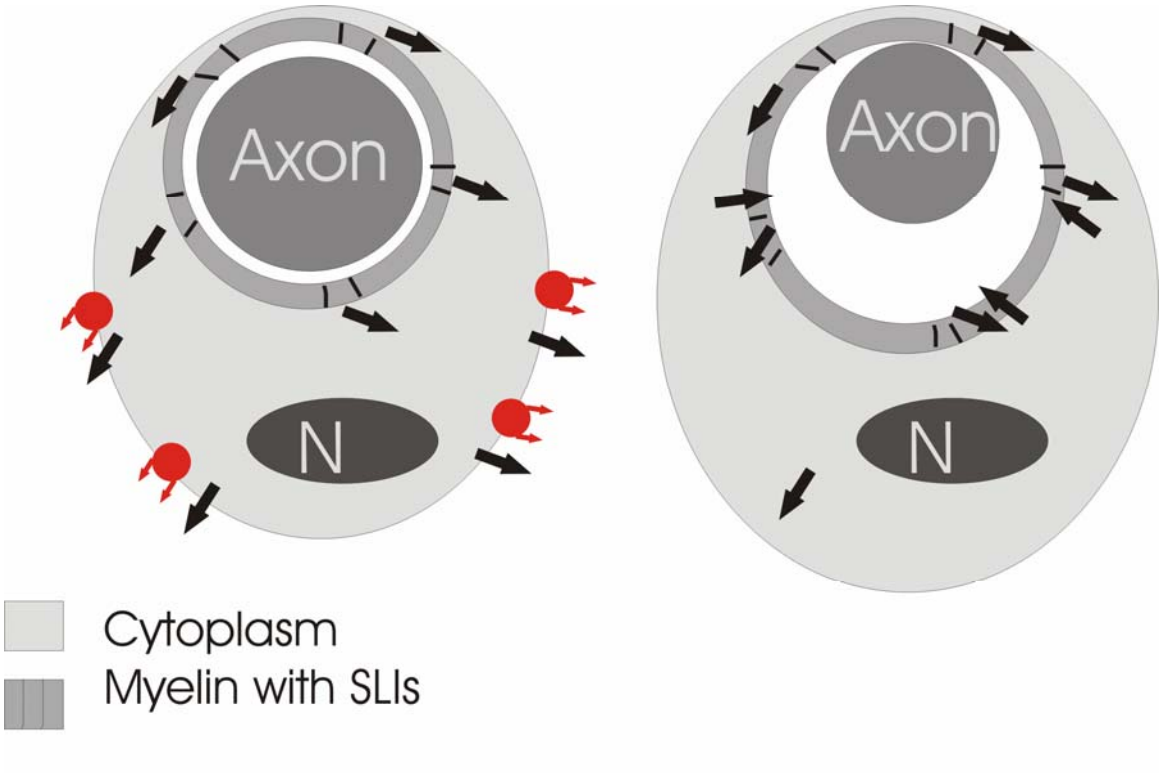

Figure 7-1. Potassium ion secretion from the Schwann cell body via KCC3

In this model, based on the localization of KCC3 on Schwann cell bodies, KCC3 (red) acts as an extrusion mechanism, releasing ions/fluid that has accumulated in the cell. This type of absorption/secretion mechanism has been well-studied in epithelial tissue. Uptake of potassium occurs via the N-K ATPase and potassium channels, and fluid follows (arrows) through Cx32 gap junctions that form radial pathways called Schmidt-Lanterman incisures (SLIs) in the myelin and serve as diffusion pathways connecting the periaxonal space and myelin with the Schwann cell body proper. The loss of KCC3 would usually lead to extensive cell swelling due to impaired RVD; the swelling may be initiated by ion uptake. However, ions/fluid that cannot be released out of the Schwann cell body can back up into the radial pathways into the empty periaxonal space. This could explain the extreme fluid accumulation in the periaxonal space in KCC3-null fibers. In this process, the axon loses contact with the myelin and atrophies. On the other hand, for axonal swelling in KCC3-null sciatic nerve, I propose that neuronal cell volume regulation is impaired as previously described for hippocampal neurons. N = nucleus.

nerve to release excessive potassium into the periaxonal space, and then assess the increase in number and size of periaxonal enlargements in the nerve compared to the unstimulated nerve. This can be done using needle electrodes used in nerve conduction studies to deliver trains of current to the sciatic nerve that activate hind leg muscles.

Besides gap junction diffusion pathways formed by Cx32, other proteins in the radial pathway could participate in ion buffering. In fact, NKCC1 is localized to SLIs (Figure 7-2), and as in traditional epithelia, could mediate ion cotransport through the incisures.

CNS

A similar pathological mechanism may be occurring in spinal cord white matter as in the sciatic nerve, and would likely also affect neurotransmission. This can be evaluated by recording somatosensory evoked potentials (SSEPs). Like the decreased NCVs in the sciatic nerve, I would expect reduced conduction velocities in the spinal cord. The peripheral neuropathy of ACCPN is likely much more complicated than the defects in sciatic nerve alone. The close to normal motor NCVs in some ACCPN patients does not seem to warrant complete wheelchair dependence; therefore, myelinated proprioceptive fibers are likely to be severely affected. Likewise, the slowed motor NCVs of KCC3-null mice compared to wild-type, are, surprisingly, not extremely low (single digits) as one would expect from their hind limb dragging. Changes in sensory perception likely plays a large role in the peripheral neuropathy. This may be related to defects at the nerve and/or spinal cord levels. We measured only one sensory modality, noxious pain; however proprioception should also be tested. A similar morphometric analysis could

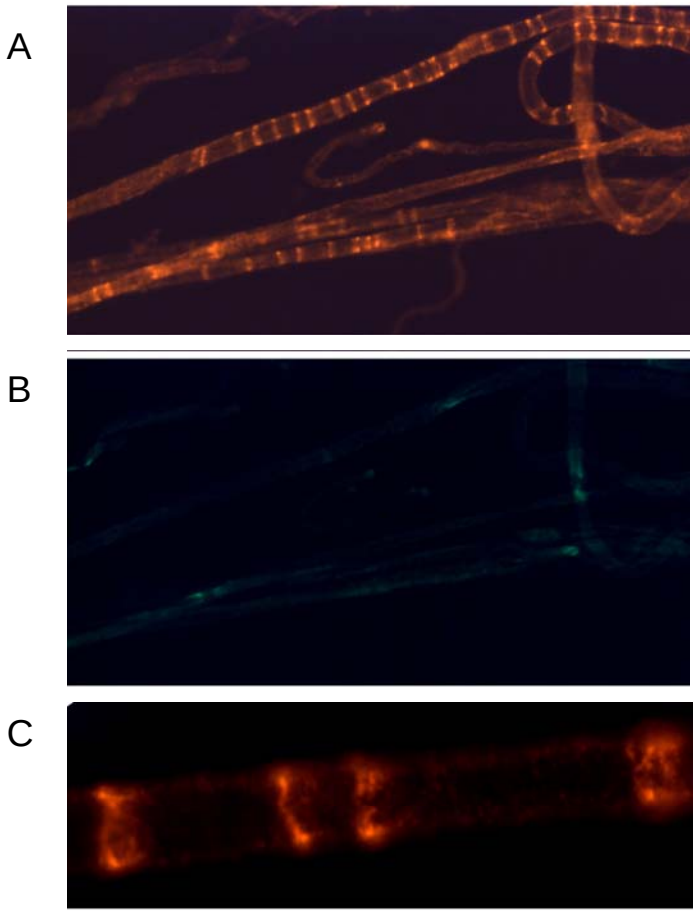

Figure 7-2. NKCC1 localizes to Schmidt-Lanterman incisures

(A) In immunostaied teased sciatic nerve fibers, NKCC1 localizes SLIs in a characteristic railroad track pattern. (B) Kv1.2 immunostaining marks the juxtaparanodes. (D) Higher magnification of panel A.

also be conducted in spinal cord sections by EM to show that the same underlying mechanism affects both the PNS and CNS. Also, cultured spinal cord oligodendrocytes can be used to test the hypothesis that central myelinating cells also regulate cell volume.

Like the psychosis of metochromatic leukodystrophy, which is correlated to damage of central myelinated axons (see Chapter 3), alteration in neurotransmission from changes in fiber tracts is a plausible explanation for schizophrenia-like symptoms from $KCC3^{-/-}$ loss of function in ACCPN. The main difference between the two disorders is primary myelin abnormalities in leukodystrophy and neuronal/axonal changes in KCC3-null brains (Boettger et al., 2003), which likely occurs in ACCPN patients. Boettger et al. detected enlarged myelinated and unmyelinated axons in $KCC3^{-/-}$ hippocampus and cerebellum (Boettger et al., 2003). Both myelin and neuronal/axonal defects can change neurotransmission. Although no abnormalities were detected in the corpus callosum of KCC3 knockout mice (Boettger et al., 2003; Howard et al., 2002b), there could be subtle differences that require morphometric analysis to differentiate. Other fiber tracts could also be involved and this should be investigated.

Additional mouse models

The expression of KCC3 in neurons and Schwann cells complicates matters since it is difficult to assess which component of the sciatic nerve contributes more to the peripheral neuropathy. Although the axonal degeneration and regeneration seem to indicate that the loss of KCC3 in the neuron leads to the neurodegeneration, we do not know if the early periaxonal swelling plays a bigger role in the locomotor defects at early ages and if this leads to axonal degeneration. Therefore cell specific knockout mice,

made utilizing Cre-loxP technology, would address this question. For example, Cre recombinase driven by the P0-promoter would delete KCC3 only in Schwann cells, while utilizing the Nav1.8-promotor to drive Cre recombinase would lead to DRG-specific KCC3 ablation.

We cannot rule out that the peripheral neuropathy phenotype induced by KCC3 disruption could be related to an interacting protein. One protein family that comes to mind is stress Ste-kinases, specifically SPAK/OSR1 (Piechotta et al., 2003; Piechotta et al., 2002) due to the evidence of their involvement in peripheral nerve. The disruption of the OSR1 *Drosophila* homolog Fray leads to focal nerve bulges containing electron-transparent regions remarkably similar to those in $KCC3^{-/-}$ fibers (Leiserson et al., 2000). Since phosphorylation inactivates KCCs, the loss of SPAK/OSR1 in mammals should lead to the activation, not the loss, of KCC3 function. However, whether there is a *Drosophila* homolog of KCC3 is not yet known; the only KCC in the fruitfly is kazachoc, a KCC2 homolog. Also, we do not know the protein targets of Fray. If Fray activated a protein that is responsible for taking up ions, such as a potassium or chloride channel or NKCC1 homolog, the loss of Fray could lead to fluid accumulation due to the lack of an ion uptake buffering mechanism. Creating a mouse with a non-functional KCC3 mutant that is expressed at the plasma membrane and capable of protein interactions would tell us if it is indeed KCC3, not the loss of a protein partner, which leads to the nerve abnormalities.

Recapitulating the disorder in mice with a KCC3 inhibitor would also show that the cotransporter is specifically involved in the peripheral neuropathy. Unfortunately, there are no specific inhibitors to KCC3. However, there is the possibility that furosemide

delivery to the sciatic nerves and/or spinal cord via pump could lead to peripheral neuropathy. More important though is the rescue of the knockout mouse either by transgenic or molecular therapeutics addressing the pathology, which should apply to other axonopthies.

Hereditary neuropathies are caused by defects in myelin and/or neuronal proteins and ACCPN is not an exception. The mouse model is important due to a lack of specific inhibitors, and a dearth of longitudinal studies. The KCC3 knockout mouse has allowed us to follow the disorder morphometrically and ultrastructurally at different ages to determine its pathogenesis. In conclusion, our data show the importance of KCC3 function in the maintenance of peripheral nerves likely through cell volume and ion/fluid regulation. Further studies on cell volume regulation in neurons and ion buffering by Schwann cells should support this proposal. We also show that after a brief period of normal development, the peripheral neuropathy in ACCPN arises from fluid-related axonal and Schwann cell deficits and progresses into a neurodegenerative axonal disorder with myelin involvement but no active demyelination/remyelination. ACCPN is a complicated disease as it also involves the CNS, which needs to be further studied in the mouse models and in patients. Our results are likely relevant for the CNS, and this hypothesis needs to be followed up with experiments since defects in the brain and spinal cord may also contribute to the peripheral neuropathy and pain phenotype as well as deficits leading to psychosis. Additional animal models should allow us to determine whether restoration of KCC3 function in childhood or early adulthood could reverse or ameliorate some of the ACCPN symptoms.

REFERENCES

Adlkofer, K., Frei, R., Neuberg, D.H., Zielasek, J., Toyka, K.V. & Suter, U. (1997). Heterozygous peripheral myelin protein 22-deficient mice are affected by a progressive demyelinating tomaculous neuropathy. *J Neurosci*, **17,** 4662-71.

Albers, J.W. & Fink, J.K. (2004). Porphyric neuropathy. *Muscle Nerve*, **30,** 410-22.

Alberti, S., Gregorio, E.A., Spadella, C.T. & Cojocel, C. (2007). Localization and irregular distribution of Na,K-ATPase in myelin sheath from rat sciatic nerve. *Tissue Cell*, **39,** 195-201.

Alexander, R.T. & Grinstein, S. (2006). Na+/H+ exchangers and the regulation of volume. *Acta Physiol (Oxf)*, **187,** 159-67.

Altevogt, B.M., Kleopa, K.A., Postma, F.R., Scherer, S.S. & Paul, D.L. (2002). Connexin29 is uniquely distributed within myelinating glial cells of the central and peripheral nervous systems. *J Neurosci*, **22,** 6458-70.

Alvarez-Leefmans, F.J., Gamino, S.M., Giraldez, F. & Nogueron, I. (1988). Intracellular chloride regulation in amphibian dorsal root ganglion neurones studied with ion-selective microelectrodes. *J Physiol*, **406,** 225-46.

Anzini, P., Neuberg, D.H., Schachner, M., Nelles, E., Willecke, K., Zielasek, J., Toyka, K.V., Suter, U. & Martini, R. (1997). Structural abnormalities and deficient maintenance of peripheral nerve myelin in mice lacking the gap junction protein connexin 32. *J Neurosci*, **17,** 4545-51.

Arroyo, E.J. & Scherer, S.S. (2000). On the molecular architecture of myelinated fibers. *Histochem Cell Biol*, **113,** 1-18.

Atanasoski, S., Notterpek, L., Lee, H.Y., Castagner, F., Young, P., Ehrengruber, M.U., Meijer, D., Sommer, L., Stavnezer, E., Colmenares, C. & Suter, U. (2004). The protooncogene Ski controls Schwann cell proliferation and myelination. *Neuron*, **43,** 499-511.

Auer-Grumbach, M., De Jonghe, P., Verhoeven, K., Timmerman, V., Wagner, K., Hartung, H.P. & Nicholson, G.A. (2003). Autosomal dominant inherited neuropathies with prominent sensory loss and mutilations: a review. *Arch Neurol*, **60,** 329-34.

Bach, M.E., Hawkins, R.D., Osman, M., Kandel, E.R. & Mayford, M. (1995). Impairment of spatial but not contextual memory in CaMKII mutant mice with a selective loss of hippocampal LTP in the range of the theta frequency. *Cell*, **81,** 905-15.

Bachmann, O., Wuchner, K., Rossmann, H., Leipziger, J., Osikowska, B., Colledge, W.H., Ratcliff, R., Evans, M.J., Gregor, M. & Seidler, U. (2003). Expression and regulation of the Na+-K+-2Cl- cotransporter NKCC1 in the normal and CFTR-deficient murine colon. *J Physiol*, **549,** 525-36.

Bachmann, S., Velazquez, H., Obermuller, N., Reilly, R.F., Moser, D. & Ellison, D.H. (1995). Expression of the thiazide-sensitive Na-Cl cotransporter by rabbit distal convoluted tubule cells. *J Clin Invest*, **96,** 2510-4.

Baker, M.D. (2002). Electrophysiology of mammalian Schwann cells. *Prog Biophys Mol Biol*, **78,** 83-103.

Ballas, N., Battaglioli, E., Atouf, F., Andres, M.E., Chenoweth, J., Anderson, M.E., Burger, C., Moniwa, M., Davie, J.R., Bowers, W.J., Federoff, H.J., Rose, D.W., Rosenfeld, M.G., Brehm, P. & Mandel, G. (2001). Regulation of neuronal traits by a novel transcriptional complex. *Neuron*, **31,** 353-65.

Ballas, N., Grunseich, C., Lu, D.D., Speh, J.C. & Mandel, G. (2005). REST and its corepressors mediate plasticity of neuronal gene chromatin throughout neurogenesis. *Cell*, **121,** 645-57.

Bao, G. & Suresh, S. (2003). Cell and molecular mechanics of biological materials. *Nat Mater*, **2,** 715-25.

Beaumont, K., Vaughn, D.A. & Fanestil, D.D. (1988). Thiazide diuretic drug receptors in rat kidney: identification with [3H]metolazone. *Proc Natl Acad Sci U S A*, **85,** 2311-4.

Ben-Ari, Y., Cherubini, E., Corradetti, R. & Gaiarsa, J.L. (1989). Giant synaptic potentials in immature rat CA3 hippocampal neurones. *J Physiol*, **416,** 303-25.

Berger, P., Niemann, A. & Suter, U. (2006). Schwann cells and the pathogenesis of inherited motor and sensory neuropathies (Charcot-Marie-Tooth disease). *Glia*, **54,** 243-57.

Bermingham, J.R., Jr., Shearin, H., Pennington, J., O'Moore, J., Jaegle, M., Driegen, S., van Zon, A., Darbas, A., Ozkaynak, E., Ryu, E.J., Milbrandt, J. & Meijer, D. (2006). The claw paw mutation reveals a role for Lgi4 in peripheral nerve development. *Nat Neurosci*, **9,** 76-84.

Bernardi, P. (1999). Mitochondrial transport of cations: channels, exchangers, and permeability transition. *Physiol Rev*, **79,** 1127-55.

Bhat, M.A. (2003). Molecular organization of axo-glial junctions. *Curr Opin Neurobiol*, **13,** 552-9.

Bhat, M.A., Rios, J.C., Lu, Y., Garcia-Fresco, G.P., Ching, W., St Martin, M., Li, J., Einheber, S., Chesler, M., Rosenbluth, J., Salzer, J.L. & Bellen, H.J. (2001). Axon-glia

interactions and the domain organization of myelinated axons requires neurexin IV/Caspr/Paranodin. *Neuron*, **30,** 369-83.
Birouk, N., Gouider, R., Le Guern, E., Gugenheim, M., Tardieu, S., Maisonobe, T., Le Forestier, N., Agid, Y., Brice, A. & Bouche, P. (1997). Charcot-Marie-Tooth disease type 1A with 17p11.2 duplication. Clinical and electrophysiological phenotype study and factors influencing disease severity in 119 cases. *Brain*, **120 (Pt 5),** 813-23.

Black, D.N., Taber, K.H. & Hurley, R.A. (2003). Metachromatic leukodystrophy: a model for the study of psychosis. *J Neuropsychiatry Clin Neurosci*, **15,** 289-93.

Blanchard, A.D., Sinanan, A., Parmantier, E., Zwart, R., Broos, L., Meijer, D., Meier, C., Jessen, K.R. & Mirsky, R. (1996). Oct-6 (SCIP/Tst-1) is expressed in Schwann cell precursors, embryonic Schwann cells, and postnatal myelinating Schwann cells: comparison with Oct-1, Krox-20, and Pax-3. *J Neurosci Res*, **46,** 630-40.

Blanz, J., Schweizer, M., Auberson, M., Maier, H., Muenscher, A., Hubner, C.A. & Jentsch, T.J. (2007). Leukoencephalopathy upon disruption of the chloride channel ClC-2. *J Neurosci*, **27,** 6581-9.

Boettger, T., Hubner, C.A., Maier, H., Rust, M.B., Beck, F.X. & Jentsch, T.J. (2002). Deafness and renal tubular acidosis in mice lacking the K-Cl co-transporter Kcc4. *Nature*, **416,** 874-8.

Boettger, T., Rust, M.B., Maier, H., Seidenbecher, T., Schweizer, M., Keating, D.J., Faulhaber, J., Ehmke, H., Pfeffer, C., Scheel, O., Lemcke, B., Horst, J., Leuwer, R., Pape, H.C., Volkl, H., Hubner, C.A. & Jentsch, T.J. (2003). Loss of K-Cl co-transporter KCC3 causes deafness, neurodegeneration and reduced seizure threshold. *Embo J*, **22,** 5422-34.

Boiko, T., Rasband, M.N., Levinson, S.R., Caldwell, J.H., Mandel, G., Trimmer, J.S. & Matthews, G. (2001). Compact myelin dictates the differential targeting of two sodium channel isoforms in the same axon. *Neuron*, **30,** 91-104.

Bolino, A., Bolis, A., Previtali, S.C., Dina, G., Bussini, S., Dati, G., Amadio, S., Del Carro, U., Mruk, D.D., Feltri, M.L., Cheng, C.Y., Quattrini, A. & Wrabetz, L. (2004). Disruption of Mtmr2 produces CMT4B1-like neuropathy with myelin outfolding and impaired spermatogenesis. *J Cell Biol*, **167,** 711-21.

Bolis, A., Coviello, S., Bussini, S., Dina, G., Pardini, C., Previtali, S.C., Malaguti, M., Morana, P., Del Carro, U., Feltri, M.L., Quattrini, A., Wrabetz, L. & Bolino, A. (2005). Loss of Mtmr2 phosphatase in Schwann cells but not in motor neurons causes Charcot-Marie-Tooth type 4B1 neuropathy with myelin outfoldings. *J Neurosci*, **25,** 8567-77.

Bossy-Wetzel, E., Barsoum, M.J., Godzik, A., Schwarzenbacher, R. & Lipton, S.A. (2003). Mitochondrial fission in apoptosis, neurodegeneration and aging. *Curr Opin Cell Biol*, **15,** 706-16.

Bouwknecht, J.A. & Paylor, R. (2002). Behavioral and physiological mouse assays for anxiety: a survey in nine mouse strains. *Behav Brain Res*, **136,** 489-501.
Boyle, M.E., Berglund, E.O., Murai, K.K., Weber, L., Peles, E. & Ranscht, B. (2001). Contactin orchestrates assembly of the septate-like junctions at the paranode in myelinated peripheral nerve. *Neuron*, **30,** 385-97.

Braff, D., Stone, C., Callaway, E., Geyer, M., Glick, I. & Bali, L. (1978). Prestimulus effects on human startle reflex in normals and schizophrenics. *Psychophysiology*, **15,** 339-43.

Braff, D.L. & Geyer, M.A. (1990). Sensorimotor gating and schizophrenia. Human and animal model studies. *Arch Gen Psychiatry*, **47,** 181-8.

Braff, D.L., Geyer, M.A. & Swerdlow, N.R. (2001). Human studies of prepulse inhibition of startle: normal subjects, patient groups, and pharmacological studies. *Psychopharmacology (Berl)*, **156,** 234-58.

Braff, D.L., Light, G.A., Ellwanger, J., Sprock, J. & Swerdlow, N.R. (2005). Female schizophrenia patients have prepulse inhibition deficits. *Biol Psychiatry*, **57,** 817-20.
Britsch, S., Goerich, D.E., Riethmacher, D., Peirano, R.I., Rossner, M., Nave, K.A., Birchmeier, C. & Wegner, M. (2001). The transcription factor Sox10 is a key regulator of peripheral glial development. *Genes Dev*, **15,** 66-78.

Brown, W.D. (2000). Osmotic demyelination disorders: central pontine and extrapontine myelinolysis. *Curr Opin Neurol*, **13,** 691-7.

Brunet, G.M., Gagnon, E., Simard, C.F., Daigle, N.D., Caron, L., Noel, M., Lefoll, M.H., Bergeron, M.J. & Isenring, P. (2005). Novel insights regarding the operational characteristics and teleological purpose of the renal Na+-K+-Cl2 cotransporter (NKCC2s) splice variants. *J Gen Physiol*, **126,** 325-37.

Capecchi, M.R. (1989). Altering the genome by homologous recombination. *Science*, **244,** 1288-92.

Chance, P.F., Alderson, M.K., Leppig, K.A., Lensch, M.W., Matsunami, N., Smith, B., Swanson, P.D., Odelberg, S.J., Disteche, C.M. & Bird, T.D. (1993). DNA deletion associated with hereditary neuropathy with liability to pressure palsies. *Cell*, **72,** 143-51.

Chilton, J.K. (2006). Molecular mechanisms of axon guidance. *Dev Biol*, **292,** 13-24.

Choleris, E., Thomas, A.W., Kavaliers, M. & Prato, F.S. (2001). A detailed ethological analysis of the mouse open field test: effects of diazepam, chlordiazepoxide and an extremely low frequency pulsed magnetic field. *Neurosci Biobehav Rev*, **25,** 235-60.

Chow, C.Y., Zhang, Y., Dowling, J.J., Jin, N., Adamska, M., Shiga, K., Szigeti, K., Shy, M.E., Li, J., Zhang, X., Lupski, J.R., Weisman, L.S. & Meisler, M.H. (2007). Mutation of

FIG4 causes neurodegeneration in the pale tremor mouse and patients with CMT4J. *Nature*, **448,** 68-72.
Colmenero-Flores, J.M., Martinez, G., Gamba, G., Vazquez, N., Iglesias, D.J., Brumos, J. & Talon, M. (2007). Identification and functional characterization of cation-chloride cotransporters in plants. *Plant J*, **50,** 278-92.

Cosgaya, J.M., Chan, J.R. & Shooter, E.M. (2002). The neurotrophin receptor p75NTR as a positive modulator of myelination. *Science*, **298,** 1245-8.

Coull, J.A., Boudreau, D., Bachand, K., Prescott, S.A., Nault, F., Sik, A., De Koninck, P. & De Koninck, Y. (2003). Trans-synaptic shift in anion gradient in spinal lamina I neurons as a mechanism of neuropathic pain. *Nature*, **424,** 938-42.

Court, F.A., Wrabetz, L. & Feltri, M.L. (2006). Basal lamina: Schwann cells wrap to the rhythm of space-time. *Curr Opin Neurobiol*, **16,** 501-7.

Crable, S.C., Hammond, S.M., Papes, R., Rettig, R.K., Zhou, G.P., Gallagher, P.G., Joiner, C.H. & Anderson, K.P. (2005). Multiple isoforms of the KC1 cotransporter are expressed in sickle and normal erythroid cells. *Exp Hematol*, **33,** 624-31.

Crawley, J.N. (1985). Exploratory behavior models of anxiety in mice. *Neurosci Biobehav Rev*, **9,** 37-44.

Crouch, J.J., Sakaguchi, N., Lytle, C. & Schulte, B.A. (1997). Immunohistochemical localization of the Na-K-Cl co-transporter (NKCC1) in the gerbil inner ear. *J Histochem Cytochem*, **45,** 773-8.

Cruz-Hofling, M.A., Love, S., Brook, G. & Duchen, L.W. (1985). Effects of Phoneutria nigriventer spider venom on mouse peripheral nerve. *Q J Exp Physiol*, **70,** 623-40.

Csomor, P.A., Stadler, R.R., Feldon, J., Yee, B.K., Geyer, M.A. & Vollenweider, F.X. (2007). Haloperidol Differentially Modulates Prepulse Inhibition and P50 Suppression in Healthy Humans Stratified for Low and High Gating Levels. *Neuropsychopharmacology*.
Darman, R.B., Flemmer, A. & Forbush, B. (2001). Modulation of ion transport by direct targeting of protein phosphatase type 1 to the Na-K-Cl cotransporter. *J Biol Chem*, **276,** 34359-62.

Davis, J.Q., Lambert, S. & Bennett, V. (1996). Molecular composition of the node of Ranvier: identification of ankyrin-binding cell adhesion molecules neurofascin (mucin+/third FNIII domain-) and NrCAM at nodal axon segments. *J Cell Biol*, **135,** 1355-67.

de Jong, J.C., Willems, P.H., Mooren, F.J., van den Heuvel, L.P., Knoers, N.V. & Bindels, R.J. (2003). The structural unit of the thiazide-sensitive NaCl cotransporter is a homodimer. *J Biol Chem*, **278,** 24302-7.

de Los Heros, P., Kahle, K.T., Rinehart, J., Bobadilla, N.A., Vazquez, N., San Cristobal, P., Mount, D.B., Lifton, R.P., Hebert, S.C. & Gamba, G. (2006). WNK3 bypasses the tonicity requirement for K-Cl cotransporter activation via a phosphatase-dependent pathway. *Proc Natl Acad Sci U S A*, **103,** 1976-81.

de Medinaceli, L., Freed, W.J. & Wyatt, R.J. (1982). An index of the functional condition of rat sciatic nerve based on measurements made from walking tracks. *Exp Neurol*, **77,** 634-43.

Decker, L., Desmarquet-Trin-Dinh, C., Taillebourg, E., Ghislain, J., Vallat, J.M. & Charnay, P. (2006). Peripheral myelin maintenance is a dynamic process requiring constant Krox20 expression. *J Neurosci*, **26,** 9771-9.

Delague, V., Jacquier, A., Hamadouche, T., Poitelon, Y., Baudot, C., Boccaccio, I., Chouery, E., Chaouch, M., Kassouri, N., Jabbour, R., Grid, D., Megarbane, A., Haase, G. & Levy, N. (2007). Mutations in FGD4 Encoding the Rho GDP/GTP Exchange Factor FRABIN Cause Autosomal Recessive Charcot-Marie-Tooth Type 4H. *Am J Hum Genet*, **81,** 1-16.

Delpire, E. (2000). Cation-Chloride Cotransporters in Neuronal Communication. *News Physiol Sci*, **15,** 309-312.

Delpire, E. & Gagnon, K.B. (2007). Genome-wide analysis of SPAK/OSR1 binding motifs. *Physiol Genomics*, **28,** 223-31.

Delpire, E. & Lauf, P.K. (1992). Kinetics of DIDS inhibition of swelling-activated K-Cl cotransport in low K sheep erythrocytes. *J Membr Biol*, **126,** 89-96.

Delpire, E., Lu, J., England, R., Dull, C. & Thorne, T. (1999). Deafness and imbalance associated with inactivation of the secretory Na-K-2Cl co-transporter. *Nat Genet*, **22,** 192-5.

Delpire, E. & Mount, D.B. (2002). Human and murine phenotypes associated with defects in cation-chloride cotransport. *Annu Rev Physiol*, **64,** 803-43.

Delpire, E., Rauchman, M.I., Beier, D.R., Hebert, S.C. & Gullans, S.R. (1994). Molecular cloning and chromosome localization of a putative basolateral Na-K-2Cl cotransporter from mouse inner medullary collecting duct (mIMCD-3) cells. *J. Biol. Chem.*, **269,** 25677-25683.

Denton, J., Nehrke, K., Yin, X., Morrison, R. & Strange, K. (2005). GCK-3, a newly identified Ste20 kinase, binds to and regulates the activity of a cell cycle-dependent ClC anion channel. *J. Gen. Physiol.*, **125,** 113-125.

Ding, J., Allen, E., Wang, W., Valle, A., Wu, C., Nardine, T., Cui, B., Yi, J., Taylor, A., Jeon, N.L., Chu, S., So, Y., Vogel, H., Tolwani, R., Mobley, W. & Yang, Y. (2006).

Gene targeting of GAN in mouse causes a toxic accumulation of microtubule-associated protein 8 and impaired retrograde axonal transport. *Hum Mol Genet*, **15,** 1451-63.
Djukic, B., Casper, K.B., Philpot, B.D., Chin, L.S. & McCarthy, K.D. (2007).

Conditional knock-out of Kir4.1 leads to glial membrane depolarization, inhibition of potassium and glutamate uptake, and enhanced short-term synaptic potentiation. *J Neurosci*, **27,** 11354-65.

Dugandzija-Novakovic, S., Koszowski, A.G., Levinson, S.R. & Shrager, P. (1995). Clustering of Na+ channels and node of Ranvier formation in remyelinating axons. *J Neurosci*, **15,** 492-503.

Dunham, P.B., Steward, G.W. & Ellory, J.C. (1980). Chloride-activated passive potassium transport in human erythrocytes. *Proc. Natl. Acad Sci. USA.* , **77,** 1711-1715.

Dupre, N., Howard, H.C., Mathieu, J., Karpati, G., Vanasse, M., Bouchard, J.P., Carpenter, S. & Rouleau, G.A. (2003). Hereditary motor and sensory neuropathy with agenesis of the corpus callosum. *Ann Neurol*, **54,** 9-18.

D'Urso, D., Brophy, P.J., Staugaitis, S.M., Gillespie, C.S., Frey, A.B., Stempak, J.G. & Colman, D.R. (1990). Protein zero of peripheral nerve myelin: biosynthesis, membrane insertion, and evidence for homotypic interaction. *Neuron*, **4,** 449-60.

Dzhala, V.I., Talos, D.M., Sdrulla, D.A., Brumback, A.C., Mathews, G.C., Benke, T.A., Delpire, E., Jensen, F.E. & Staley, K.J. (2005). NKCC1 transporter facilitates seizures in the developing brain. *Nat Med*, **11,** 1205-13.

Ecelbarger, C.A., Kim, G.H., Wade, J.B. & Knepper, M.A. (2001). Regulation of the abundance of renal sodium transporters and channels by vasopressin. *Exp Neurol*, **171,** 227-34.

Edmonds, B.T. & Koenig, E. (1990). Volume regulation in response to hypo-osmotic stress in goldfish retinal ganglion cell axons regenerating in vitro. *Brain Res*, **520,** 159-65.

Ellison, D.H., Velazquez, H. & Wright, F.S. (1987). Thiazide-sensitive sodium chloride cotransport in early distal tubule. *Am J Physiol*, **253,** F546-54.

Evans, R.L., Park, K., Turner, R.J., Watson, G.E., Nguyen, H.V., Dennett, M.R., Hand, A.R., Flagella, M., Shull, G.E. & Melvin, J.E. (2000). Severe impairment of salivation in Na+/K+/2Cl- cotransporter (NKCC1)-deficient mice. *J Biol Chem*, **275,** 26720-6.

Evgrafov, O.V., Mersiyanova, I., Irobi, J., Van Den Bosch, L., Dierick, I., Leung, C.L., Schagina, O., Verpoorten, N., Van Impe, K., Fedotov, V., Dadali, E., Auer-Grumbach, M., Windpassinger, C., Wagner, K., Mitrovic, Z., Hilton-Jones, D., Talbot, K., Martin, J.J., Vasserman, N., Tverskaya, S., Polyakov, A., Liem, R.K., Gettemans, J., Robberecht,

W., De Jonghe, P. & Timmerman, V. (2004). Mutant small heat-shock protein 27 causes axonal Charcot-Marie-Tooth disease and distal hereditary motor neuropathy. *Nat Genet*, **36,** 602-6.

Fabrizi, G.M., Cavallaro, T., Angiari, C., Bertolasi, L., Cabrini, I., Ferrarini, M. & Rizzuto, N. (2004). Giant axon and neurofilament accumulation in Charcot-Marie-Tooth disease type 2E. *Neurology*, **62,** 1429-31.

Fabrizi, G.M., Cavallaro, T., Angiari, C., Cabrini, I., Taioli, F., Malerba, G., Bertolasi, L. & Rizzuto, N. (2007). Charcot-Marie-Tooth disease type 2E, a disorder of the cytoskeleton. *Brain*, **130,** 394-403.

Feltri, M.L., Graus Porta, D., Previtali, S.C., Nodari, A., Migliavacca, B., Cassetti, A., Littlewood-Evans, A., Reichardt, L.F., Messing, A., Quattrini, A., Mueller, U. & Wrabetz, L. (2002). Conditional disruption of beta 1 integrin in Schwann cells impedes interactions with axons. *J Cell Biol*, **156,** 199-209.

Finn, D.A., Rutledge-Gorman, M.T. & Crabbe, J.C. (2003). Genetic animal models of anxiety. *Neurogenetics*, **4,** 109-35.

Fiumelli, H., Cancedda, L. & Poo, M.M. (2005). Modulation of GABAergic transmission by activity via postsynaptic Ca2+-dependent regulation of KCC2 function. *Neuron*, **48,** 773-86.

Flagella, M., Clarke, L.L., Miller, M.L., Erway, L.C., Giannella, R.A., Andringa, A., Gawenis, L.R., Kramer, J., Duffy, J.J., Doetschman, T., Lorenz, J.N., Yamoah, E.N., Cardell, E.L. & Shull, G.E. (1999). Mice lacking the basolateral Na-K-2Cl cotransporter have impaired epithelial chloride secretion and are profoundly deaf. *J. Biol. Chem.*, **274,** 26946-26955.

Flemmer, A.W., Gimenez, I., Dowd, B.F., Darman, R.B. & Forbush, B. (2002). Activation of the Na-K-Cl otransporter NKCC1 detected with a phospho-specific antibody. *J Biol Chem*, **277,** 37551-8.

Flood, D.G., Reaume, A.G., Gruner, J.A., Hoffman, E.K., Hirsch, J.D., Lin, Y.G., Dorfman, K.S. & Scott, R.W. (1999). Hindlimb motor neurons require Cu/Zn superoxide dismutase for maintenance of neuromuscular junctions. *Am J Pathol*, **155,** 663-72.

Frankenhaeuser, B. & Hodgkin, A.L. (1956). The after-effects of impulses in the giant nerve fibres of Loligo. *J Physiol*, **131,** 341-76.

Friede, R.L. & Bischhausen, R. (1980). The precise geometry of large internodes. *J Neurol Sci*, **48,** 367-81.

Friede, R.L., Meier, T. & Diem, M. (1981). How is the exact length of an internode determined. *J Neurol Sci*, **50,** 217-28.

Gagnon, E., Forbush, B., Caron, L. & Isenring, P. (2003). Functional comparison of renal Na-K-Cl cotransporters between distant species. *Am J Physiol Cell Physiol*, **284,** C365-70.

Gagnon, K.B., Adragna, N.C., Fyffe, R.E. & Lauf, P.K. (2007). Characterization of glial cell k-cl cotransport. *Cell Physiol Biochem*, **20,** 121-30.

Gagnon, K.B., England, R. & Delpire, E. (2006). Volume sensitivity of cation-Cl- cotransporters is modulated by the interaction of two kinases: Ste20-related proline-alanine-rich kinase and WNK4. *Am J Physiol Cell Physiol*, **290,** C134-42.

Gamba, G., Miyanoshita, A., Lombardi, M., Lytton, J., Lee, W.S., Hediger, M.A. & Hebert, S.C. (1994). Molecular cloning, primary structure, and characterization of two members of the mammalian electroneutral sodium-(potassium)-chloride cotransporter family expressed in kidney. *J Biol Chem*, **269,** 17713-22.

Gamba, G., Saltzberg, S.N., Lombardi, M., Miyanoshita, A., Lytton, J., Hediger, M.A., Brenner, B.M. & Hebert, S.C. (1993). Primary structure and functional expression of a cDNA encoding the thiazide-sensitive, electroneutral sodium-chloride cotransporter. *Proc Natl Acad Sci U S A*, **90,** 2749-53.

Ganguly, K., Schinder, A.F., Wong, S.T. & Poo, M. (2001). GABA itself promotes the developmental switch of neuronal GABAergic responses from excitation to inhibition. *Cell*, **105,** 521-32.

Garbay, B., Heape, A.M., Sargueil, F. & Cassagne, C. (2000). Myelin synthesis in the peripheral nervous system. *Prog Neurobiol*, **61,** 267-304.

Garzon-Muvdi, T., Pacheco-Alvarez, D., Gagnon, K.B., Vazquez, N., Ponce-Coria, J., Moreno, E., Delpire, E. & Gamba, G. (2007). WNK4 kinase is a negative regulator of K+-Cl- cotransporters. *Am J Physiol Renal Physiol*, **292,** F1197-207.

Geck, P., Pietrzyk, C., Burckhardt, B.-C., Pfeiffer, B. & Heinz, E. (1980). Electrically silent cotransport of Na^+, K^+ and Cl^- in Ehrlich cells. *Biochim. Biophys. Acta*, **600,** 432-447.

Ghislain, J. & Charnay, P. (2006). Control of myelination in Schwann cells: a Krox20 cis-regulatory element integrates Oct6, Brn2 and Sox10 activities. *EMBO Rep*, **7,** 52-8.

Giese, K.P., Martini, R., Lemke, G., Soriano, P. & Schachner, M. (1992). Mouse P0 gene disruption leads to hypomyelination, abnormal expression of recognition molecules, and degeneration of myelin and axons. *Cell*, **71,** 565-76.

Gillen, C.M., Brill, S., Payne, J.A. & Forbush, B., 3rd. (1996). Molecular cloning and functional expression of the K-Cl cotransporter from rabbit, rat, and human. A new member of the cation-chloride cotransporter family. *J Biol Chem*, **271,** 16237-44.

Gillespie, C.S., Sherman, D.L., Fleetwood-Walker, S.M., Cottrell, D.F., Tait, S., Garry, E.M., Wallace, V.C., Ure, J., Griffiths, I.R., Smith, A. & Brophy, P.J. (2000). Peripheral demyelination and neuropathic pain behavior in periaxin-deficient mice. *Neuron,* **26,** 523-31.

Gimenez, I. & Forbush, B. (2003). Short-term stimulation of the renal Na-K-Cl cotransporter (NKCC2) by vasopressin involves phosphorylation and membrane translocation of the protein. *J Biol Chem*, **278,** 26946-51.

Gimenez, I., Isenring, P. & Forbush, B. (2002). Spatially distributed alternative splice variants of the renal Na-K-Cl cotransporter exhibit dramatically different affinities for the transported ions. *J Biol Chem*, **277,** 8767-70.

Gomez, T.M., Robles, E., Poo, M. & Spitzer, N.C. (2001). Filopodial calcium transients promote substrate-dependent growth cone turning. *Science*, **291,** 1983-7.

Gomez, T.M. & Spitzer, N.C. (1999). In vivo regulation of axon extension and pathfinding by growth-cone calcium transients. *Nature*, **397,** 350-5.

Good, D.W. (1994). Ammonium transport by the thick ascending limb of Henle's loop. *Annu Rev Physiol*, **56,** 623-47.

Gordon, N. (1999). The acute porphyrias. *Brain Dev*, **21,** 373-7.

Graham, F.K. (1975). Presidential Address, 1974. The more or less startling effects of weak prestimulation. *Psychophysiology*, **12,** 238-48.

Grubb, B.R., Lee, E., Pace, A.J., Koller, B.H. & Boucher, R.C. (2000). Intestinal ion transport in NKCC1-deficient mice. *Am J Physiol Gastrointest Liver Physiol*, **279,** G707-18.

Guertin, A.D., Zhang, D.P., Mak, K.S., Alberta, J.A. & Kim, H.A. (2005). Microanatomy of axon/glial signaling during Wallerian degeneration. *J Neurosci*, **25,** 3478-87.

Haas, M. (1994). The Na-K-Cl cotransporters. . *Am. J. Physiol. (Cell Physiol.),* **267,** C869-C885.

Hahn, A.F., Ainsworth, P.J., Bolton, C.F., Bilbao, J.M. & Vallat, J.M. (2001). Pathological findings in the x-linked form of Charcot-Marie-Tooth disease: a morphometric and ultrastructural analysis. *Acta Neuropathol (Berl)*, **101,** 129-39.

Hahn, A.F., Ainsworth, P.J., Naus, C.C., Mao, J. & Bolton, C.F. (2000). Clinical and pathological observations in men lacking the gap junction protein connexin 32. *Muscle Nerve Suppl*, **9,** S39-48.

Harding, A.E. & Thomas, P.K. (1980). The clinical features of hereditary motor and sensory neuropathy types I and II. *Brain*, **103,** 259-80.

Hartline, D.K. & Colman, D.R. (2007). Rapid conduction and the evolution of giant axons and myelinated fibers. *Curr Biol*, **17,** R29-35.

Hebert, S.C., Mount, D.B. & Gamba, G. (2004). Molecular physiology of cation-coupled Cl(-) cotransport: the SLC12 family. *Pflugers Arch.*, **447,** 580-593.

Hediger, M.A., Romero, M.F., Peng, J.B., Rolfs, A., Takanaga, H. & Bruford, E.A. (2004). The ABCs of solute carriers: physiological, pathological and therapeutic implications of human membrane transport proteinsIntroduction. *Pflugers Arch*, **447,** 465-8.

Hekmat-Scafe, D.S., Lundy, M.Y., Ranga, R. & Tanouye, M.A. (2006). Mutations in the K+/Cl- cotransporter gene kazachoc (kcc) increase seizure susceptibility in Drosophila. *J Neurosci*, **26,** 8943-54.

Herrick-Davis, K., Weaver, B.A., Grinde, E. & Mazurkiewicz, J.E. (2006). Serotonin 5-HT2C receptor homodimer biogenesis in the endoplasmic reticulum: real-time visualization with confocal fluorescence resonance energy transfer. *J Biol Chem*, **281,** 27109-16.

Hiki, K., D'Andrea, R.J., Furze, J., Crawford, J., Woollatt, E., Sutherland, G.R., Vadas, M.A. & Gamble, J.R. (1999). Cloning, characterization, and chromosomal location of a novel human K+-Cl- cotransporter. *J Biol Chem*, **274,** 10661-7.

Hirano, A. & Dembitzer, H.M. (1981). The periaxonal space in an experimental model of neuropathy: the mutant Syrian hamster with hindleg paralysis. *J Neurocytol*, **10,** 261-9.
Hoenig, K., Hochrein, A., Quednow, B.B., Maier, W. & Wagner, M. (2005). Impaired prepulse inhibition of acoustic startle in obsessive-compulsive disorder. *Biol Psychiatry*, **57,** 1153-8.

Hoffmann, E.K., Schettino, T. & Marshall, W.S. (2006). The role of volume-sensitive ion transport systems in regulation of epithelial transport. *Comp Biochem Physiol A Mol Integr Physiol*.

Holden, S., Cox, J. & Raymond, F.L. (2004). Cloning, genomic organization, alternative splicing and expression analysis of the human gene WNK3 (PRKWNK3). *Gene*, **335,** 109-19.

Hoopfer, E.D., McLaughlin, T., Watts, R.J., Schuldiner, O., O'Leary, D.D. & Luo, L. (2006). Wlds protection distinguishes axon degeneration following injury from naturally occurring developmental pruning. *Neuron*, **50,** 883-95.

Howard, H.C., Dube, M.P., Prevost, C., Bouchard, J.P., Mathieu, J. & Rouleau, G.A. (2002a). Fine mapping the candidate region for peripheral neuropathy with or without agenesis of the corpus callosum in the French Canadian population. *Eur J Hum Genet*, **10,** 406-12.

Howard, H.C., Mount, D.B., Rochefort, D., Byun, N., Dupre, N., Lu, J., Fan, X., Song, L., Riviere, J.B., Prevost, C., Horst, J., Simonati, A., Lemcke, B., Welch, R., England, R., Zhan, F.Q., Mercado, A., Siesser, W.B., George, A.L., Jr., McDonald, M.P., Bouchard, J.P., Mathieu, J., Delpire, E. & Rouleau, G.A. (2002b). The K-Cl cotransporter KCC3 is mutant in a severe peripheral neuropathy associated with agenesis of the corpus callosum. *Nat Genet*, **32,** 384-92.

Hsieh, M.H., Swerdlow, N.R. & Braff, D.L. (2006). Effects of background and prepulse characteristics on prepulse inhibition and facilitation: implications for neuropsychiatric research. *Biol Psychiatry*, **59,** 555-9.

Hu, X., Hicks, C.W., He, W., Wong, P., Macklin, W.B., Trapp, B.D. & Yan, R. (2006). Bace1 modulates myelination in the central and peripheral nervous system. *Nat Neurosci*, **9,** 1520-5.

Hubner, C.A., Stein, V., Hermans-Borgmeyer, I., Meyer, T., Ballanyi, K. & Jentsch, T.J. (2001). Disruption of KCC2 reveals an essential role of K-Cl cotransport already in early synaptic inhibition. *Neuron*, **30,** 515-24.

Hyde, T.M., Ziegler, J.C. & Weinberger, D.R. (1992). Psychiatric disturbances in metachromatic leukodystrophy. Insights into the neurobiology of psychosis. *Arch Neurol*, **49,** 401-6.

Ichimura, T. & Ellisman, M.H. (1991). Three-dimensional fine structure of cytoskeletal-membrane interactions at nodes of Ranvier. *J Neurocytol*, **20,** 667-81.

Igarashi, P., Vanden Heuvel, G.B., Payne, J.A. & Forbush, B., 3rd. (1995). Cloning, embryonic expression, and alternative splicing of a murine kidney-specific Na-K-Cl cotransporter. *Am J Physiol*, **269,** F405-18.

Igarashi, P., Whyte, D.A., Li, K. & Nagami, G.T. (1996). Cloning and kidney cell-specific activity of the promoter of the murine renal Na-K-C1 cotransporter gene. *J Biol Chem*, **271,** 9666-74.

Irobi, J., Van Impe, K., Seeman, P., Jordanova, A., Dierick, I., Verpoorten, N., Michalik, A., De Vriendt, E., Jacobs, A., Van Gerwen, V., Vennekens, K., Mazanec, R., Tournev, I., Hilton-Jones, D., Talbot, K., Kremensky, I., Van Den Bosch, L., Robberecht, W., Van Vandekerckhove, J., Van Broeckhoven, C., Gettemans, J., De Jonghe, P. & Timmerman, V. (2004). Hot-spot residue in small heat-shock protein 22 causes distal motor neuropathy. *Nat Genet*, **36,** 597-601.

Irwin, S. (1968). Comprehensive observational assessment: Ia. A systematic, quantitative procedure for assessing the behavioral and physiologic state of the mouse. *Psychopharmacologia*, **13,** 222-57.

Isenring, P., Jacoby, S.C. & Forbush, B., 3rd. (1998). The role of transmembrane domain 2 in cation transport by the Na-K-Cl cotransporter. *Proc Natl Acad Sci U S A*, **95,** 7179-84.

Jablonka, S., Wiese, S. & Sendtner, M. (2004). Axonal defects in mouse models of motoneuron disease. *J Neurobiol*, **58,** 272-86.

Jennings, M.L. & Adame, M.F. (2001). Direct estimate of 1:1 stoichiometry of K(+)-Cl(-) cotransport in rabbit erythrocytes. *Am J Physiol Cell Physiol*, **281,** C825-32.

Jennings, M.L. & Schulz, R.K. (1991). Okadaic acid inhibition of KCl cotransport. Evidence that protein dephosphorylation is necessary for activation of transport by either cell swelling or N-ethylmaleimide. *J Gen Physiol*, **97,** 799-817.

Jentsch, T.J. (2005). Chloride transport in the kidney: lessons from human disease and knockout mice. *J Am Soc Nephrol*, **16,** 1549-61.

Jentsch, T.J., Neagoe, I. & Scheel, O. (2005). CLC chloride channels and transporters. *Curr Opin Neurobiol*, **15,** 319-25.

Jessen, K.R. & Mirsky, R. (2002). Signals that determine Schwann cell identity. *J Anat*, **200,** 367-76.

Jessen, K.R. & Mirsky, R. (2005). The origin and development of glial cells in peripheral nerves. *Nat Rev Neurosci*, **6,** 671-82.

Johnson, K.M., Tao, J.Z., Kennan, R.P. & Gore, J.C. (1998). Gadolinium-bearing red cells as blood pool MRI contrast agents. *Magn Reson Med*, **40,** 133-42.

Johnston, A.M., Naselli, G., Gonez, L.J., Martin, R.M., Harrison, L.C. & Deaizpurua, H.J. (2000). SPAK, a Ste20/SPS1-related kinase that activates the p38 pathway. *Oncogene*, **19,** 4290-4297.

Jones, H.C. & Keep, R.F. (1987). The control of potassium concentration in the cerebrospinal fluid and brain interstitial fluid of developing rats. *J Physiol*, **383,** 441-53.

Kahle, K.T., Rinehart, J., de Los Heros, P., Louvi, A., Meade, P., Vazquez, N., Hebert, S.C., Gamba, G., Gimenez, I. & Lifton, R.P. (2005). WNK3 modulates transport of Cl- in and out of cells: implications for control of cell volume and neuronal excitability. *Proc. Natl. Acad Sci. USA.*, **102,** 16783-16788.

Kaji, D.M. & Tsukitani, Y. (1991). Role of protein phosphatase in activation of KCl cotransport in human erythrocytes. *Am J Physiol*, **260,** C176-80.

Kalil, K. & Dent, E.W. (2005). Touch and go: guidance cues signal to the growth cone cytoskeleton. *Curr Opin Neurobiol*, **15,** 521-6.

Kanaka, C., Ohno, K., Okabe, A., Kuriyama, K., Itoh, T., Fukuda, A. & Sato, K. (2001). The differential expression patterns of messenger RNAs encoding K-Cl cotransporters (KCC1,2) and Na-K-2Cl cotransporter (NKCC1) in the rat nervous system. *Neuroscience*, **104,** 933-46.

Kaplan, M.R., Plotkin, M.D., Lee, W.S., Xu, Z.C., Lytton, J. & Hebert, S.C. (1996). Apical localization of the Na-K-Cl cotransporter, rBSC1, on rat thick ascending limbs. *Kidney Int*, **49,** 40-7.

Karadsheh, M.F., Byun, N., Mount, D.B. & Delpire, E. (2004). Localization of the KCC4 potassium-chloride cotransporter in the nervous system. *Neuroscience*, **123,** 381-91.

Karadsheh, M.F. & Delpire, E. (2001). Neuronal restrictive silencing element is found in the KCC2 gene: molecular basis for KCC2-specific expression in neurons. *J Neurophysiol*, **85,** 995-7.

Karolyi, L., Koch, M.C., Grzeschik, K.H. & Seyberth, H.W. (1998). The molecular genetic approach to "Bartter's syndrome". *J Mol Med*, **76,** 317-25.

Kiernan, M.C., Walters, R.J., Andersen, K.V., Taube, D., Murray, N.M. & Bostock, H. (2002). Nerve excitability changes in chronic renal failure indicate membrane depolarization due to hyperkalaemia. *Brain*, **125,** 1366-78.

Kim, J., Lo, L., Dormand, E. & Anderson, D.J. (2003). SOX10 maintains multipotency and inhibits neuronal differentiation of neural crest stem cells. *Neuron*, **38,** 17-31.

Kim, S.W., de Seigneux, S., Sassen, M.C., Lee, J., Kim, J., Knepper, M.A., Frokiaer, J. & Nielsen, S. (2006). Increased apical targeting of renal ENaC subunits and decreased expression of 11betaHSD2 in HgCl2-induced nephrotic syndrome in rats. *Am J Physiol Renal Physiol*, **290,** F674-87.

King, R. (1999). *Atlas of Peripheral Nerve Pathology*. Arnold: London.
Kleinschmidt-Demasters, B.K., Rojiani, A.M. & Filley, C.M. (2006). Central and extrapontine myelinolysis: then...and now. *J Neuropathol Exp Neurol*, **65,** 1-11.

Knepper, M.A., Kim, G.H., Fernandez-Llama, P. & Ecelbarger, C.A. (1999). Regulation of thick ascending limb transport by vasopressin. *J Am Soc Nephrol*, **10,** 628-34.

Koch, M. (1999). The neurobiology of startle. *Prog Neurobiol*, **59,** 107-28.

Kofuji, P. & Newman, E.A. (2004). Potassium buffering in the central nervous system. *Neuroscience*, **129,** 1045-56.

Koirala, S. & Ko, C.P. (2004). Pruning an axon piece by piece: a new mode of synapse elimination. *Neuron*, **44,** 578-80.

Konishi, T. (1990). Voltage-gated potassium currents in myelinating Schwann cells in the mouse. *J Physiol*, **431,** 123-39.

Koszowski, A.G., Owens, G.C. & Levinson, S.R. (1998). The effect of the mouse mutation claw paw on myelination and nodal frequency in sciatic nerves. *J Neurosci*, **18,** 5859-68.

Krajewski, K.M., Lewis, R.A., Fuerst, D.R., Turansky, C., Hinderer, S.R., Garbern, J., Kamholz, J. & Shy, M.E. (2000). Neurological dysfunction and axonal degeneration in Charcot-Marie-Tooth disease type 1A. *Brain*, **123 (Pt 7),** 1516-27.

Kraner, S.D., Chong, J.A., Tsay, H.J. & Mandel, G. (1992). Silencing the type II sodium channel gene: a model for neural-specific gene regulation. *Neuron*, **9,** 37-44.

Krarup, T. & Dunham, P.B. (1996). Reconstitution of calyculin-inhibited K-Cl cotransport in dog erythrocyte ghosts by exogenous PP-1. *Am J Physiol*, **270,** C898-902.

Krarup, T., Jakobsen, L.D., Jensen, B.S. & Hoffmann, E.K. (1998). Na+-K+-2Cl- cotransport in Ehrlich cells: regulation by protein phosphatases and kinases. *Am J Physiol*, **275,** C239-50.

Kubicki, M., McCarley, R.W. & Shenton, M.E. (2005). Evidence for white matter abnormalities in schizophrenia. *Curr Opin Psychiatry*, **18,** 121-34.

Kucheryavykh, Y.V., Kucheryavykh, L.Y., Nichols, C.G., Maldonado, H.M., Baksi, K., Reichenbach, A., Skatchkov, S.N. & Eaton, M.J. (2007). Downregulation of Kir4.1 inward rectifying potassium channel subunits by RNAi impairs potassium transfer and glutamate uptake by cultured cortical astrocytes. *Glia*, **55,** 274-81.

Kumari, V. & Sharma, T. (2002). Effects of typical and atypical antipsychotics on prepulse inhibition in schizophrenia: a critical evaluation of current evidence and directions for future research. *Psychopharmacology (Berl)*, **162,** 97-101.

Laird, J.M., Garcia-Nicas, E., Delpire, E.J. & Cervero, F. (2004). Presynaptic inhibition and spinal pain processing in mice: a possible role of the NKCC1 cation-chloride co-transporter in hyperalgesia. *Neurosci. Lett.*, **361,** 200-203.

Landau, D. (2006). Potassium-related inherited tubulopathies. *Cell Mol Life Sci*, **63,** 1962-8.

Lauf, P.K., Bauer, J., Adragna, N.C., Fujise, H., Zade-Oppen, A.M., Ryu, K.H. & Delpire, E. (1992). Erythrocyte K-Cl cotransport: properties and regulation. *Am J Physiol*, **263,** C917-32.

Lauf, P.K. & Theg, B.E. (1980). A chloride dependent K^+ flux induced by N-ethylmaleimide in genetically low K^+ sheep and goat erythrocytes. *Biochem. Biophys. Res. Comm.*, **70,** 221-242.

Lee, D.Y., Choo, I.H., Kim, K.W., Jhoo, J.H., Youn, J.C., Lee, U.Y. & Woo, J.I. (2006). White matter changes associated with psychotic symptoms in Alzheimer's disease patients. *J Neuropsychiatry Clin Neurosci*, **18,** 191-8.

Leiserson, W.M., Harkins, E.W. & Keshishian, H. (2000). Fray, a Drosophila serine/threonine kinase homologous to mammalian PASK, is required for axonal ensheathment. *Neuron*, **28,** 793-806.

Lentz, S.I., Knudson, C.M., Korsmeyer, S.J. & Snider, W.D. (1999). Neurotrophins support the development of diverse sensory axon morphologies. *J Neurosci*, **19,** 1038-48.
Li, H., Tornberg, J., Kaila, K., Airaksinen, M.S. & Rivera, C. (2002). Patterns of cation-chloride cotransporter expression during embryonic rodent CNS development. *Eur J Neurosci*, **16,** 2358-70.

Lijam, N., Paylor, R., McDonald, M.P., Crawley, J.N., Deng, C.X., Herrup, K., Stevens, K.E., Maccaferri, G., McBain, C.J., Sussman, D.J. & Wynshaw-Boris, A. (1997). Social interaction and sensorimotor gating abnormalities in mice lacking Dvl1. *Cell*, **90,** 895-905.

Liu, P., Sudhaharan, T., Koh, R.M., Hwang, L.C., Ahmed, S., Maruyama, I.N. & Wohland, T. (2007). Investigation of the dimerization of proteins from the epidermal growth factor receptor family by single wavelength fluorescence cross-correlation spectroscopy. *Biophys J*, **93,** 684-98.

Lu, J., Karadsheh, M. & Delpire, E. (1999). Developmental regulation of the neuronal-specific isoform of K-Cl cotransporter KCC2 in postnatal rat brains. *J Neurobiol*, **39,** 558-68.

Ludewig, S., Geyer, M.A., Ramseier, M., Vollenweider, F.X., Rechsteiner, E. & Cattapan-Ludewig, K. (2005). Information-processing deficits and cognitive dysfunction in panic disorder. *J Psychiatry Neurosci*, **30,** 37-43.

Luo, L. (2000). Rho GTPases in neuronal morphogenesis. *Nat Rev Neurosci*, **1,** 173-80.
Lytle, C. & McManus, T. (2002). Coordinate modulation of Na-K-2Cl cotransport and K-Cl cotransport by cell volume and chloride. *Am J Physiol Cell Physiol*, **283,** C1422-31.

Ma, L. & Tessier-Lavigne, M. (2007). Dual branch-promoting and branch-repelling actions of Slit/Robo signaling on peripheral and central branches of developing sensory axons. *J Neurosci,* **27,** 6843-51.

MacDonald, J.M., Beach, M.G., Porpiglia, E., Sheehan, A.E., Watts, R.J. & Freeman, M.R. (2006). The Drosophila cell corpse engulfment receptor Draper mediates glial clearance of severed axons. *Neuron,* **50,** 869-81.

MacKenzie, S., Vaitkevicius, H. & Lockette, W. (2001). Sequencing and characterization of the human thiazide-sensitive Na-Cl cotransporter (SLC12A3) gene promoter. *Biochem Biophys Res Commun,* **282,** 991-1000.

Madi, S., Hasan, K.M. & Narayana, P.A. (2005). Diffusion tensor imaging of in vivo and excised rat spinal cord at 7 T with an icosahedral encoding scheme. *Magn Reson Med,* **53,** 118-25.

Mandemakers, W., Morais, V.A. & De Strooper, B. (2007). A cell biological perspective on mitochondrial dysfunction in Parkinson disease and other neurodegenerative diseases. *J Cell Sci,* **120,** 1707-16.

Mantyh, P.W. & Hunt, S.P. (2004). Setting the tone: superficial dorsal horn projection neurons regulate pain sensitivity. *Trends Neurosci,* **27,** 582-4.

Martin, E.D. & Decima, E.E. (2003). Epinephrine reduces the nerve conduction blockage induced by high-potassium in mammalian sciatic nerve. *Brain Res,* **983,** 237-41.

Martini, R., Bollensen, E. & Schachner, M. (1988). Immunocytological localization of the major peripheral nervous system glycoprotein P0 and the L2/HNK-1 and L3 carbohydrate structures in developing and adult mouse sciatic nerve. *Dev Biol,* **129,** 330-8.

Martini, R. & Schachner, M. (1986). Immunoelectron microscopic localization of neural cell adhesion molecules (L1, N-CAM, and MAG) and their shared carbohydrate epitope and myelin basic protein in developing sciatic nerve. *J Cell Biol,* **103,** 2439-48.

Martini, R., Zielasek, J., Toyka, K.V., Giese, K.P. & Schachner, M. (1995). Protein zero (P0)-deficient mice show myelin degeneration in peripheral nerves characteristic of inherited human neuropathies. *Nat Genet,* **11,** 281-6.

Masilamani, S., Wang, X., Kim, G.H., Brooks, H., Nielsen, J., Nielsen, S., Nakamura, K., Stokes, J.B. & Knepper, M.A. (2002). Time course of renal Na-K-ATPase, NHE3, NKCC2, NCC, and ENaC abundance changes with dietary NaCl restriction. *Am J Physiol Renal Physiol,* **283,** F648-57.

Mathias, R.T. (1985). Epithelial water transport in a balanced gradient system. *Biophys J,* **47,** 823-36.

Mayan, H., Vered, I., Mouallem, M., Tzadok-Witkon, M., Pauzner, R. & Farfel, Z. (2002). Pseudohypoaldosteronism type II: marked sensitivity to thiazides, hypercalciuria, normomagnesemia, and low bone mineral density. *J Clin Endocrinol Metab*, **87,** 3248-54.

Meeks, J.P. & Mennerick, S. (2004). Selective effects of potassium elevations on glutamate signaling and action potential conduction in hippocampus. *J Neurosci*, **24,** 197-206.

Menichella, D.M., Goodenough, D.A., Sirkowski, E., Scherer, S.S. & Paul, D.L. (2003). Connexins are critical for normal myelination in the CNS. *J Neurosci*, **23,** 5963-73.

Menichella, D.M., Majdan, M., Awatramani, R., Goodenough, D.A., Sirkowski, E., Scherer, S.S. & Paul, D.L. (2006). Genetic and physiological evidence that oligodendrocyte gap junctions contribute to spatial buffering of potassium released during neuronal activity. *J Neurosci*, **26,** 10984-91.

Mercado, A., Broumand, V., Zandi-Nejad, K., Enck, A.H. & Mount, D.B. (2006). A C-terminal domain in KCC2 confers constitutive K+-Cl- cotransport. *J Biol Chem*, **281,** 1016-26.

Mercado, A., Song, L., Vazquez, N., Mount, D.B. & Gamba, G. (2000). Functional comparison of the K+-Cl- cotransporters KCC1 and KCC4. *J Biol Chem*, **275,** 30326-34.

Mercado, A., Vazquez, N., Song, L., Cortes, R., Enck, A.H., Welch, R., Delpire, E., Gamba, G. & Mount, D.B. (2005). NH2-terminal heterogeneity in the KCC3 K+-Cl- cotransporter. *Am. J. Physiol. Renal Physiol.*, **289,** F1246-F1261.

Metzger, K.L., Shoemaker, J.M., Kahn, J.B., Maxwell, C.R., Liang, Y., Tokarczyk, J., Kanes, S.J., Hans, M., Lowman, A.M., Dan, N., Winey, K.I., Swerdlow, N.R. & Siegel, S.J. (2007). Pharmacokinetic and behavioral characterization of a long-term antipsychotic delivery system in rodents and rabbits. *Psychopharmacology (Berl)*, **190,** 201-11.

Meyer, G. & Feldman, E.L. (2002). Signaling mechanisms that regulate actin-based motility processes in the nervous system. *J Neurochem*, **83,** 490-503.

Meyer, J., Johannssen, K., Freitag, C.M., Schraut, K., Teuber, I., Hahner, A., Mainhardt, C., Mossner, R., Volz, H.P., Wienker, T.F., McKeane, D., Stephan, D.A., Rouleau, G., Reif, A. & Lesch, K.P. (2005). Rare variants of the gene encoding the potassium chloride co-transporter 3 are associated with bipolar disorder. *Int J Neuropsychopharmacol*, **8,** 495-504.

Meyer, J.W., Flagella, M., Sutliff, R.L., Lorenz, J.N., Nieman, M.L., Weber, C.S., Paul, R.J. & Shull, G.E. (2002). Decreased blood pressure and vascular smooth muscle tone in mice lacking basolateral Na(+)-K(+)-2Cl(-) cotransporter. *Am J Physiol Heart Circ Physiol*, **283,** H1846-55.

Michailov, G.V., Sereda, M.W., Brinkmann, B.G., Fischer, T.M., Haug, B., Birchmeier, C., Role, L., Lai, C., Schwab, M.H. & Nave, K.A. (2004). Axonal neuregulin-1 regulates myelin sheath thickness. *Science*, **304,** 700-3.

Mongeluzi, D.L., Hoppe, T.A. & Frost, W.N. (1998). Prepulse inhibition of the Tritonia escape swim. *J Neurosci*, **18,** 8467-72.

Moore-Hoon, M.L. & Turner, R.J. (2000). The structural unit of the secretory Na+-K+-2Cl- cotransporter (NKCC1) is a homodimer. *Biochemistry*, **39,** 3718-3724.

Morales-Aza, B.M., Chillingworth, N.L., Payne, J.A. & Donaldson, L.F. (2004). Inflammation alters cation chloride cotransporter expression in sensory neurons. *Neurobiol Dis*, **17,** 62-9.

Morris, R.G., Garrud, P., Rawlins, J.N. & O'Keefe, J. (1982). Place navigation impaired in rats with hippocampal lesions. *Nature*, **297,** 681-3.

Mount, D.B. (2006). Membrane trafficking and the regulation of NKCC2. *Am J Physiol Renal Physiol*, **290,** F606-7.

Mount, D.B., Mercado, A., Song, L., Xu, J., George, A.L., Jr., Delpire, E. & Gamba, G. (1999). Cloning and characterization of KCC3 and KCC4, new members of the cation-chloride cotransporter gene family. *J Biol Chem*, **274,** 16355-62.

Munoz, E., Cervera, A. & Valls-Sole, J. (2003). Neurophysiological study of facial chorea in patients with Huntington's disease. *Clin Neurophysiol*, **114,** 1246-52.

Muntoni, F., Mateddu, A., Marchei, F., Clerk, A. & Serra, G. (1993). Muscular weakness in the mdx mouse. *J Neurol Sci*, **120,** 71-7.

Murata, T., Ohnishi, H., Okazawa, H., Murata, Y., Kusakari, S., Hayashi, Y., Miyashita, M., Itoh, H., Oldenborg, P.A., Furuya, N. & Matozaki, T. (2006). CD47 promotes neuronal development through Src- and FRG/Vav2-mediated activation of Rac and Cdc42. *J Neurosci*, **26,** 12397-407.

Nejsum, L.N., Praetorius, J. & Nielsen, S. (2005). NKCC1 and NHE1 are abundantly expressed in the basolateral plasma membrane of secretory coil cells in rat, mouse, and human sweat glands. *Am J Physiol Cell Physiol*, **289,** C333-40.

Neusch, C., Rozengurt, N., Jacobs, R.E., Lester, H.A. & Kofuji, P. (2001). Kir4.1 potassium channel subunit is crucial for oligodendrocyte development and in vivo myelination. *J Neurosci*, **21,** 5429-38.

Nickols, J.C., Valentine, W., Kanwal, S. & Carter, B.D. (2003). Activation of the transcription factor NF-kappaB in Schwann cells is required for peripheral myelin formation. *Nat Neurosci*, **6,** 161-7.

Nicolet-Barousse, L., Blanchard, A., Roux, C., Pietri, L., Bloch-Faure, M., Kolta, S., Chappard, C., Geoffroy, V., Morieux, C., Jeunemaitre, X., Shull, G.E., Meneton, P., Paillard, M., Houillier, P. & De Vernejoul, M.C. (2005). Inactivation of the Na-Cl co-transporter (NCC) gene is associated with high BMD through both renal and bone mechanisms: analysis of patients with Gitelman syndrome and Ncc null mice. *J Bone Miner Res*, **20,** 799-808.

Niemann, A., Ruegg, M., La Padula, V., Schenone, A. & Suter, U. (2005). Ganglioside-induced differentiation associated protein 1 is a regulator of the mitochondrial network: new implications for Charcot-Marie-Tooth disease. *J Cell Biol*, **170,** 1067-78.

Nomura, H., Sakai, A., Nagano, M., Umino, M. & Suzuki, H. (2006). Expression changes of cation chloride cotransporters in the rat spinal cord following intraplantar formalin. *Neurosci Res*, **56,** 435-40.

Nusbaum, M.P. & Contreras, D. (2004). Sensorimotor gating: startle submits to presynaptic inhibition. *Curr Biol*, **14,** R247-9.

Obermuller, N., Bernstein, P., Velazquez, H., Reilly, R., Moser, D., Ellison, D.H. & Bachmann, S. (1995). Expression of the thiazide-sensitive Na-Cl cotransporter in rat and human kidney. *Am J Physiol*, **269,** F900-10.

Odermatt, B., Wellershaus, K., Wallraff, A., Seifert, G., Degen, J., Euwens, C., Fuss, B., Bussow, H., Schilling, K., Steinhauser, C. & Willecke, K. (2003). Connexin 47 (Cx47)-deficient mice with enhanced green fluorescent protein reporter gene reveal predominant oligodendrocytic expression of Cx47 and display vacuolized myelin in the CNS. *J Neurosci*, **23,** 4549-59.

Okada, Y., Maeno, E., Shimizu, T., Dezaki, K., Wang, J. & Morishima, S. (2001). Receptor-mediated control of regulatory volume decrease (RVD) and apoptotic volume decrease (AVD). *J Physiol*, **532,** 3-16.

Oppermann, M., Mizel, D., Huang, G., Li, C., Deng, C., Theilig, F., Bachmann, S., Briggs, J., Schnermann, J. & Castrop, H. (2006). Macula densa control of renin secretion and preglomerular resistance in mice with selective deletion of the B isoform of the Na,K,2Cl co-transporter. *J Am Soc Nephrol*, **17,** 2143-52.

Oppermann, M., Mizel, D., Kim, S.M., Chen, L., Faulhaber-Walter, R., Huang, Y., Li, C., Deng, C., Briggs, J., Schnermann, J. & Castrop, H. (2007). Renal function in mice with targeted disruption of the A isoform of the Na-K-2Cl co-transporter. *J Am Soc Nephrol*, **18,** 440-8.

Ouagazzal, A., Grottick, A.J., Moreau, J. & Higgins, G.A. (2001). Effect of LSD on prepulse inhibition and spontaneous behavior in the rat. A pharmacological analysis and comparison between two rat strains. *Neuropsychopharmacology*, **25,** 565-75.

Pace, A.J., Lee, E., Athirakul, K., Coffman, T.M., O'Brien, D.A. & Koller, B.H. (2000). Failure of spermatogenesis in mouse lines deficient in the Na(+)-K(+)-2Cl(-) cotransporter. *J Clin Invest,* **105,** 441-50.

Parmantier, E., Lynn, B., Lawson, D., Turmaine, M., Namini, S.S., Chakrabarti, L., McMahon, A.P., Jessen, K.R. & Mirsky, R. (1999). Schwann cell-derived Desert hedgehog controls the development of peripheral nerve sheaths. *Neuron,* **23,** 713-24.

Pasantes-Morales, H., Cardin, V. & Tuz, K. (2000). Signaling events during swelling and regulatory volume decrease. *Neurochem Res,* **25,** 1301-14.

Patel, T.D., Jackman, A., Rice, F.L., Kucera, J. & Snider, W.D. (2000). Development of sensory neurons in the absence of NGF/TrkA signaling in vivo. *Neuron,* **25,** 345-57.

Payne, J.A. & Forbush, B., 3rd. (1994). Alternatively spliced isoforms of the putative renal Na-K-Cl cotransporter are differentially distributed within the rabbit kidney. *Proc Natl Acad Sci U S A,* **91,** 4544-8.

Payne, J.A., Rivera, C., Voipio, J. & Kaila, K. (2003). Cation-chloride co-transporters in neuronal communication, development and trauma. *Trends Neurosci,* **26,** 199-206.

Payne, J.A., Stevenson, T.J. & Donaldson, L.F. (1996). Molecular characterization of a putative K-Cl cotransporter in rat brain. A neuronal-specific isoform. *J Biol Chem,* **271,** 16245-52.

Payne, J.A., Xu, J.C., Haas, M., Lytle, C.Y., Ward, D. & Forbush, B., 3rd. (1995). Primary structure, functional expression, and chromosomal localization of the bumetanide-sensitive Na-K-Cl cotransporter in human colon. *J Biol Chem,* **270,** 17977-85.

Pearson, M.M., Lu, J., Mount, D.B. & Delpire, E. (2001). Localization of the K(+)-Cl(-) cotransporter, KCC3, in the central and peripheral nervous systems: expression in the choroid plexus, large neurons and white matter tracts. *Neuroscience,* **103,** 481-91.

Pfister, B.J., Iwata, A., Meaney, D.F. & Smith, D.H. (2004). Extreme stretch growth of integrated axons. *J Neurosci,* **24,** 7978-83.

Piechotta, K., Garbarini, N., England, R. & Delpire, E. (2003). Characterization of the interaction of the stress kinase SPAK with the Na+-K+-2Cl- cotransporter in the nervous system: evidence for a scaffolding role of the kinase. *J Biol Chem,* **278,** 52848-56.

Piechotta, K., Lu, J. & Delpire, E. (2002). Cation chloride cotransporters interact with the stress-related kinases Ste20-related proline-alanine-rich kinase (SPAK) and oxidative stress response 1 (OSR1). *J Biol Chem,* **277,** 50812-9.

Plata, C., Meade, P., Vazquez, N., Hebert, S.C. & Gamba, G. (2002). Functional properties of the apical Na+-K+-2Cl- cotransporter isoforms. *J Biol Chem*, **277,** 11004-12.

Plotkin, M.D., Kaplan, M.R., Peterson, L.N., Gullans, S.R., Hebert, S.C. & Delpire, E. (1997). Expression of the Na^+-K^+-2Cl^- cotransporter BSC2 in the nervous system. *Am. J. Physiol. (Cell Physiol.)*, **272,** C173-C183.

Poet, M., Kornak, U., Schweizer, M., Zdebik, A.A., Scheel, O., Hoelter, S., Wurst, W., Schmitt, A., Fuhrmann, J.C., Planells-Cases, R., Mole, S.E., Hubner, C.A. & Jentsch, T.J. (2006). Lysosomal storage disease upon disruption of the neuronal chloride transport protein ClC-6. *Proc Natl Acad Sci U S A*, **103,** 13854-9.

Poliak, S. & Peles, E. (2003). The local differentiation of myelinated axons at nodes of Ranvier. *Nat Rev Neurosci*, **4,** 968-80.

Previtali, S.C., Feltri, M.L., Archelos, J.J., Quattrini, A., Wrabetz, L. & Hartung, H. (2001). Role of integrins in the peripheral nervous system. *Prog Neurobiol*, **64,** 35-49.

Price, G., Cercignani, M., Parker, G.J., Altmann, D.R., Barnes, T.R., Barker, G.J., Joyce, E.M. & Ron, M.A. (2007). Abnormal brain connectivity in first-episode psychosis: a diffusion MRI tractography study of the corpus callosum. *Neuroimage*, **35,** 458-66.

Puccio, H. & Koenig, M. (2002). Friedreich ataxia: a paradigm for mitochondrial diseases. *Curr Opin Genet Dev*, **12,** 272-7.

Pullarkat, P.A., Dommersnes, P., Fernandez, P., Joanny, J.F. & Ott, A. (2006).

Osmotically driven shape transformations in axons. *Phys Rev Lett*, **96,** 048104.

Race, J.E., Makhlouf, F.N., Logue, P.J., Wilson, F.H., Dunham, P.B. & Holtzman, E.J. (1999). Molecular cloning and functional characterization of KCC3, a new K-Cl cotransporter. *Am J Physiol*, **277,** C1210-9.

Randall, J., Thorne, T. & Delpire, E. (1997). Partial cloning and characterization of Slc12a2: the gene encoding the secretory Na+-K+-2Cl- cotransporter. *Am J Physiol*, **273,** C1267-77.

Ransom, B.R., Yamate, C.L. & Connors, B.W. (1985). Activity-dependent shrinkage of extracellular space in rat optic nerve: a developmental study. *J Neurosci*, **5,** 532-5.

Ransom, C.B., Ransom, B.R. & Sontheimer, H. (2000). Activity-dependent extracellular K+ accumulation in rat optic nerve: the role of glial and axonal Na+ pumps. *J Physiol*, **522 Pt 3,** 427-42.

Rasband, M.N., Trimmer, J.S., Schwarz, T.L., Levinson, S.R., Ellisman, M.H., Schachner, M. & Shrager, P. (1998). Potassium channel distribution, clustering, and function in remyelinating rat axons. *J Neurosci*, **18,** 36-47.

Reisert, J., Lai, J., Yau, K.W. & Bradley, J. (2005). Mechanism of the excitatory Cl- response in mouse olfactory receptor neurons. *Neuron*, **45,** 553-61.

Rinehart, J., Kahle, K.T., de Los Heros, P., Vazquez, N., Meade, P., Wilson, F.H., Hebert, S.C., Gimenez, I., Gamba, G. & Lifton, R.P. (2005). WNK3 kinase is a positive regulator of NKCC2 and NCC, renal cation-Cl- cotransporters required for normal blood pressure homeostasis. *Proc Natl Acad Sci U S A*, **102,** 16777-82.

Rios, J.C., Rubin, M., St Martin, M., Downey, R.T., Einheber, S., Rosenbluth, J., Levinson, S.R., Bhat, M. & Salzer, J.L. (2003). Paranodal interactions regulate expression of sodium channel subtypes and provide a diffusion barrier for the node of Ranvier. *J Neurosci*, **23,** 7001-11.

Rivera, C., Voipio, J., Payne, J.A., Ruusuvuori, E., Lahtinen, H., Lamsa, K., Pirvola, U., Saarma, M. & Kaila, K. (1999). The K+/Cl- co-transporter KCC2 renders GABA hyperpolarizing during neuronal maturation. *Nature*, **397,** 251-5.

Rojo, M., Legros, F., Chateau, D. & Lombes, A. (2002). Membrane topology and mitochondrial targeting of mitofusins, ubiquitous mammalian homologs of the transmembrane GTPase Fzo. *J Cell Sci*, **115,** 1663-74.

Ronen, G.M., Rosenbaum, P., Law, M. & Streiner, D.L. (1999). Health-related quality of life in childhood epilepsy: the results of children's participation in identifying the components. *Dev Med Child Neurol*, **41,** 554-9.

Roopra, A., Sharling, L., Wood, I.C., Briggs, T., Bachfischer, U., Paquette, A.J. & Buckley, N.J. (2000). Transcriptional repression by neuron-restrictive silencer factor is mediated via the Sin3-histone deacetylase complex. *Mol Cell Biol*, **20,** 2147-57.

Rozsa, G., Morgan, C., Szent-Gyorgyi, A. & Wyckoff, R.W. (1950). The electron microscopy of sectioned nerve. *Science*, **112,** 42-3.

Runker, A.E., Kobsar, I., Fink, T., Loers, G., Tilling, T., Putthoff, P., Wessig, C., Martini, R. & Schachner, M. (2004). Pathology of a mouse mutation in peripheral myelin protein P0 is characteristic of a severe and early onset form of human Charcot-Marie-Tooth type 1B disorder. *J Cell Biol*, **165,** 565-73.

Russell, J.M. (2000). Sodium-potassium-chloride cotransport. *Physiol Rev*, **80,** 211-76.

Rust, M.B., Alper, S.L., Rudhard, Y., Shmukler, B.E., Vicente, R., Brugnara, C., Trudel, M., Jentsch, T.J. & Hubner, C.A. (2007). Disruption of erythroid K-Cl cotransporters

alters erythrocyte volume and partially rescues erythrocyte dehydration in SAD mice. *J Clin Invest*, **117,** 1708-17.

Salzer, J.L. (2003). Polarized domains of myelinated axons. *Neuron*, **40,** 297-318.

Sato, T., Hasan, K., Alexander, A.L. & Minato, K. (2001). Structural connectivity in white matter using the projected diffusion-tensor distance. *Medinfo*, **10,** 929-32.

Scherer, S.S. (2006). Finding the causes of inherited neuropathies. *Arch. Neurol.*, **63,** 812-816.

Scherer, S.S. & Arroyo, E.J. (2002). Recent progress on the molecular organization of myelinated axons. *J Peripher Nerv Syst*, **7,** 1-12.

Scherer, S.S. & Chance, P.F. (1995). Myelin genes: getting the dosage right. *Nat Genet*, **11,** 226-8.

Scherer, S.S., Deschenes, S.M., Xu, Y.T., Grinspan, J.B., Fischbeck, K.H. & Paul, D.L. (1995). Connexin32 is a myelin-related protein in the PNS and CNS. *J Neurosci*, **15,** 8281-94.

Scherer, S.S., Xu, Y.T., Nelles, E., Fischbeck, K., Willecke, K. & Bone, L.J. (1998). Connexin32-null mice develop demyelinating peripheral neuropathy. *Glia*, **24,** 8-20.

Schultheis, P.J., Lorenz, J.N., Meneton, P., Nieman, M.L., Riddle, T.M., Flagella, M., Duffy, J.J., Doetschman, T., Miller, M.L. & Shull, G.E. (1998). Phenotype resembling Gitelman's syndrome in mice lacking the apical Na+-Cl- cotransporter of the distal convoluted tubule. *J Biol Chem*, **273,** 29150-5.

Seeger, T., Fedorova, I., Zheng, F., Miyakawa, T., Koustova, E., Gomeza, J., Basile, A.S., Alzheimer, C. & Wess, J. (2004). M2 muscarinic acetylcholine receptor knock-out mice show deficits in behavioral flexibility, working memory, and hippocampal plasticity. *J Neurosci*, **24,** 10117-27.

Segal, D., Koschnick, J.R., Slegers, L.H. & Hof, P.R. (2007). Oligodendrocyte pathophysiology: a new view of schizophrenia. *Int J Neuropsychopharmacol*, **10,** 503-11.

Shapiro, L., Doyle, J.P., Hensley, P., Colman, D.R. & Hendrickson, W.A. (1996). Crystal structure of the extracellular domain from P0, the major structural protein of peripheral nerve myelin. *Neuron*, **17,** 435-49.

Shen, M.R., Chou, C.Y. & Ellory, J.C. (2000). Volume-sensitive KCI cotransport associated with human cervical carcinogenesis. *Pflugers Arch*, **440,** 751-60.

Shen, M.R., Chou, C.Y., Hsu, K.F., Liu, H.S., Dunham, P.B., Holtzman, E.J. & Ellory, J.C. (2001). The KCl cotransporter isoform KCC3 can play an important role in cell growth regulation. *Proc Natl Acad Sci U S A*, **98,** 14714-9.

Shrager, P. (1989). Sodium channels in single demyelinated mammalian axons. *Brain Res*, **483,** 149-54.

Shy, M.E. (2006). Peripheral neuropathies caused by mutations in the myelin protein zero. *J Neurol Sci*, **242,** 55-66.

Simard, C.F., Bergeron, M.J., Frenette-Cotton, R., Carpentier, G.A., Pelchat, M.E., Caron, L. & Isenring, P. (2007). Homooligomeric and Heterooligomeric Associations between K+-Cl- Cotransporter Isoforms and between K+-Cl- and Na+-K+-Cl- Cotransporters. *J Biol Chem*, **282,** 18083-93.

Simard, C.F., Brunet, G.M., Daigle, N.D., Montminy, V., Caron, L. & Isenring, P. (2004). Self-interacting domains in the C terminus of a cation-Cl- cotransporter described for the first time. *J Biol Chem*, **279,** 40769-77.

Simon, D.B., Nelson-Williams, C., Bia, M.J., Ellison, D., Karet, F.E., Molina, A.M., Vaara, I., Iwata, F., Cushner, H.M., Koolen, M., Gainza, F.J., Gitleman, H.J. & Lifton, R.P. (1996). Gitelman's variant of Bartter's syndrome, inherited hypokalaemic alkalosis, is caused by mutations in the thiazide-sensitive Na-Cl cotransporter. *Nat Genet*, **12,** 24-30.

Smart, S.L., Lopantsev, V., Zhang, C.L., Robbins, C.A., Wang, H., Chiu, S.Y., Schwartzkroin, P.A., Messing, A. & Tempel, B.L. (1998). Deletion of the K(V)1.1 potassium channel causes epilepsy in mice. *Neuron*, **20,** 809-19.

Smith, K.J., Blakemore, W.F., Murray, J.A. & Patterson, R.C. (1982). Internodal myelin volume and axon surface area. A relationship determining myelin thickness? *J Neurol Sci*, **55,** 231-46.

Song, X.Y., Zhou, F.H., Zhong, J.H., Wu, L.L. & Zhou, X.F. (2006). Knockout of p75(NTR) impairs re-myelination of injured sciatic nerve in mice. *J Neurochem*, **96,** 833-42.

Spencer, C.M., Serysheva, E., Yuva-Paylor, L.A., Oostra, B.A., Nelson, D.L. & Paylor, R. (2006). Exaggerated behavioral phenotypes in Fmr1/Fxr2 double knockout mice reveal a functional genetic interaction between Fragile X-related proteins. *Hum Mol Genet*, **15,** 1984-94.

Starke, L.C. & Jennings, M.L. (1993). K-Cl cotransport in rabbit red cells: further evidence for regulation by protein phosphatase type 1. *Am J Physiol*, **264,** C118-24.

Starremans, P.G., Kersten, F.F., Van Den Heuvel, L.P., Knoers, N.V. & Bindels, R.J. (2003). Dimeric architecture of the human bumetanide-sensitive Na-K-Cl Co-transporter. *J Am Soc Nephrol*, **14,** 3039-46.

Stein, V., Hermans-Borgmeyer, I., Jentsch, T.J. & Hubner, C.A. (2004). Expression of the KCl cotransporter KCC2 parallels neuronal maturation and the emergence of low intracellular chloride. *J Comp Neurol*, **468,** 57-64.

Steinlein, O.K., Neubauer, B.A., Sander, T., Song, L., Stoodt, J. & Mount, D.B. (2001). Mutation analysis of the potassium chloride cotransporter KCC3 (SLC12A6) in rolandic and idiopathic generalized epilepsy. *Epilepsy Res*, **44,** 191-5.

Stendel, C., Roos, A., Deconinck, T., Pereira, J., Castagner, F., Niemann, A., Kirschner, J., Korinthenberg, R., Ketelsen, U.P., Battaloglu, E., Parman, Y., Nicholson, G., Ouvrier, R., Seeger, J., Jonghe, P.D., Weis, J., Kruttgen, A., Rudnik-Schoneborn, S., Bergmann, C., Suter, U., Zerres, K., Timmerman, V., Relvas, J.B. & Senderek, J. (2007). Peripheral Nerve Demyelination Caused by a Mutant Rho GTPase Guanine Nucleotide Exchange Factor, Frabin/FGD4. *Am J Hum Genet*, **81,** 158-64.

Stolt, C.C., Rehberg, S., Ader, M., Lommes, P., Riethmacher, D., Schachner, M., Bartsch, U. & Wegner, M. (2002). Terminal differentiation of myelin-forming oligodendrocytes depends on the transcription factor Sox10. *Genes Dev*, **16,** 165-70.

Strange, K., Denton, J. & Nehrke, K. (2006). Ste20-type kinases: evolutionarily conserved regulators of ion transport and cell volume. *Physiology (Bethesda)*, **21,** 61-8.

Su, W., Shmukler, B.E., Chernova, M.N., Stuart-Tilley, A.K., de Franceschi, L., Brugnara, C. & Alper, S.L. (1999). Mouse K-Cl cotransporter KCC1: cloning, mapping, pathological expression, and functional regulation. *Am J Physiol*, **277,** C899-912.

Sung, K.W., Kirby, M., McDonald, M.P., Lovinger, D.M. & Delpire, E. (2000). Abnormal GABAA receptor-mediated currents in dorsal root ganglion neurons isolated from Na-K-2Cl cotransporter null mice. *J Neurosci*, **20,** 7531-8.

Suter, U. & Scherer, S.S. (2003). Disease mechanisms in inherited neuropathies. *Nat Rev Neurosci*, **4,** 714-26.

Swerdlow, N.R., Braff, D.L. & Geyer, M.A. (1999). Cross-species studies of sensorimotor gating of the startle reflex. *Ann N Y Acad Sci*, **877,** 202-16.

Swerdlow, N.R., Paulsen, J., Braff, D.L., Butters, N., Geyer, M.A. & Swenson, M.R. (1995). Impaired prepulse inhibition of acoustic and tactile startle response in patients with Huntington's disease. *J Neurol Neurosurg Psychiatry*, **58,** 192-200.

Swerdlow, N.R., Sprock, J., Light, G.A., Cadenhead, K., Calkins, M.E., Dobie, D.J., Freedman, R., Green, M.F., Greenwood, T.A., Gur, R.E., Mintz, J., Olincy, A.,

Nuechterlein, K.H., Radant, A.D., Schork, N.J., Seidman, L.J., Siever, L.J., Silverman, J.M., Stone, W.S., Tsuang, D.W., Tsuang, M.T., Turetsky, B.I. & Braff, D.L. (2007). Multi-site studies of acoustic startle and prepulse inhibition in humans: initial experience and methodological considerations based on studies by the Consortium on the Genetics of Schizophrenia. *Schizophr Res*, **92,** 237-51.

Takahashi, N., Chernavvsky, D.R., Gomez, R.A., Igarashi, P., Gitelman, H.J. & Smithies, O. (2000). Uncompensated polyuria in a mouse model of Bartter's syndrome. *Proc Natl Acad Sci U S A*, **97,** 5434-9.

Tateyama, M., Abe, H., Nakata, H., Saito, O. & Kubo, Y. (2004). Ligand-induced rearrangement of the dimeric metabotropic glutamate receptor 1alpha. *Nat Struct Mol Biol*, **11,** 637-42.

Tenhumberg, S., Schuster, B., Zhu, L., Kovaleva, M., Scheller, J., Kallen, K.J. & Rose-John, S. (2006). gp130 dimerization in the absence of ligand: preformed cytokine receptor complexes. *Biochem Biophys Res Commun*, **346,** 649-57.

Tessier-Lavigne, M. & Goodman, C.S. (1996). The molecular biology of axon guidance. *Science*, **274,** 1123-33.

Thaisetthawatkul, P., Logigian, E.L. & Herrmann, D.N. (2002). Dispersion of the distal compound muscle action potential as a diagnostic criterion for chronic inflammatory demyelinating polyneuropathy. *Neurology*, **59,** 1526-32.

Thomas, P.K. (1999). Overview of Charcot-Marie-Tooth disease type 1A. *Ann N Y Acad Sci*, **883,** 1-5.

Trapp, B.D., Quarles, R.H. & Suzuki, K. (1984). Immunocytochemical studies of quaking mice support a role for the myelin-associated glycoprotein in forming and maintaining the periaxonal space and periaxonal cytoplasmic collar of myelinating Schwann cells. *J Cell Biol*, **99,** 594-606.

Tsukamoto, Y. (1995). Pathophysiology and treatment of secondary hyperparathyroidism in patients with chronic renal failure. *Nephrol Dial Transplant*, **10 Suppl 3,** 22-4.

Tsutsumi, T., Ushiro, H., Kosaka, T., Kayahara, T. & Nakano, K. (2002). Proline- and alanine-rich Ste20-related kinase associates with F-actin and translocates from the cytosol to cytoskeleton upon cellular stresses. *J. Biol. Chem.*, **275,** 9157-9162.

Tucker, K.L., Meyer, M. & Barde, Y.A. (2001). Neurotrophins are required for nerve growth during development. *Nat Neurosci*, **4,** 29-37.

Turetsky, B.I., Calkins, M.E., Light, G.A., Olincy, A., Radant, A.D. & Swerdlow, N.R. (2007). Neurophysiological endophenotypes of schizophrenia: the viability of selected candidate measures. *Schizophr Bull*, **33,** 69-94.

Ushiro, H., Tsutsumi, T., Suzuki, K., Kayahara, T. & Nakano, K. (1998). Molecular Cloning and Characterization of a novel Ste20-related protein kinase enriched in neurons and transporting epithelia. *Arch. Biochem. Biophys.*, **355,** 233-240.

Van Dam, D., Errijgers, V., Kooy, R.F., Willemsen, R., Mientjes, E., Oostra, B.A. & De Deyn, P.P. (2005). Cognitive decline, neuromotor and behavioural disturbances in a mouse model for fragile-X-associated tremor/ataxia syndrome (FXTAS). *Behav Brain Res*, **162,** 233-9.

Vargas, F.F. (1968). Filtration coefficient of the axon membrane as measured with hydrostatic and osmotic methods. *J Gen Physiol*, **51,** 13-27.

Verhoeven, K., De Jonghe, P., Coen, K., Verpoorten, N., Auer-Grumbach, M., Kwon, J.M., FitzPatrick, D., Schmedding, E., De Vriendt, E., Jacobs, A., Van Gerwen, V., Wagner, K., Hartung, H.P. & Timmerman, V. (2003). Mutations in the small GTP-ase late endosomal protein RAB7 cause Charcot-Marie-Tooth type 2B neuropathy. *Am J Hum Genet*, **72,** 722-7.

Vitari, A.C., Deak, M., Morrice, N.A. & Alessi, D.R. (2005). The WNK1 and WNK4 protein kinases that are mutated in Gordon's hypertension syndrome, phosphorylate and active SPAK and OSR1 protein kinases. *Biochem. J.*, **391,** 17-24.

Vitoux, D., Olivieri, O., Garay, R.P., Cragoe, E.J., Jr., Galacteros, F. & Beuzard, Y. (1989). Inhibition of K+ efflux and dehydration of sickle cells by [(dihydroindenyl)oxy]alkanoic acid: an inhibitor of the K+ Cl- cotransport system. *Proc Natl Acad Sci U S A*, **86,** 4273-6.

Walcott, B., Birzgalis, A., Moore, L.C. & Brink, P.R. (2005). Fluid secretion and the Na+-K+-2Cl- cotransporter in mouse exorbital lacrimal gland. *Am J Physiol Cell Physiol*, **289,** C860-7.

Wall, S.M., Knepper, M.A., Hassell, K.A., Fischer, M.P., Shodeinde, A., Shin, W., Pham, T.D., Meyer, J.W., Lorenz, J.N., Beierwaltes, W.H., Dietz, J.R., Shull, G.E. & Kim, Y.H. (2006). Hypotension in NKCC1 null mice: role of the kidneys. *Am J Physiol Renal Physiol*, **290,** F409-16.

Warner, L.E., Hilz, M.J., Appel, S.H., Killian, J.M., Kolodry, E.H., Karpati, G., Carpenter, S., Watters, G.V., Wheeler, C., Witt, D., Bodell, A., Nelis, E., Van Broeckhoven, C. & Lupski, J.R. (1996). Clinical phenotypes of different MPZ (P0) mutations may include Charcot-Marie-Tooth type 1B, Dejerine-Sottas, and congenital hypomyelination. *Neuron*, **17,** 451-60.

Warner, L.E., Mancias, P., Butler, I.J., McDonald, C.M., Keppen, L., Koob, K.G. & Lupski, J.R. (1998). Mutations in the early growth response 2 (EGR2) gene are associated with hereditary myelinopathies. *Nat Genet*, **18,** 382-4.

Wehner, F., Olsen, H., Tinel, H., Kinne-Saffran, E. & Kinne, R.K. (2003). Cell volume regulation: osmolytes, osmolyte transport, and signal transduction. *Rev Physiol Biochem Pharmacol*, **148,** 1-80.

Weiss, M.D., Luciano, C.A. & Quarles, R.H. (2001). Nerve conduction abnormalities in aging mice deficient for myelin-associated glycoprotein. *Muscle Nerve*, **24,** 1380-7.

Willem, M., Garratt, A.N., Novak, B., Citron, M., Kaufmann, S., Rittger, A., DeStrooper, B., Saftig, P., Birchmeier, C. & Haass, C. (2006). Control of peripheral nerve myelination by the beta-secretase BACE1. *Science*, **314,** 664-6.

Williams, J.R., Sharp, J.W., Kumari, V.G., Wilson, M. & Payne, J.A. (1999). The neuron-specific K-Cl cotransporter, KCC2. Antibody development and initial characterization of the protein. *J Biol Chem*, **274,** 12656-64.

Willis, W.D. (1999). Dorsal root potentials and dorsal root reflexes: a double-edged sword. *Exp. Brain Res.*, **124,** 395-421.

Wilson, F.H., Kahle, K.T., Sabath, E., Lalioti, M.D., Rapson, A.K., Hoover, R.S., Hebert, S.C., Gamba, G. & Lifton, R.P. (2003). Molecular pathogenesis of inherited hypertension with hyperkalemia: the Na-Cl cotransporter is inhibited by wild-type but not mutant WNK4. *Proc. Natl. Acad. Sci. U.S.A.*, **100,** 680-684.

Wilson, G.F. & Chiu, S.Y. (1990). Ion channels in axon and Schwann cell membranes at paranodes of mammalian myelinated fibers studied with patch clamp. *J Neurosci*, **10,** 3263-74.

Winseck, A.K., Caldero, J., Ciutat, D., Prevette, D., Scott, S.A., Wang, G., Esquerda, J.E. & Oppenheim, R.W. (2002). In vivo analysis of Schwann cell programmed cell death in the embryonic chick: regulation by axons and glial growth factor. *J Neurosci*, **22,** 4509-21.

Wolpowitz, D., Mason, T.B., Dietrich, P., Mendelsohn, M., Talmage, D.A. & Role, L.W. (2000). Cysteine-rich domain isoforms of the neuregulin-1 gene are required for maintenance of peripheral synapses. *Neuron*, **25,** 79-91.

Woo, N.S., Lu, J., England, R., McClellan, R., Dufour, S., Mount, D.B., Deutch, A.Y., Lovinger, D.M. & Delpire, E. (2002). Hyperexcitability and epilepsy associated with disruption of the mouse neuronal-specific K-Cl cotransporter gene. *Hippocampus*, **12,** 258-68.

Wouters, M., De Laet, A., Ver Donck, L., Delpire, E., van Bogaert, P.P., Timmermans, J.P., de Kerchove d'Exaerde, A., Smans, K. & Vanderwinden, J.M. (2006). Subtractive hybridization unravels a role for the ion co-transporter NKCC1 in the murine intestinal pacemaker. *Am. J. Physiol. Gastrointest. Liver Physiol.*, **290,** G1219-G1227.

Wrabetz, L., Feltri, M.L., Quattrini, A., Imperiale, D., Previtali, S., D'Antonio, M., Martini, R., Yin, X., Trapp, B.D., Zhou, L., Chiu, S.Y. & Messing, A. (2000). P(0) glycoprotein overexpression causes congenital hypomyelination of peripheral nerves. *J Cell Biol*, **148,** 1021-34.

Wright, D.E., Zhou, L., Kucera, J. & Snider, W.D. (1997). Introduction of a neurotrophin-3 transgene into muscle selectively rescues proprioceptive neurons in mice lacking endogenous neurotrophin-3. *Neuron*, **19,** 503-17.

Xu, J.C., Lytle, C., Zhu, T.T., Payne, J.A., Benz, E., Jr. & Forbush, B., 3rd. (1994). Molecular cloning and functional expression of the bumetanide-sensitive Na-K-Cl cotransporter. *Proc Natl Acad Sci U S A*, **91,** 2201-5.

Yamada, J., Okabe, A., Toyoda, H., Kilb, W., Luhmann, H.J. & Fukuda, A. (2004). Cl- uptake promoting depolarizing GABA actions in immature rat neocortical neurones is mediated by NKCC1. *J Physiol*, **557,** 829-41.

Yang, S.S., Morimoto, T., Rai, T., Chiga, M., Sohara, E., Ohno, M., Uchida, K., Lin, S.H., Moriguchi, T., Shibuya, H., Kondo, Y., Sasaki, S. & Uchida, S. (2007a). Molecular pathogenesis of pseudohypoaldosteronism type II: generation and analysis of a Wnk4(D561A/+) knockin mouse model. *Cell Metab*, **5,** 331-44.

Yang, T., Huang, Y.G., Singh, I., Schnermann, J. & Briggs, J.P. (1996). Localization of bumetanide- and thiazide-sensitive Na-K-Cl cotransporters along the rat nephron. *Am J Physiol*, **271,** F931-9.

Yang, Y., Allen, E., Ding, J. & Wang, W. (2007b). Giant axonal neuropathy. *Cell Mol Life Sci*, **64,** 601-9.

Yeiser, E.C., Rutkoski, N.J., Naito, A., Inoue, J. & Carter, B.D. (2004). Neurotrophin signaling through the p75 receptor is deficient in traf6-/- mice. *J Neurosci*, **24,** 10521-9.

Yeomans, J.S., Li, L., Scott, B.W. & Frankland, P.W. (2002). Tactile, acoustic and vestibular systems sum to elicit the startle reflex. *Neurosci Biobehav Rev*, **26,** 1-11.

Zhao, C., Takita, J., Tanaka, Y., Setou, M., Nakagawa, T., Takeda, S., Yang, H.W., Terada, S., Nakata, T., Takei, Y., Saito, M., Tsuji, S., Hayashi, Y. & Hirokawa, N. (2001). Charcot-Marie-Tooth disease type 2A caused by mutation in a microtubule motor KIF1Bbeta. *Cell*, **105,** 587-97.

Zhu, L., Lovinger, D. & Delpire, E. (2005a). Cortical neurons lacking KCC2 expression show impaired regulation of intracellular chloride. *J. Neurophysiol.*, **93,** 1557-1568.

Zuchner, S. & Vance, J.M. (2006). Mechanisms of disease: a molecular genetic update on hereditary axonal neuropathies. *Nat Clin Pract Neurol*, **2,** 45-53.